Spatial Bias in Unsaturated Hydraulic Property Estimates:

Origin, Impact, and Relevance

By

Robert M. Holt

Submitted in Partial Fulfillment

of the Requirements for a

Doctorate of Philosophy in Earth and Environmental Science

with a Dissertation in Hydrology

New Mexico Institute of Mining and Technology

Department of Earth and Environmental Science

Socorro, New Mexico

August 2000

ABSTRACT

In this dissertation, we show for the first time that bias in property measurements hinders our ability to characterize spatial variability and model flow and transport in heterogeneous systems. Spatial statistics of hydraulic properties can be accurately estimated when measurement errors are unbiased. Unfortunately, measurements are usually spatially biased (i.e., their spatial pattern is systematically distorted) because random observation errors are propagated through non-linear inversion models that may incorrectly describe experimental physics. Measurement bias can be experimentally evaluated and removed through the use of calibration standards. The entire instrument including the inversion model must be calibrated to overcome the inversion non-linearity, and this is often infeasible in hydrology because physical standards do not exist and inversion-model errors vary unpredictably between individual samples. It is also impossible to fully calibrate estimates of the spatial statistics. Therefore, the effect of bias on spatial statistics cannot be directly quantified, and instead must be examined indirectly.

We develop a new Monte Carlo approach for indirectly determining the spatial bias in field- and laboratory-estimated unsaturated hydraulic properties subject to measurement errors. We find that hydraulic properties are strongly biased by small, simple observation and inversion-model errors. This bias can lead to order-of-magnitude errors in spatial statistics, artificial cross-correlation between measured properties, and the inclusion of parameters in the inversion model that are simply artifacts of the errors, yet show realistic spatial statistics. We also find that measurement errors amplify

uncertainty in experimental variograms caused by limited spatial sampling and can preclude identification of variogram-model parameters. The use of biased spatial statistics in stochastic flow and transport models causes in order-of-magnitude errors in critical transport results, including the mean velocity, velocity variance, and velocity integral scale. The effects of observation and inversion-model errors are insidious, as hydraulic property estimates may appear reasonable and generate realistic looking spatial statistics that are, however, inaccurate and misleading.

Robust estimation of unsaturated hydraulic properties for spatial variability studies and stochastic modeling is not possible with most current instruments and inversion models, because spatial bias cannot easily be removed by calibration or error analyses such as presented here. Bias is extremely sensitive to different inversion-model errors, and it is not possible to identify *a priori* all types of inversion-model error that affect a particular property estimation method. Error analyses cannot be used to uniquely identify all material types or conditions under which a particular instrument or inversion model will perform best or to remove bias caused by measurement errors.

ACKNOWLEDGEMENTS

I would first like to thank all of those who supported me with love and encouragement throughout this endeavor. I would especially like to thank my parents Joseph and Sally Holt, my brother Bill Holt, and my friends Christine Hunter, Mary Jo O'Rourke, Kristine Baker, John Sigda, and Dan and Debbie Golden. Your support at critical times helped me to reach this goal.

I am also grateful to all my colleagues at the Flow Visualization Lab, including Mehdi Eliassi, Don Fox, Scott Pringle, Jim Brainard, Will Peplinski, Lee O'Rear, Vince Tidwell, and Mike Nicholl. I would be less without the interactions we had and friendships we've developed. I would have succumbed to stress without all of your lame jokes.

I would especially like to thank my mentors, who have offered guidance, friendship, and assistance throughout this process. I extend my most sincere thanks to my advisor John Wilson. His example inspired and motivated me to strive for excellence. He was patient with me while I chased dead ends, worked on other things, and struggled through difficult times. My debt to him cannot be measured. I am deeply indebted to Bob Glass who aroused my interest in unsaturated flow and encouraged me to chase this dream. Allan Gutjahr gave me confidence when I needed it and taught me geostatistics, no small feat. I will always remember him and his kindness. Peter Mozely helped me, a geologist, to ease into hydrology. I would like to give a special thanks to Dennis Powers, who first taught me how to think and do meaningful research. By their

example, they have set a high professional standard for me to aspire. It has been a privilege to work with all of you.

Throughout my Ph.D. education, I was sustained by a variety of sources of funding. I am grateful for the consulting opportunities on the Waste Isolation Pilot Plant Project and would like to thank my friends at Sandia National Laboratories including Tom Corbet, Hans Papenguth, and Lucy Meigs. These projects helped me to grow professionally. At a critical time in this endeavor, I received financial support from Idaho National Engineering and Environmental Laboratory. For this I would like to thank, Bob Smith. Finally, I would like to recognize the support of Sandia National Laboratories and the U.S. Department of Energy.

TABLE OF CONTENTS

LIST OF FIGURES

CHAPTER 1 – INTRODUCTION

Despite over twenty-five years of environmental clean up and restoration, environmental pollution continues to be a major problem for the United States. At the end of 1995 the U.S. Environmental Protection Agency (EPA) inventoried over 40,000 contaminated sites and had 1,296 contaminated sites on the National Priorities List (Browner, 1995). Recently, the EPA estimated that there may be as many as 600,000 other contaminated sites within the U.S. (EPA, 2000). The estimated cumulative clean-up costs of these sites could reach over $1 trillion (Russel et al., 1991). Groundwater contamination is an important component of the problem at many contaminated sites. Unfortunately, the groundwater problem is not limited to the saturated zone. The unsaturated zone is the primary conduit for contaminants to reach the water table and may act as a continuing source of contamination long after removal of the contaminant source. In fact, the U.S. Department of Energy (DOE) estimates that approximately half of it's total clean up costs, or $113 billion, will be spent remediating unsaturated zone materials (ERRRD, 1997).

Remediation of unsaturated media is hampered by the lack of a comprehensive understanding of critical processes affecting flow and transport. Predictive models often lack the appropriate physics, and model boundary conditions may be poorly defined, both temporally and spatially. The hydraulic properties that are required by these models are difficult to accurately measure and are distributed heterogeneously in the subsurface. It has long been recognized that unsaturated hydraulic properties are heterogeneous (e.g., Russo and Bresler, 1981; Wierenga et al, 1991; Shouse and Mohanty, 1998) and a

geostatistical approach is commonly employed to characterize observed heterogeneity in terms of spatial statistics (e.g., Mohanty et al., 1994; Russo et al., 1997). Statistical parameters can easily be incorporated in probabilistic models of flow and contaminant transport (e.g., Yeh et al., 1985a,b; Zhang et al., 1998). While a number of workers have focused on improving estimates of spatial statistics (e.g., Russo, 1984; Warrick and Myers, 1987), none have investigated the impact of property measurement errors on estimates of spatial statistics, the focus of this dissertation.

1.1 MOTIVATION

The primary motivation driving this work is the need for adequate characterization of unsaturated hydraulic properties at contaminated sites. The spatial variability of unsaturated hydraulic properties directly influences the movement of contaminated water and non-aqueous phase liquids. In unsaturated materials, capillary forces amplify the influence of heterogeneity on flow and transport processes, because permeability is a function of both geologic heterogeneity and the fluid saturation. Local contrasts of the unsaturated permeability in adjacent strata are significantly greater than for saturated permeability, and the orientation of bedding layers may cause convergence or divergence of a mobile contaminant.

These processes strongly affect the design, final cost, and effectiveness of remedial actions at contaminated sites. Poor characterization of site-specific heterogeneity may lead to ineffective remedial designs and increased risk, requiring subsequent additional remedial actions at increased cost and time. Although many

techniques exist for incorporating site-specific heterogeneity into a probabilistic risk framework for decision analysis, they cannot be reliably applied without first quantifying the uncertainty in hydraulic parameter data and assessing data worth.

A number of researchers have focused on evaluations of data worth, with the goal of optimizing data sampling locations. In particular various strategies have been proposed to optimize sampling locations for determining spatial statistics (e.g., Russo, 1984; Warrick and Myers, 1987). Some workers consider the trade off between the number of samples and remediation costs (e.g., James and Gorelick, 1994). Other workers have examined the relationship between scales of individual measurements and field heterogeneity (e.g., Beckie, 1996; Tidwell, 1999). Still others (e.g., Maxwell et al., 1999) integrate site characterization activities into the prediction of human health risk. Most of these treatments of data worth assume that parameter uncertainty mainly arises from incomplete sampling and non-ideal sample locations. Measurement errors are typically neglected, or it is assumed that measurement errors are unbiased. As we show in this dissertation, these assumptions are generally invalid because measurement errors are often biased, or systematically distorted, in space, and this bias amplifies sampling uncertainty.

1.2   THE BIAS PROBLEM

Bias in property measurements is a serious potential problem that could affect our ability to characterize spatial variability and model flow and transport in heterogeneous systems. Hydraulic property measurements are prone to bias because most properties

(e.g., hydraulic conductivity) are estimated indirectly using: 1) instruments that observe the response of a hydrologic system to a time-varying or steady boundary condition, and 2) non-linear mathematical-inversion models that infer property values from the observed responses. Because properties depend on non-linear inversion models, purely random error in the observation can lead to a systematic error, or bias, in the derived property value (Mandel, 1964). Bias may also result when the inversion model is inadequate (Kempthorne and Allmaras, 1986). Throughout this dissertation, we refer to these two contributions to measurement error as "observation error" and "inversion-model error", respectively.

Most texts on error analysis (e.g., Mandel, 1964, Doebelin, 1966) suggest that measurement bias can be directly evaluated and removed through the use of calibration standards. While individual components of an instrument may be calibrated, such as transducers used to observe response, the entire instrument including the inversion model must be calibrated to overcome the inversion non-linearity. Unfortunately, most instruments and methods for estimating hydraulic properties are not directly calibrated because physical standards do not exist, and furthermore may never be calibrated because inversion-model errors vary unpredictably between individual field samples. In spatial variability studies, it is also impossible to fully calibrate estimates of the spatial statistics. Therefore, the effect of bias on spatial statistics cannot be directly quantified, and instead must be examined indirectly.

We hypothesize that measurement bias is potentially disastrous in the context of spatial variability studies and modeling of flow and transport in heterogeneous media. Property measurement errors are likely to be correlated to the sampled hydraulic property

4

because the observed response depends upon the hydraulic properties of the system. The spatial pattern of estimated hydraulic properties may become distorted in space, and estimated spatial statistics could also become biased and no longer representative. Deterministic and stochastic flow and transport results will also show systematic errors if biased spatial statistics are used in the models.

1.3   OBJECTIVE AND APPROACH

The objective of this dissertation is to evaluate for the first time the origin, impact and relevance of spatial bias in field- and laboratory-estimated unsaturated hydraulic properties due to simple errors in observations and inversion models. To fulfill this objective, we focus on these fundamental questions:

1) Do simple observation and inversion-model errors cause bias in spatial statistics; if so, how does this bias originate and what is its magnitude?

2) Can we characterize the spatial statistics of unsaturated hydraulic properties in the presence of measurement errors?

3) Are probabilistic models of flow and transport sensitive to spatial bias caused by measurement error?

To answer these questions, we develop a new Monte Carlo approach for indirectly determining the spatial bias in estimates of hydraulic properties subject to simple observation and inversion-model errors.

Our approach is straightforward (Figure 1-1). Using standard methods (e.g., Robin et al., 1993), we generate and sample a series of artificial spatial realities (sets of parameter fields). At each sampled location, observation and inversion-model errors are propagated through numerical simulations of parameter measurements. The spatial structure of the resulting parameter estimates is compared to the spatial structure of the underlying reality, revealing the extent of spatial bias. To evaluate the sensitivity of bias to the true field statistics, this procedure is repeated a across parameter spaces selected to represent a range of realistic materials.

To estimate properties three different types of models are used: 1) models for determining the system response due to a perturbation, 2) models for errors affecting observations of the perturbation and state variables, and 3) technique-specific inversion models for estimating parameters. When inversion-models are simple and require only steady-state data (e.g., the tension infiltrometer), the system response is modeled using analytical models. Otherwise, finite-difference methods are used to simulate the unsaturated system response. Inversion-model errors are incorporated within the system-response model, while observation errors are added to observations of the perturbation and state variables prior to use in inversion models for estimating parameters. Inversion-models for estimating parameters follow published methods.

Observation-error models are constructed using data collected for instruments in our laboratories (New Mexico Institute of Mining and Technology and Sandia National Laboratories). Models for inversion-model errors are developed based on our experiences in the laboratory and field. It is not our objective to study these errors in detail, but to examine their influence on estimates of spatial statistics.
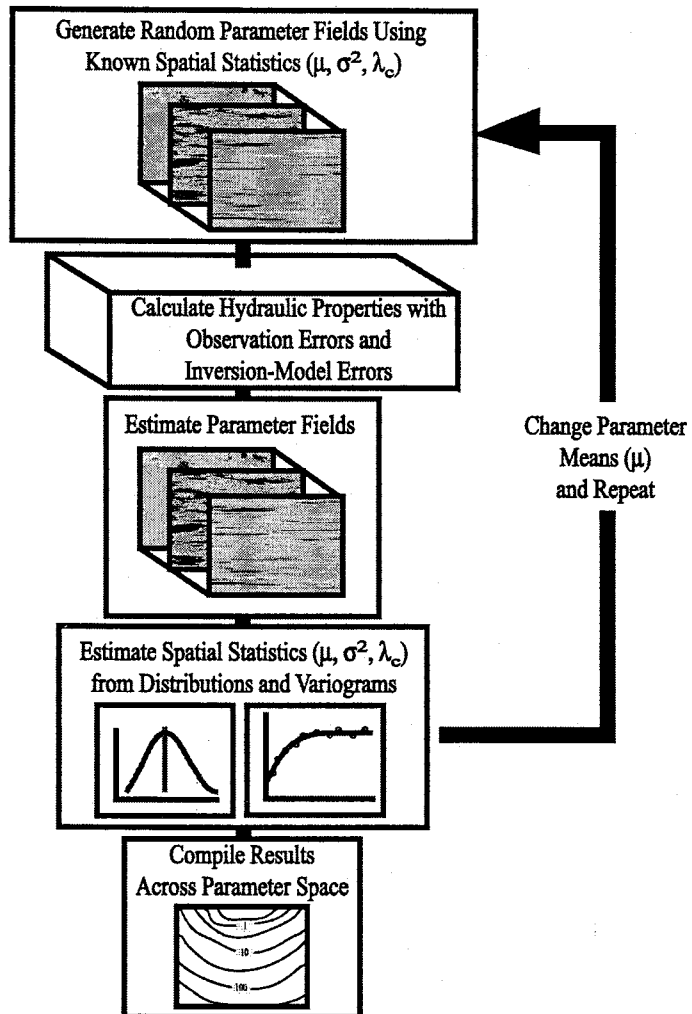
Figure 1-1. Schematic of the Monte Carlo process used to evaluate bias in spatial statistics.

1.4 ORGANIZATION

This dissertation is written in the style where each chapter, except Chapters 1 and 5, has been composed as an independent, peer-reviewed journal publication. As a result, each chapter contains its own literature review and references. Short summaries of each chapter are provided below.

Chapter 2 – This chapter focuses on spatial bias in field-estimated unsaturated hydraulic properties. We use a Monte Carlo error analysis to evaluate spatial bias in unsaturated hydraulic properties estimated using a tension infiltrometer, a device commonly employed for spatial variability studies. Two types of observation error (error in steady flux rate and applied tension) are considered, along with one inversion-model error resulting from poor contact between the instrument and the medium. Bias in estimates of spatial statistics, including the mean, variance, and variogram-model parameters, is evaluated across a parameter space representative of poorly- to well-sorted sandy silt to very coarse sand. Within the parameter space, we conduct 221 Monte Carlo simulations using random parameter fields consisting of 262,144 (512×512) points.

Chapter 3 – In this chapter, we consider bias in laboratory-estimated hydraulic properties, including the saturated hydraulic conductivity, porosity, and parameters that describe the moisture characteristic curve. Only observation errors (volume, length, weight, pressure and time) are considered when estimating the saturated hydraulic

conductivity and porosity. Moisture-characteristic curves are estimated in four different error scenarios with progressively larger errors, including observation, equilibrium, boundary, and repacking errors. The geometric mean n is systematically varied from 1.5 to 7.0, representing materials from soils to eolian sands. Because of computational expense, random fields used in this study are smaller consisting of only 16,384 (128×128) points. The chapter ends by evaluating the relative impact of spatial bias in structural error, due to incomplete sampling of spatial locations.

Chapter 4 – We evaluate the impact of measurement errors in field-estimated hydraulic properties on 1D and 3D unconditional unsaturated stochastic models of unsaturated flow and transport. Hydraulic properties are determined by simulating tension-infiltrometer measurements across a parameter space representative of poorly- to well-sorted, sandy silt to coarse sand. Within the parameter space, we conduct 221 Monte Carlo simulations using random parameter fields consisting of 262,144 (512×512) points. Two types of observation error are considered, along with one inversion-model error resulting from poor contact between the instrument and the medium, the same types of errors studied in Chapter 2. Bias in estimates of the mean, variance, and integral scale of vertical unsaturated velocity and longitudinal macrodispersivity is determined.

1.5   REFERENCES CITED

Beckie, R., 1996, Measurement scale, network sampling scale, and groundwater model
parameters, *Water Resources Research*, v. 32, p. 65-76.

Browner, C., 1995, *Testimony to the Subcommittee on Commerce, Trade, and Hazardous
Materials*, Committee on Commerce, U.S. House of Representatives,
Washington, DC, October 26.

Doebelin, E. O., 1966, *Measurement Systems: Application & Design*, McGraw Hill, NY,
NY, 1966, 743 pp.

EPA, 2000, A decade of progress: Innovation at the Environmental Protection Agency,
EPA100-R-00-020, U.S. EPA Office of Policy, Economics, and Innovation,
Washington, DC.

ERRRD, 1997, Environmental Restoration Remediation Requirements Definition, URL:
http://emsp.em.doe.gov/define/rd_3.html.

James, B. R., and S. M. Gorelick, 1994, When enough is enough: The worth of
monitoring data in aquifer remediation design, *Water Resources Research*, v. 30,
p. 3499-3513.

Kempthorne, O. and R. R. Allmaras, 1986, Errors and variability of observations, in A.
Klute, Ed., *Methods of Soil Analysis, Part 1, Physical and Mineralogical
Methods, 2nd ed.*, American Society of Agronomy and Soil Science Society of
America, Madison, WI, p. 1-31.

Mandel, J., 1964, *The Statistical Analysis of Experimental Data*, Dover Publications,
New York, NY, pp. 410.

Maxwell, R. M., Kastenberg, W. E., and Y. Rubin, 1999, A methodology to integrate site characterization information into groundwater-driven health risk assessment, *Water Resources Research*, v. 35, p. 2841-2855.

Mohanty, B. P., M. D. Ankeny, R. Horton, and R. S. Kanwar, 1994, Spatial analysis of hydraulic conductivity measured using disc infiltrometers, *Water Resources Research*, v. 30, p. 2489-2498.

Robin, M. J. L., A. L. Gutjahr, E. A. Sudicky, and J. L. Wilson, 1993, Cross-correlated random field generation with the direct Fourier transform method, *Water Resources Research*, v. 29, p. 2385-2397.

Russel, M., Colglazier, E. M., and M. R. English, 1991, *Hazardous Waste Remediation: The Task Ahead*, University of Tennessee, Knoxville, TN, A-3.10

Russo, D., 1984, Design of an optimal sampling network for estimating the variogram, *Soil Science Society of America Journal*, v. 48, p. 708-716.

Russo, D., and E. Bresler, 1981, Soil hydraulic properties as stochastic processes: I. An analysis of field spatial variability, *Soil Science Society of America Journal*, v. 45, p. 682-687.

Russo, D., I. Russo, and A. Laufer, 1997, On the spatial variability of parameters of the unsaturated hydraulic conductivity, *Water Resources Research*, v. 33, p. 947-956.

Shouse, P. J., and B. P. Mohanty, 1998, Scaling of near-saturated hydraulic conductivity measured using disc infiltrometers, *Water Resources Research*, v. 23, p. 1195-1205.

Tidwell, V. C., 1999, *Laboratory Investigation of Permeability Upscaling*, unpublished Ph.D. Dissertation, New Mexico Institute of Mining and Technology, Socorro, NM.

Warrick, A. W., and D. E. Myers, 1987, Optimization of sampling locations for variogram calculations, *Water Resources Research*, v. 23, p. 496-500.

Wierenga, P. J., R. G. Hills, and D. B. Hudson, 1991, The Las Cruses Trench site: characterization, experimental Results, and one-dimensional flow predictions, *Water Resources Research*, v. 27, p. 2695-2705.

Yeh, T. -C. Jim, L. W. Gelhar, and A. L. Gutjahr, 1985a, Stochastic analysis of unsaturated flow in heterogeneous soils: 1. Statistically isotropic media, *Water Resources Research*, v. 21, p. 447-456.

Yeh, T. -C. Jim, L. W. Gelhar, and A. L. Gutjahr, 1985b, Stochastic analysis of unsaturated flow in heterogeneous soils: 2. Statistically isotropic media with variable α, *Water Resources Research*, v. 21, p. 457-464.

Zhang, D. Z., T. C. Wallstrom, and C. L. Winter, 1998, Stochastic analysis of steady-state unsaturated flow in heterogeneous media: Comparison of the Brooks-Corey and Gardner-Russo models, *Water Resources Research*, v. 34, p. 1437-1449.

CHAPTER 2 - SPATIAL BIAS IN FIELD-ESTIMATED UNSATURATED HYDRAULIC PROPERTIES

2.1 ABSTRACT

Hydraulic property measurements often rely on non-linear inversion models whose errors vary between samples. In non-linear physical measurement systems, bias can be directly quantified and removed using calibration standards. In hydrologic systems, field calibration is often infeasible and bias must be quantified indirectly. We use a Monte Carlo error analysis to indirectly quantify spatial bias in the saturated hydraulic conductivity, K_s, and the exponential relative permeability parameter, α, estimated using a tension infiltrometer. Two types of observation error are considered, along with one inversion-model error resulting from poor contact between the instrument and the medium. Estimates of spatial statistics, including the mean, variance, and variogram-model parameters, show significant bias across a parameter space representative of poorly- to well-sorted silty sand to very coarse sand. When only observation errors are present, spatial statistics for both parameters are best estimated in materials with high hydraulic conductivity, like very coarse sand. When simple contact errors are included, the nature of the bias changes dramatically. Spatial statistics are poorly estimated, even in highly conductive materials. Conditions that permit accurate estimation of the statistics for one of the parameters prevent accurate estimation for the other; accurate regions for the two parameters do not overlap in parameter space. False cross-correlation between estimated parameters is created because estimates of K_s also depend on estimates of α and both parameters are estimated from the same data.

13

2.2 INTRODUCTION

In recent years, there has been an increased focus on characterizing the spatial variability of unsaturated hydraulic properties. Because laboratory methods for estimating unsaturated properties are expensive, time-consuming, and may not yield results representative of heterogeneous field conditions, simple and rapid field methods for estimating *in situ* unsaturated properties are appealing and potentially cost-effective. As a result, a variety of field methods for estimating *in situ* hydraulic properties have been developed (e.g., Reynolds and Elrick, 1985; Ankeny et al., 1991; Simunek and van Genuchten, 1996), and applied in spatial variability studies (e.g., Istok et al., 1994; Jarvis and Messing, 1995; Mohanty et al., 1994; Russo, et al., 1997; Shouse and Mohanty, 1998). Although most studies carefully document instrument procedures, little attention has been paid to examining hydraulic property measurement errors in the field. The absence of a rigorous treatment of property measurement errors in many of these studies is a potentially serious oversight, especially when hydraulic property data are used to characterize spatial variability.

Field measurement methods are often validated through limited testing in a known medium (e.g., Reynolds and Elrick, 1987; Simunek, et al., 1999) or by numerically simulating experimental results (e.g., Reynolds and Elrick, 1987; Simunek and van Genuchten, 1996; Wu, et al., 1997). In some cases, a cursory examination of errors has been performed (e.g., Simunek and van Genuchten, 1996; Russo et al., 1997). These types of validation can show that a method is useful for measuring *in situ* properties in

the studied material. However, it is not sufficient for validating the use of a method in spatial variability studies where material properties vary over orders of magnitude. Measurements are only useful when they are sufficiently accurate for their intended purpose (e.g., Doebelin, 1966). Proper validation of a measurement technique for spatial variability studies should include systematic error analyses that considers the impact of measurement error on estimated spatial statistics, including the variogram. Without such a systematic evaluation, the reliability of data collected in spatial variability studies of unsaturated hydraulic properties remains suspect.

Errors in measured hydraulic properties are difficult to quantify. Most *in situ* hydraulic properties (e.g., hydraulic conductivity) are estimated indirectly using: 1) instruments that observe the response of a hydrologic system to a time-varying or steady boundary condition, and 2) non-linear mathematical-inversion models that infer property values from the observed responses. Because properties depend on non-linear inversion models, purely random error in the observation can lead to a systematic error, or bias, in the derived property value (Mandel, 1964). Bias may also result when the inversion model is inadequate (Kempthorne and Allmaras, 1986). We refer to these two contributions to measurement error as "observation error" and "inversion-model error", respectively.

Most texts on error analysis (e.g., Mandel, 1964, Doebelin, 1966) suggest that measurement bias can be experimentally evaluated and removed through the use of calibration standards. While individual components of an instrument may be calibrated, such as transducers used to observe response, the entire instrument including the inversion model must be calibrated to overcome the inversion non-linearity.

15

Unfortunately, most instruments and methods for estimating *in situ* hydraulic properties are not directly calibrated because physical standards do not exist, and furthermore may never be calibrated because inversion-model errors vary unpredictably between individual field samples. In spatial variability studies, it is also impossible to fully calibrate estimates of the spatial statistics. Therefore, the effect of bias on spatial statistics cannot be directly quantified, and instead must be examined indirectly.

Measurement bias is potentially disastrous in the context of spatial variability studies. Because the observed response depends upon the hydraulic properties of the system, property measurement errors are correlated to the sampled hydraulic property. The spatial pattern of estimated hydraulic properties is distorted in space and estimated spatial statistics are also corrupted by bias and no longer representative. In summary, we hypothesize that field measurements of unsaturated hydraulic properties, and their spatial statistics, are spatially biased.

In this chapter, we use a Monte Carlo error analysis to systematically evaluate for the first time the extent of bias in the spatial statistics of unsaturated hydraulic properties. Although the total inaccuracy of a measurement includes the effects of both bias and random errors (e.g., Mandel, 1964; Doebelin, 1966), bias is the most insidious component of error because it is difficult to identify or remove without calibration. Unsaturated property field instruments are seldom calibrated. We therefore focus on the issue of bias in this study. In particular, we consider tension-infiltrometer estimates of the saturated hydraulic conductivity and the pore-size distribution parameter for the exponential unsaturated hydraulic conductivity model. To keep our analysis tractable, we create an artificial reality in which the only errors affecting measurements are simple observation

and inversion-model errors. This paper is not intended to be a detailed evaluation of all measurement error induced bias in spatial statistics tension-infiltrometer-estimated hydraulic properties. Instead, we focus on quantitatively revealing for the first time the impacts of measurement error bias on estimated spatial statistics. We do not consider sampling bias or uncertainty due to non-ideal sample locations or incomplete sampling.

2.3   METHODS

The tension infiltrometer is an instrument commonly used for examining the spatial variability of unsaturated hydraulic properties (e.g., DOE, 1993; Mohanty, et al., 1994; Jarvis and Messing, 1995; Shouse and Mohanty, 1998). It is a simple device for applying a constant (negative) pressure boundary condition to unsaturated soil (Figure 2-1). Contact with the soil is established using a porous membrane on the base-plate ring. Typically, a ring is placed on the soil surface and filled with fine sand. The base plate is placed upon the sand, which provides contact with the soil. Flow from the instrument is primarily caused by a capillary gradient. The flux from the instrument is determined by monitoring the declining water level in the Mariotte bottle (Figure 2-1). The design and operation of the tension infiltrometer is described by Ankeny et al. (1988).

A common inversion approach for the tension infiltrometer requires that the unsaturated hydraulic conductivity be described by an exponential relative permeability model, $\exp(\alpha\psi)$, where

$$K(\psi) = K_s \exp(-\alpha\psi), \tag{2-1}$$

ψ is the tension or the absolute value of the matric potential, α is the slope of

17
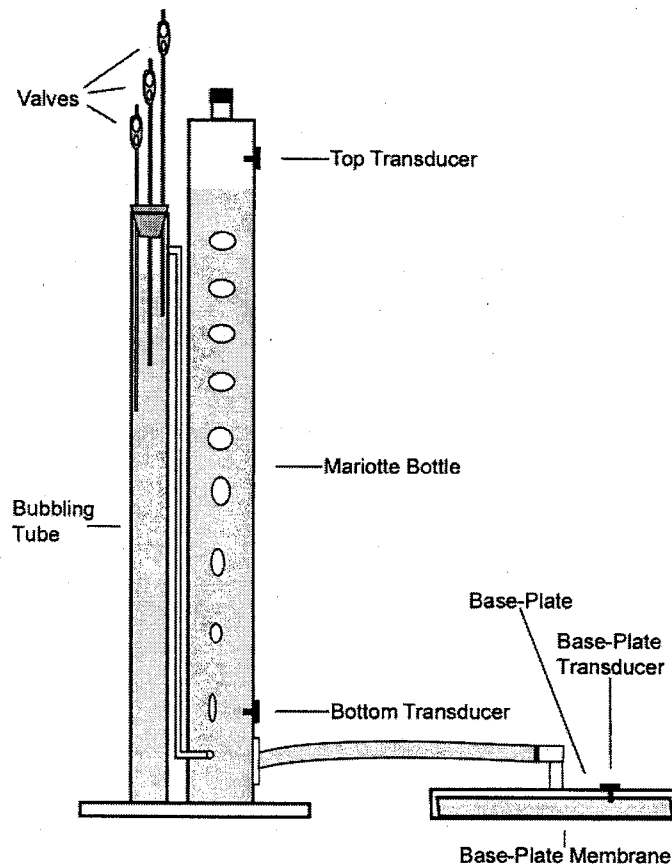
Figure 2-1. Schematic of the tension infiltrometer. The base plate (on the right) is in contact with the sampled medium.

$\ln[K(\psi)]/\psi$, and K_s is the saturated hydraulic conductivity. The exponential relative permeability model is commonly used in stochastic models of unsaturated flow (e.g., Yeh et al., 1985a, b, c; Mantoglou and Gelhar, 1987a, b; Polmann, et al., 1991; Indelman, et al., 1993; Russo, 1995; Harter and Yeh, 1996; Zhang et al., 1998). With knowledge of two applied tensions (ψ_1 and ψ_2) and corresponding observed steady-state flux rates (Q_1

and Q_2), parameters α and K_s can be estimated using the analytical approximation of Wooding (1968).

We employ a Monte Carlo approach to conduct our analysis. We generate 221 pairs of statistically homogeneous independent Gaussian random fields of $\ln(\alpha)$ and $\ln(K_s)$, with a zero specified point covariance between $\ln(\alpha)$ and $\ln(K_s)$. The pore-size parameter, α, is typically assumed to follow a normal distribution in most unsaturated stochastic models (e.g., Yeh et al., 1985a, 1985b, 1985c; Mantoglou and Gelhar, 1987a, 1987b; Indelman, et al., 1993; Zhang et al., 1998). However, we have chosen to describe α with a log-normal distribution because a log-normal distribution may be more realistic (e.g., White and Sulley, 1992; Russo et al., 1997). At each spatial location in a Monte Carlo simulation, we estimate the true flux and applied tension, add observation error to these values, and re-estimate $\ln(\alpha)$ and $\ln(K_s)$. To simplify our analysis, we assume that (2-1) describes the unsaturated hydraulic conductivity, Wooding's (1968) approximation is exact, and that sub-sample-scale heterogeneity (including macropores) does not exist. We consider only two types of observation error, error in estimated steady flux and error in applied tension, and only one type of model inversion error, error in contact between the disk and the medium. As in practice, we reject physically implausible results during the re-estimation. We examine biases affecting the mean, variance, and variogram model parameters for $\ln(\alpha)$ and $\ln(K_s)$ and define the parameter space in which these statistics can be predicted with minimal bias.

In this study, we do not consider the effects of structural errors, caused by a limited number of samples and non-ideal sampling locations, on variogram estimation.

Most spatial variability studies are based on several hundred points or less, and structural errors introduce significant uncertainty in spatial statistics (e.g., Russo, 1984; Warrick and Myers, 1987; Russo et al., 1987a, b).

2.3.1 Random Fields

For each Monte Carlo simulation we generate over 262,000 pairs (a 512 by 512 random field) of log-normal α and K_s with a fixed geometric mean and variance of α (α^G and $\sigma^2_{\ln(\alpha)}$) and K_s (K_s^G and $\sigma^2_{\ln(K_s)}$). The geometric means of α and K_s are varied between simulations. Philip (1969) suggests that the parameter α ranges between 0.002 to 0.05 cm^{-1}, although other reported values are both smaller than 0.002 cm^{-1} (e.g., Bresler, 1978; Russo and Bouton, 1992) and greater than 0.05 cm^{-1} (e.g., Clothier et al., 1985; Russo et al., 1997). α^G is varied from 10^{-4} to 0.1 cm^{-1} to encompass this range of values. Similarly, we vary K_s^G from 10^{-5} cm/s to 0.1 cm/s. This range is consistent with the range of hydraulic conductivity values reported in tension infiltrometer studies (e.g., Ankeny et al., 1991; Hussen and Warrick, 1993; Shouse and Mohanty, 1998) and is representative of silty sand to coarse sand (e.g., Freeze and Cherry, 1979). The variances of $\ln(\alpha)$ and $\ln(K_s)$ remain arbitrarily fixed at 1.0 which are consistent with the range of values reported from field studies (e.g., Russo and Bouton, 1992; Mohanty et al., 1994; Istok et al., 1994; Russo et al., 1997). Across our entire parameter space, we conduct 13 × 17 = 221 Monte Carlo simulations, in which the means of $\ln(K_s)$ and $\ln(\alpha)$ are each incremented by steps of size 0.576 between simulations.

In Richard's equation, the parameter α scales the influence of gravity (e.g., Philip, 1969). As α is increases, the slope of the $K(\psi)$ relationship increases indicating a narrowing of the pore-size distribution. By assuming that the pore-size distribution is proportional to the grain-size distribution, we can imply that the degree of sorting is inversely proportional to α. We can also infer that K_s increases with the average grain size. Across the parameter space the geometric mean values of α and K_s represent poorly to well-sorted silty sand to very coarse sand.

Random fields are generated using the FFT method (e.g., Robin et al., 1993). We employ a 2D, isotropic, exponential variogram model

$$\gamma^{e}(\mathbf{h}) = \sigma^{2}\left[1 - \exp\left(-\frac{\mathbf{h}}{\lambda_{c}}\right)\right] \qquad (2\text{-}2)$$

where σ^2 is the variance of the random process, $\mathbf{h}$ is a separation vector, and λ_c is the correlation length. In stochastic models, it is often assumed that the correlation lengths of unsaturated parameters are the same (e.g., Yeh et al., 1985a, b, c; Mantoglou and Gelhar, 1987a, b) and, for convenience, we set all correlation lengths equal to 10 length units.

2.3.2   Observation Errors

Two sets of observations, each consisting of an applied tension and an observed steady-state flux, are required to estimate α and K_s. We assume that the applied tension is observed using a standard pressure transducer in the base plate (Figure 2-1). The flux from the Mariotte bottle is estimated by observing the height of water in the bottle with pressure transducers at two different times (e.g., Ankeny et al., 1988). Errors, in this

21

case, are limited to transducer error and changes in tension due to bubbling within the Mariotte bottle.

The estimated tension, $\hat{\psi}$, at the base-plate membrane is expressed as

$$\hat{\psi} = \psi + \xi \tag{2-3}$$

where ψ is the true tension and ξ is the error due to transducer noise and drift and bubbling error. Because bubbling error is a time dependant phenomena, ξ has a temporal correlation. Ankeny et al. (1988) examined this issue and concluded that, in most cases, temporal correlation can be neglected. We assume that ξ is an independent, mean-zero, normally-distributed random variable and neglect transducer drift, implying that the transducers themselves are perfectly calibrated. With the assumption of independence, the variance of $\hat{\psi}$ is defined as

$$\sigma_{\hat{\psi}}^2 = \frac{\sigma_{\xi}^2}{M} \tag{2-4}$$

where σ_{ξ}^2 is the variance of ξ and M is the number of times the transducer is polled. Ankeny et al. (1988) reports that the standard deviation of observed pressure within their tension infiltrometer device is 0.62 cm. We assume that this variability is representative of the tension variation at the disk and set $\sigma_{\xi}^2 = 0.4 \, \text{cm}^2$.

Estimates of the flux rate from a tension infiltrometer are most commonly based upon a method described by Ankeny, et al. (1988). Two transducers in the Mariotte tube are used to minimize, but not eliminate, the effect of bubbling errors. The flux rate, $\hat{Q}$, is estimated by determining the decline of water-level in the Mariotte tube as infiltration occurs and applying

22

$$\hat{Q} = \frac{\Delta \hat{H}}{\Delta t} \pi r_t^2 \tag{2-5}$$

where $\Delta \hat{H} = \hat{H}(t_2) - \hat{H}(t_1)$, $\Delta t = t_2 - t_1$ (the polling interval for the transducers), r_t is the radius of the Mariotte tube, and $\hat{H}(t)$ is the estimated height of the water in the Mariotte tube at time t. Flux errors are caused by errors in estimating the height of the water in the Mariotte tube,

$$\hat{H}(t) = H(t) + \varepsilon \tag{2-6}$$

where $H(t)$ is the true height of the water in the bubbling tube at time t and ε is an independent, mean-zero, normally-distributed error with variance σ_ε^2. As with the error in observed tension, the assumed distribution and assumption of independence of ε is an approximation that improves when the sampling period is much greater than the bubble frequency. If N flux estimates are averaged, then the variance of this estimate is

$$\sigma_q^2 = \frac{2\sigma_\varepsilon^2 \pi^2 r_t^4}{\Delta t^2 N} \tag{2-7}$$

We estimate $\sigma_\varepsilon^2 = 0.0025\,\mathrm{cm}^2$ from the results of Figure 2 of Ankeny et al. (1988), with spurious data removed. We also assume that the radius of the bubbling tube r_t is 1 cm, that the pressure transducer is polled once per second, and 30 seconds worth of data are averaged to estimate the steady-state flux rate. Using (2-7), the variance of estimated flux rates is $\sigma_q^2 = 0.00165\ \mathrm{cm}^6/\mathrm{s}^2$.

23

2.3.3 Contact Error

We consider only one type of inversion-model error, a "contact error" resulting from poor contact between the base-plate membrane and the sample medium. It is a common problem during use of the tension infiltrometer and, in our experience, appears to occur more frequently for observations made at higher tensions. This type of error reduces the area for flow and alters the flow geometry. Flaws in the sand contact between the disk and the medium act as large pores, which do not fill at high tensions. At lower tensions, these pores fill eliminating or reducing the error. Since the tension infiltrometer requires at least two observations, one at a higher tension, this error is often more pronounced at the higher tension.

We are not interested in studying contact error in detail, but only its impact on estimating spatial statistics. Consequently, we develop and apply a simple approximation based upon the reduction of area for flow. We assume that the flow geometry does not change and that only the disk area is reduced due to poor contact. We apply this error only at the highest applied tension. The disk area is multiplied by a scaling factor $(1-f)$, where f is selected from a uniform random distribution over 0.0 to 0.1. Because estimates of α and K_s require two flux observations, this error introduces an additional bias in the estimated hydraulic properties. In the following sections, the contact error scenario includes both the contact and observation errors.

2.3.4 Hydraulic Property Estimates

We assume that the tension values used for each observation are estimated to be $\hat{\psi}_1 = 2.0$ cm and $\hat{\psi}_2 = 7.0$ cm. The true tensions (ψ_n) are calculated by subtracting ξ from $\hat{\psi}_n$, for $n = 1,2$. For each observation, the value of ξ is determined by randomly sampling a mean-zero normal distribution with $\sigma_\xi^2 = 0.4$ cm^2. Given ψ_n, α, and K_s, we calculate the true flux from the tension infiltrometer using (Wooding, 1968)

$$Q_n = \frac{K_s}{\alpha} e^{-\alpha \psi_n} \left(\alpha + \frac{4}{\pi r_d} \right) \pi r_d^2 \qquad (2\text{-}8)$$

where r_d is the radius of the disk and is equal to 10 cm.

Once the true flux rate is determined, we calculate the estimated flux $\hat{Q}_n$ by adding mean-zero, normally distributed error with $\sigma_q^2 = 0.00165$ cm^4/s^2. Sampling locations where $\hat{Q}_1 \leq \hat{Q}_2$ are discarded, as they would be in practice. Although we and others (e.g., Mohanty, pers. comm., 2000; Ankeny, pers. comm., 2000) have both observed and followed this practice in field studies, it is not well documented in the literature. The percentage of discarded points is usually small. For our field studies it is typically around 5%.

When contact errors are considered, $\hat{Q}_1$ is estimated using the procedure outlined above, while $\hat{Q}_2$ is estimated using the same variance for σ_q^2 but is estimated using an altered disk radius

$$r_d^* = r_d \sqrt{1-f} \qquad (2\text{-}9)$$

where f is sampled from a uniform distribution over 0.0 to 0.1. This means that the disk radius may be reduced from 10 cm to a minimum of ~ 9.5 cm.

The relative permeability parameter, α, is then estimated with (Reynolds and Elrick, 1991)

$$\hat{\alpha} = \frac{\ln(\hat{Q}_1 / \hat{Q}_2)}{\hat{\psi}_2 - \hat{\psi}_1} \qquad (2\text{-}10)$$

and the saturated hydraulic conductivity, K_s, is estimated with

$$\hat{K}_s = \frac{\hat{\alpha}\, \hat{Q}_1 e^{\hat{\alpha}\hat{\psi}_1}}{\hat{\alpha}\, \pi r_d^2 + 4 r_d} \qquad (2\text{-}11)$$

This procedure is repeated for all pairs of α and K_s values.

2.3.5   Statistical Property Estimates

For each spatially correlated random field, the mean, variance, and cross-covariance between $\ln(\alpha)$ and $\ln(K_s)$ are determined. In addition, local variograms are calculated for $\ln(\alpha)$, $\ln(K_s)$, $\ln(\hat{\alpha})$, and $\ln(\hat{K}_s)$ using the GSLIB subroutines gam2 (Deutsch and Journel, 1998)

$$\gamma(\mathbf{h}) = \frac{1}{2\,N(\mathbf{h})} \sum_{i=1}^{N(\mathbf{h})} \left[U(\mathbf{x}_i + \mathbf{h}) - U(\mathbf{x}_i) \right]^2 \qquad (2\text{-}12)$$

where $N(\mathbf{h})$ is the number of samples in lag interval $\mathbf{h}$ and $U(x)$ is the random field. All of the resulting 221 experimental variograms are fit using a Levenberg-Marquardt algorithm with the exponential variogram model

$$\hat{\gamma}^m(\mathbf{h}) = \sigma_m^2 \left[1 - \exp\left(-\frac{3\mathbf{h}}{\hat{\lambda}_c} \right) \right] + \sigma_n^2 \qquad (2\text{-}13)$$

where $\hat{\lambda}_c$ is the estimated "correlation length", $\hat{\sigma}_m^2$ is the "model variance", and $\hat{\sigma}_n^2$ is the nugget variance. It is important to note that the model variance differs from the variance

26

in that it is a fitting parameter while the variance is a directly calculated statistic. The variance of the fitted data is the sum of model and nugget variances. When a variogram is constant for all lag distances, we refer to it as a "nugget variogram" in which $\hat{\sigma}_m^2 = 0.0$ and $\hat{\lambda}_c = 0.0$. In classical geostatistics, nugget variograms represent white noise processes that have no spatial correlation. Bias for each statistical parameter is shown using a ratio

$$\hat{P}_E / \hat{P}_T \tag{2-14}$$

where $\hat{P}_E$ is the statistical parameter (e.g., mean, variance, or variogram model parameters) for a random field of estimates and $\hat{P}_T$ is the statistical parameter determined for the true random field. The ratio equals 1.0 for an unbiased statistic.

2.4   RESULTS

Here, we present the results of our Monte Carlo analysis. We show that both the fraction of points discarded because of a physically implausible result ($\hat{Q}_1 \leq \hat{Q}_2$), and the bias in the mean, variance, and variogram-model parameters for $\ln(\hat{\alpha})$ and $\ln(\hat{K}_s)$, are functions of the field values of K_s^G and α^G. In addition, we illustrate how measurement errors introduce false cross-correlation between $\ln(\hat{\alpha})$ and $\ln(\hat{K}_s)$. When only measurement errors are considered, bias in spatial statistics increases for those geometric mean values that produce low flux rates (e.g., small K_s and high α) and appears to correlate with the fraction of points discarded. When inversion-model errors, in the form

27

of a contact error, are included, the pattern of bias in spatial statistics changes significantly and depends less on the fraction of points discarded.

2.4.1 Fraction of Points Discarded

Figures 2-2a and 2-2b plots across parameter space the fraction of points discarded (FPD) because of an unrealistic result, $\hat{Q}_1 \leq \hat{Q}_2$. When only observation errors are considered (Figure 2-2a), the FPD is a function of both K_s^G and α^G. The FPD increases with α^G and decreases with K_s^G. This result is not surprising, because relative errors in flux rates increase when the flux rates are small and small flux rates result from high α and small K_s (2-8). In the upper left corner (high α^G and small K_s^G), estimated fluxes $\hat{Q}_1$ and $\hat{Q}_2$ are dominated by errors and are nearly independent of the sampled values of α and K_s. In these regions, the likelihood that $\hat{Q}_1 \leq \hat{Q}_2$ is high, and the FPD increases. When contact error is included (Figure 2-2b), the FPD tends to become less dependent on the value of K_s at low α^G, and the FPD decreases across much of the parameter space. This occurs because contact error tends to decrease $\hat{Q}_2$, reducing the likelihood that $\hat{Q}_1 \leq \hat{Q}_2$.

2.4.2 Bias in Estimated Mean

Figure 2-3a presents the bias, expressed as a ratio, in the geometric mean of $\hat{\alpha}$, or $\hat{\alpha}^G$, across parameter space. As the field value of either α^G or K_s^G decreases (lower left
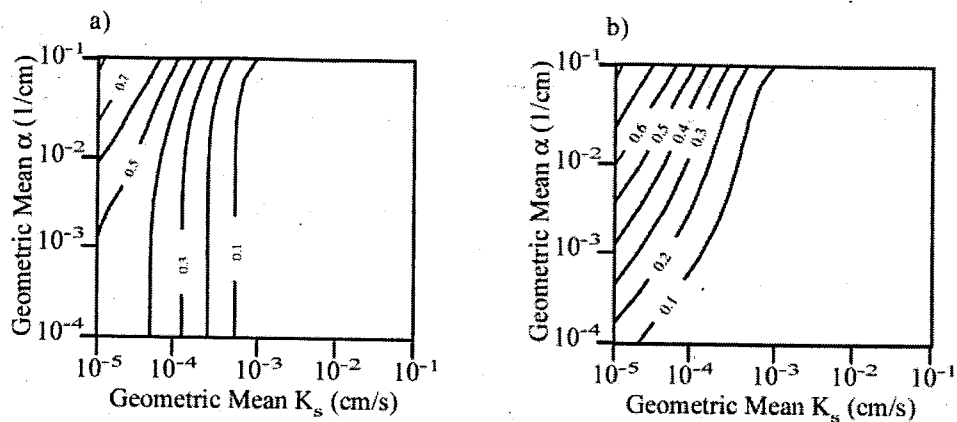
Figure 2-2. Fraction of points rejected as a function of parameter space with a) observation error and b) also with contact error.
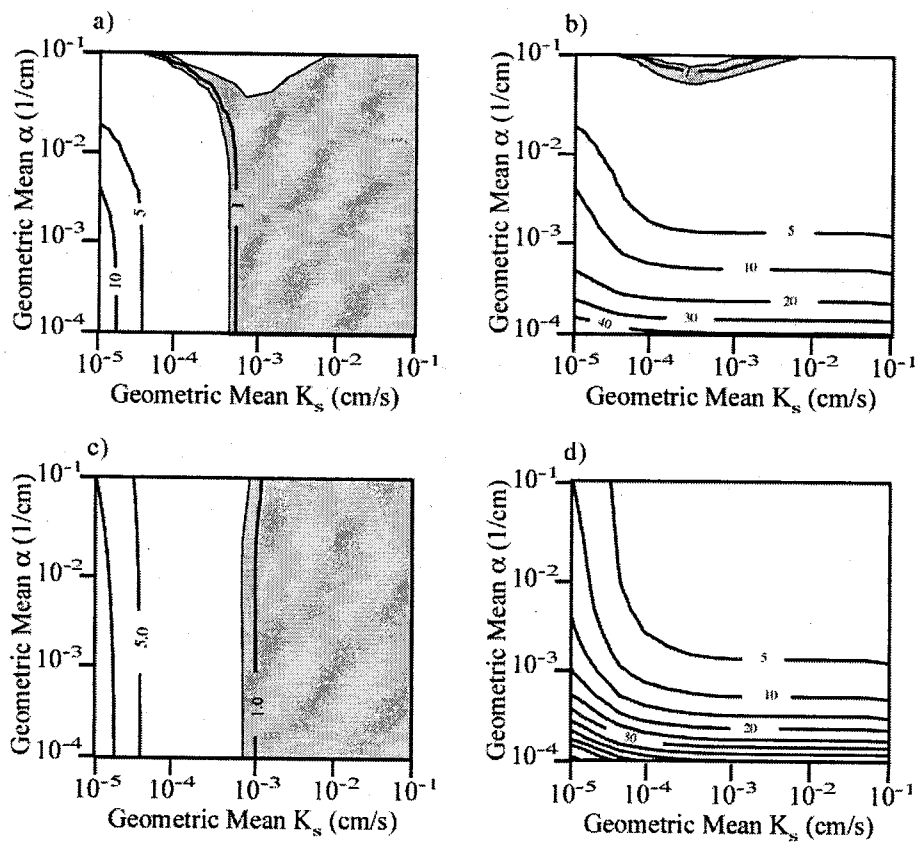
Figure 2-3. The ratio $\hat{\alpha}^G / \alpha^G$ with a) observation error and b) also with contact error. The $\hat{K}_s^G / K_s^G$ with c) observation error and d) also with contact error. The most accurate region, relative error between 0.95 and 1.05, is shaded.

29

portion of parameter space), the amount of bias in $\hat{\alpha}^G$ increases significantly to over five

times the true value. It is not surprising that bias would increase at small K_s^G, because

$\hat{Q}_1$ tends to be overestimated and $\hat{Q}_2$ tends to be underestimated as the FPD increases.

However, it seems contradictory that bias is less at high α^G, because the FPD increases

there. This occurs because bias in the log flux ratio, $\ln\left(\hat{Q}_1/\hat{Q}_2\right)$ from (2-10) differs from

bias in the flux rates themselves, $\hat{Q}_1$ and $\hat{Q}_2$. At a small α^G, flux-rate errors are

relatively small, but errors in the log ratio are very large. Therefore, relatively small

errors in flux-rates cause large, positively biased errors in the flux ratio and $\hat{\alpha}$.

The bias in the geometric mean of the estimated K_s, or $\hat{K}_s^G$, is shown in Figure

2-3c and is similar to the bias in $\hat{\alpha}^G$, except that it is less sensitive to α^G. The parameter

$\hat{K}_s$ is a linear function of $\hat{Q}_1$ (2-11), and, as K_s^G decreases, $\hat{Q}_1$ is overestimated because

the FPD increases. Therefore, bias in $\hat{K}_s^G$ is nearly independent of α^G.

Figures 2-3b and 2-3d show that the bias in $\hat{\alpha}^G$ and $\hat{K}_s^G$ changes drastically when

contact error is added. $\hat{\alpha}^G$ is only accurately estimated in a narrow region at high α^G,

near the top of parameter space, while $\hat{K}_s^G$ is overestimated across the entire parameter

space. There is much less dependence on K_s^G, and the bias is much greater at low α^G.

The contact errors decrease $\hat{Q}_2$, leading to an increase in the flux ratio and overestimation

of $\hat{\alpha}$ and $\hat{K}_s$. For low α's the biased estimates, $\hat{\alpha}^G$ and $\hat{K}_s^G$, are both well over an order

of magnitude too high.

2.4.3 Bias in Estimated Variance

Bias in the variance of $\ln(\hat{\alpha})$ is depicted across parameter space in Figure 2-4a. The bias increases as α^G and K_s^G decreases (lower left corner of parameter space), except at very small K_s^G (far left portion of parameter space) where the bias decreases again. As α^G or K_s^G decreases, the variability of the log ratio in (2-10) increases, causing the variance of $\ln(\hat{\alpha})$ to increase. At very small K_s^G, however, $\hat{Q}_1$ and $\hat{Q}_2$ are dominated by errors and are independent of sampled α and K_s. The variability of the log ratio is reduced, and the variance of $\ln(\hat{\alpha})$ decreases.

Figure 2-4b illustrates bias in the variance of $\ln(\hat{\alpha})$ when contact errors are added. There is much less dependence on the K_s^G, and the variance of $\ln(\hat{\alpha})$ is underestimated at large K_s^G. In this case, $\hat{Q}_2$ tends to underestimate Q_2 because the disk area is reduced. The log ratio in (2-10) is consistently overestimated, and the amount of overestimation increases at low α^G where the true flux ratio is small. This effect is most pronounced for higher K_s^G, where $\hat{Q}_1$ and $\hat{Q}_2$ are strongly dependent upon the values of K_s and α. The variability of the log ratio and the variance of $\ln(\hat{\alpha})$ decreases. Contact effects decrease as K_s^G decreases, because both $\hat{Q}_1$ and $\hat{Q}_2$ become increasingly independent of α and K_s (i.e. independent of Q_1 and Q_2).

Figure 2-4c shows bias in the variance of $\ln(\hat{K}_s)$. Bias increases at high α^G and small K_s^G. Recalling that $\hat{K}_s$ is a function of both $\hat{\alpha}$ and $\hat{Q}_1$, this relationship appears counter-

31
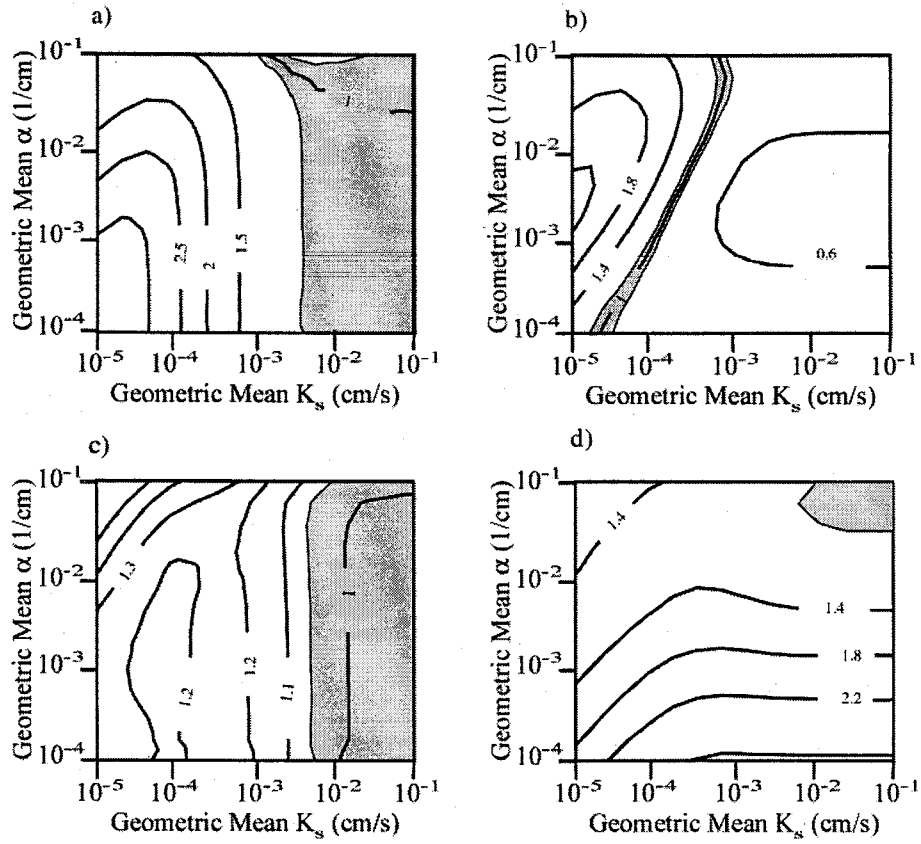
Figure 2-4. The variance of $\hat{\alpha}$ shown as a ratio $(\sigma^2_{\ln(\hat{\alpha})} / \sigma^2_{\ln(\alpha)})$ with a) observation error only and b) also with contact error. The variance of $\hat{K}_s$ shown as a ratio $(\sigma^2_{\ln(\hat{K}_s)} / \sigma^2_{\ln(K_s)})$ with c) observation error and d) also with contact error. The most accurate region, relative error between 0.95 and 1.05, is shaded.

intuitive, because the variance of $\ln(\hat{\alpha})$ decreases as α increases and the variability of $\hat{Q}_1$ decreases at high α^G and low K_s^G. Compensating effects, however, cause the observed behavior. Consider the covariance between $\hat{Q}_1$ and $\hat{\alpha}$ in

$$\text{var}\left[\ln(\hat{K}_s)\right] \propto \text{var}\left[\ln(\hat{\alpha})\right] + \text{var}\left[\ln(\hat{Q}_1)\right] + 2\,\text{cov}\left[\ln(\hat{\alpha}), \ln(\hat{Q}_1)\right] \qquad (2\text{-}15)$$

In general, estimated $\ln\left(\hat{Q}_1\right)$ and $\ln(\hat{\alpha})$ exhibit a large negative covariance, except for that portion of our parameter space where the fluxes become independent of α and K_s. Independence occurs at high α^G or small K_s^G, where more points are discarded (Figure 2-2). Here the negative covariance between $\ln(\hat{\alpha})$ and $\ln(\hat{Q}_1)$ approaches zero faster than the positive variances of $\ln(\hat{\alpha})$ and $\ln(\hat{Q}_1)$ decrease. Therefore, the variance of $\ln(\hat{K}_s)$ increases for high α^G or small K_s^G.

The bias in the variance of $\ln(\hat{K}_s)$ changes significantly when contact errors are present (Figure 2-4d), as overestimation increases. At high K_s^G, the bias is nearly independent of K_s^G and increases dramatically as α^G decreases. When contact errors are present, $\hat{\alpha}$ tends to be overestimated leading to overestimation of $\hat{K}_s$ (Figures 2-3c and 2-3d). This effect is most pronounced in parameter space where the flux rates are strongly dependent on α and K_s, that is in the lower right corner of the parameter space where K_s^G is large and α^G is small. In this region, $\hat{\alpha}$ depends primarily on the errors in the estimate of $\hat{Q}_2$, and the correlation between $\hat{Q}_1$ and $\hat{\alpha}$ decreases. Consequently, the variance of $\ln(\hat{K}_s)$ tends to increase (2-15).

33

2.4.4 Bias in Variograms

Bias in the variogram model variance and correlation length for $\ln(\hat{\alpha})$ are shown in Figures 2-5a and 2-5b, respectively. The model variance is mostly overestimated, while the correlation length is underestimated. The pattern of error in the model variance is similar to the pattern of error in the variance of $\ln(\hat{\alpha})$ (Figure 2-4a), except in the upper left corner of parameter space (high α^G and small K_s^G) where the model variance approaches zero. Correlation lengths are accurately estimated, with bias values near one, across most of the parameter space. As with the model variance, correlation lengths become inaccurate in the upper left corner of parameter space (Figure 2-5b), with a bias ratio approaching zero. Correlation lengths and model variances approach zero as estimates of the flux rates become dominated by errors, rather than the true values of α and K_s. At low α^G and small K_s^G, flux-rate errors greatly increase the variance of $\ln(\hat{\alpha})$ (Figure 2-4a), but do not disrupt estimation of spatial correlation, because bias in the flux-rates accentuates spatial differences of $\ln(\hat{\alpha})$.

Figures 2-5c and 2-5d display the bias in the model variance and correlation length for $\ln(\hat{\alpha})$ when contact errors are added. Both are underestimated. The underestimation is significant at high α^G and small K_s^G and across a broad region characterized by low α^G. In the upper left corner of parameter space where α^G is high and K_s^G is small, as with the case with no contact error (Figures 2-5a and 2-5b), flux rates are dominated by errors, and $\ln(\hat{\alpha})$ loses spatial correlation. However, along the bottom of the figure, with low α^G, estimates of $\hat{Q}_2$ are too small leading to consistent

34
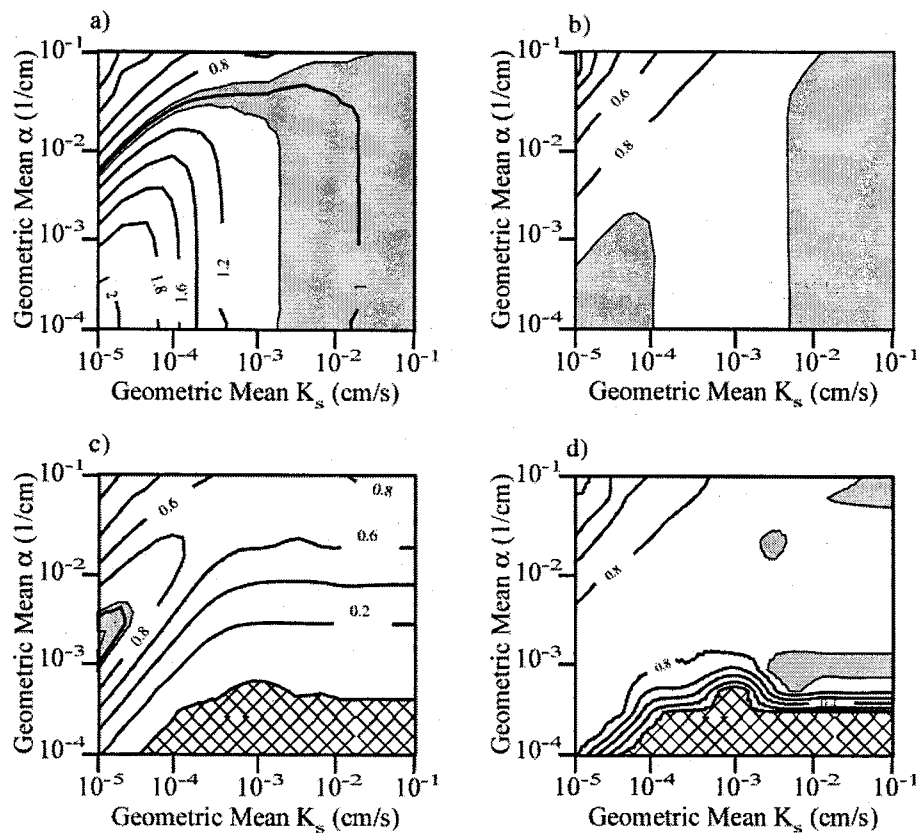
Figure 2-5. Variogram model parameters for ln($\hat{\alpha}$), shown as a ratio of "estimated"/"true": a) model variance with measurement errors only, b) correlation length with measurement error only, c) model variance with contact error, and d) correlation length with contact error. The most accurate region, ratio value between 0.95 and 1.05, is shaded. Regions equal to zero are patterned indicating nugget variograms.

overestimation of $\ln(\hat{\alpha})$ and a reduction of spatial correlation. The spatial statistics are those of a nugget.

Figures 2-6a and 2-6b present the bias in the model variance and correlation length for $\ln(\hat{K}_s)$. Model variances and correlation lengths are accurately estimated across most of the parameter space, but greatly underestimated at small K_s^G, especially in combination with a low α^G. The variogram of $\ln(\hat{K}_s)$ is proportional to

$\gamma_{\ln(\hat{\alpha})} + \gamma_{\ln(\hat{Q}_1)} + 2\gamma_{\ln(\hat{\alpha}),\ln(\hat{Q}_1)}$, where $\gamma_{\ln(\hat{\alpha})}$ is the variogram of $\ln(\hat{\alpha})$, $\gamma_{\ln(\hat{Q}_1)}$ is the variogram of $\ln(\hat{Q}_1)$, and $\gamma_{\ln(\hat{\alpha}),\ln(\hat{Q}_1)}$ is the cross-variogram between $\ln(\hat{\alpha})$ and $\ln(\hat{Q}_1)$. This relationship is primarily responsible for the patterns displayed by errors in the model variance and correlation length. Of particular importance is $\gamma_{\ln(\hat{\alpha}),\ln(\hat{Q}_1)}$, which tends to reduce the variogram of $\ln(\hat{K}_s)$ because $\ln(\hat{\alpha})$ and $\ln(\hat{Q}_1)$ are negatively correlated. At high α^G and small K_s^G (upper left corner), flux rates are dominated by errors, and $\gamma_{\ln(\hat{\alpha})}$, $\gamma_{\ln(\hat{Q}_1)}$, and $\gamma_{\ln(\hat{\alpha}),\ln(\hat{Q}_1)}$ have little correlated spatial structure. Consequently, the model variance and correlation length of $\ln(\hat{K}_s)$ are reduced in this region. At low α^G, however, spatial structure is preserved in $\gamma_{\ln(\hat{\alpha})}$, $\gamma_{\ln(\hat{Q}_1)}$, and $\gamma_{\ln(\hat{\alpha}),\ln(\hat{Q}_1)}$, but the negative correlation between $\ln(\hat{\alpha})$ and $\ln(\hat{Q}_1)$ is strong, and little spatial structure is preserved in the variogram of $\ln(\hat{K}_s)$. At low α^G and small K_s^G (lower left corner), $\ln(\hat{\alpha})$ is dominated by errors in $\hat{Q}_1$, as $\hat{Q}_1$ tends to have more error than $\hat{Q}_2$, and the magnitude of the cross-covariance between $\ln(\hat{\alpha})$ and $\ln(\hat{Q}_1)$ increases.

36
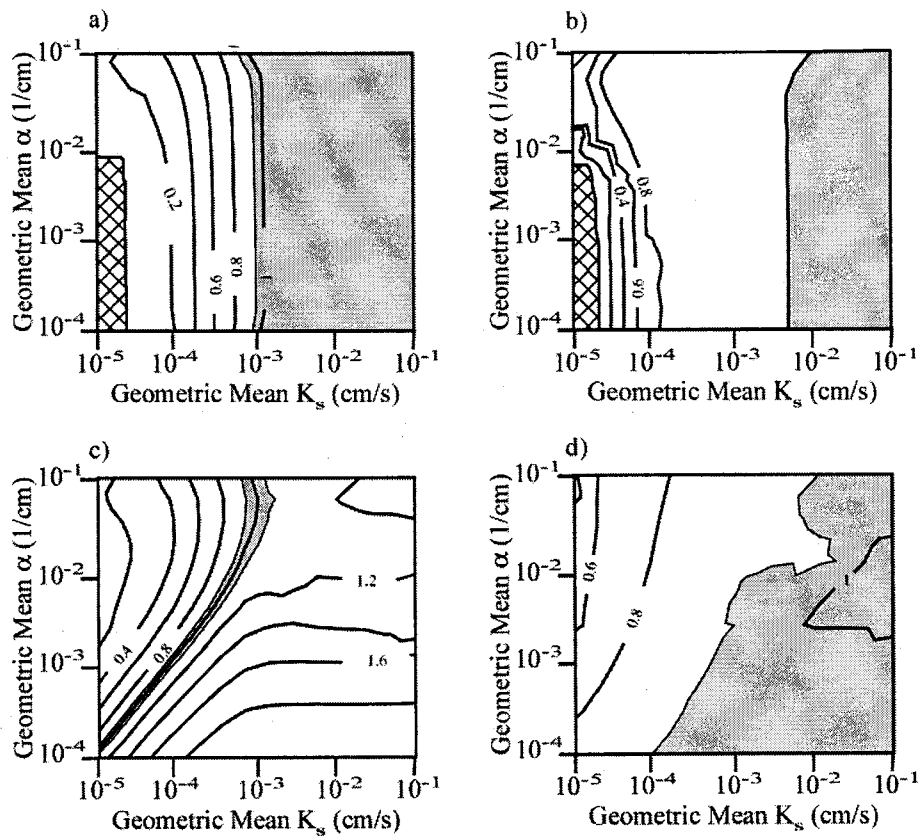
Figure 2-6. Variogram model parameters for $\ln(\hat{K}_s)$, shown as a ratio of "estimated"/"true": a) model variance with measurement errors only, b) correlation length with measurement error only, c) model variance with contact error, and d) correlation length with contact error. The most accurate region, ratio value between 0.95 and 1.05, is shaded. Regions equal to zero are patterned.

When contact error is added, patterns of bias in the model variance and correlation length of $\ln(\hat{K}_s)$ change (Figures 2-6c and 2-6d). Similar to errors in the variance of $\ln(\hat{K}_s)$ (Figure 2-4d), model variance bias increases significantly at low α^G. Errors in the cross-variogram between $\ln(\hat{\alpha})$ and $\ln(\hat{Q}_1)$ still strongly control the variogram of $\ln(\hat{K}_s)$. At low α^G, $\ln(\hat{\alpha})$ is controlled by errors in $\hat{Q}_2$, and $\gamma_{\ln(\hat{\alpha}),\ln(\hat{Q}_1)}$ is small. As a result, the estimated correlation length of $\ln(\hat{K}_s)$ is fairly accurate (Figure 2-6d), but the model variance is greatly overestimated (Figure 2-6c). As with the case with no contact error, model variances and correlation lengths approach zero at high α^G and small K_s^G (upper left corner), because flux rate estimates are dominated by errors.

2.4.5   Cross-Correlation

Although true properties $\ln(\alpha)$ and $\ln(K_s)$ are statistically independent, we observe significant cross-correlation between estimated properties $\ln(\hat{\alpha})$ and $\ln(\hat{K}_s)$ (Figure 2-7). False cross-correlation between $\ln(\hat{\alpha})$ and $\ln(\hat{K}_s)$ results because both $\hat{\alpha}$ and $\hat{K}_s$ depend on $\hat{Q}_1$ (2-10 and 2-11), and $\hat{K}_s$ depends on and increases with $\hat{\alpha}$ (2-11), yielding positive point correlation functions. When only measurement errors are present, the correlation coefficient for $\ln(\hat{\alpha})$ and $\ln(\hat{K}_s)$ appears to increase as K_s^G decreases, reflecting increasing errors in the flux rates. When contact errors are also present, the pattern of the correlation coefficient changes, and strong cross-correlation is observed at both large K_s^G and low α^G (lower right corner), and small K_s^G and high α^G
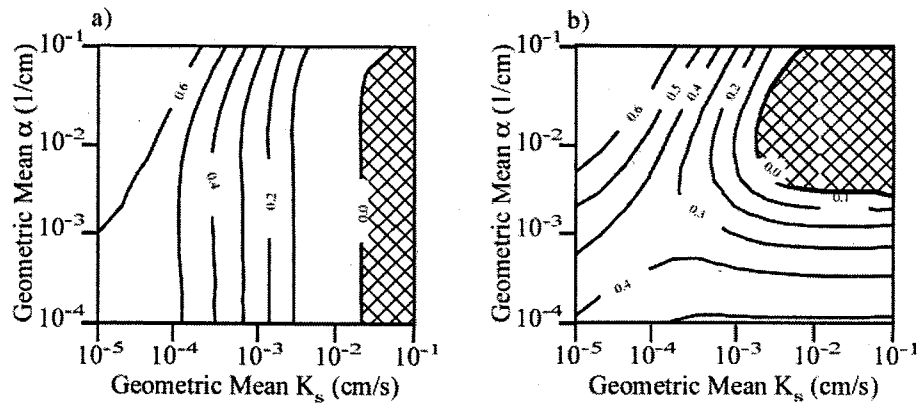
Figure 2-7. Correlation coefficients for $\ln(\hat{\alpha})$ and $\ln(\hat{K}_s)$ as a function of parameter space: a) with measurement error only and b) also with contact error. Regions equal to zero are patterned.

(upper left corner of parameter space). This occurs because $\hat{\alpha}$ tends to be overestimated in this region of parameter space (Figure 2-3b).

With the tension infiltrometer we use one parameter ($\hat{\alpha}$) to estimate another ($\hat{K}_s$). Errors in the first parameter generate errors in the second, resulting in apparent cross-correlation. Similar cross-correlation can occur if a single data set is used to estimate multiple parameters, because errors in the data set will propagate through multiple inversions. Cross-correlation due to measurement error may enhance or obscure the true cross-correlation between hydraulic parameters.

2.5 DISCUSSION

In this paper, we focus on revealing some of the impacts of tension infiltrometer measurement error on estimated spatial statistics. In the following discussion, we argue that our results are over optimistic for many applied field situations. We first show that observation errors are likely to be much greater than those used in this study. We have also neglected a large number of inversion-model errors that can cause spatial bias. We then discuss the implications this work for tension infiltrometer field studies. Finally, we illuminate the general problem of bias in hydrologic property measurements.

2.5.1 Range of Observation Errors

In most field studies, observation errors are likely to be greater than those used for this study. The flux-rate errors used here were based on instrument observations reported by Ankeny et al. (1988). Because their observations were made under highly controlled laboratory conditions (Ankeny, pers. com., 1998), we conducted a series of laboratory repeatability studies to directly evaluate the flux-rate variance, σ_q^2, during realistic tension infiltrometer operation. A large sandbox was constructed and filled with well-sorted, fine sand. The tension infiltrometer (manufactured by Soil Measurement Systems of Tucson, Arizona) was calibrated using standard methods (e.g., Soil Measurement Systems, 1992), and applied following normal procedures. After each test, the sand was returned to a constant initial condition by applying a vacuum to a pressure plate at the base of the box. For these tests, σ_q^2 was determined to be 0.06 cm^6/s^2. This value may

be a more representative more representative of field studies than the flux-error variance used here ($\sigma_q^2 = 0.00165 \text{ cm}^6/\text{s}^2$).

Errors in applied tension at the disk source may also be much larger than considered here. Many tension infiltrometers do not have a pressure transducer located at the disk source. Instead the applied tension at the disk is traditionally calibrated at a given bubble rate (e.g., Soil Measurement Systems, 1992). A constant bubble rate is achieved by establishing a vacuum on the Mariotte bottle, and a manometer is connected to the source tube for the disk. The depth of the air entry tubes is adjusted until the desired tension in the source tube is reached. This approach, however, is subject to a variety of errors. Because temperature changes will affect the expansion of bubbles, effective steady-state tensions will systematically vary from the calibrated values. In addition, some tension infiltrometers have a separate disk, and errors will be introduced if the disk is not at the correct elevation relative to the Mariotte bottle.

2.5.2   Neglected Inversion-Model Errors

Infiltrometer operators generally try to minimize observation errors by calibrating some of the components of infiltrometer and changing the diameter of the Mariotte bottle (Ankeny et al., 1988). In principle, bias due to observation errors can be significantly reduced by virtually eliminating these errors, provided that the inversion model is not too non-linear. Changing the inversion model can also reduce bias due to inversion-model error. Because it is virtually impossible to completely and accurately incorporate all of the physics relevant to a hydraulic property measurements at every sampled location

(Beckie, 1996), it is unlikely an inversion model can be found that is completely free of error. As our results show, a simple inversion-model error, contact between the disk source and the sampled medium, can lead to large amounts of spatial bias. A variety of other types of inversion-model error could cause a different, yet still significant, bias in spatial statistics.

Consider the effects of viscosity errors due to temperature changes. Standard inversion models for the tension infiltrometer assume that the viscosity of the infiltrating water remains constant (e.g., Ankeny, 1991; Reynolds and Elrick; 1991). This is very unlikely, especially in the field where the temperature of water in the infiltrometer will almost certainly be different from the soil temperature. A temperature drop of 1° C will result in an increase in the viscosity of pure water of ~2% (Weast, 1972), resulting in a ~2% decrease in unsaturated hydraulic conductivity. This change could cause significant bias in properties estimated with the tension infiltrometer.

In a field situation, bias due to viscosity errors would be temporal. In the morning, the water temperature in the infiltrometer could be greater than that of the soil and soil water. Infiltrating water would cooler during the measurement of $\hat{Q}_2$ and warmer during the measurement of $\hat{Q}_1$. These differences would lead to a smaller FPD and an overestimation of the flux ratio, $\hat{\alpha}$, and $\hat{K}_s$. In the afternoon, the situation could be reversed. In this situation, the temporal bias due to viscosity errors would appear as noise that may cause underestimation of the model variance and the correlation length.

A variety of other inversion-model errors will also produce bias that affects spatial statistics. Other potential sources of bias include sub-sample-scale heterogeneity,

42

changes in the medium due to infiltration, soils with non-exponential hydraulic conductivity functions, and air entrapment. As with our contact error, many of these errors could cause significant bias in estimated spatial statistics, and their impact should be studied.

2.5.3 Implications for Tension Infiltrometer Studies

Our results indicate that tension infiltrometer observation and contact errors will lead to overestimation of both $\hat{\alpha}$ and $\hat{K}_s$. This is consistent with Ankeny et al. (1991), who observed that on average tension infiltrometer measurements of $\hat{K}_s$ overestimate laboratory measurements by a factor of 3. The mathematical character of tension infiltrometer inversion models leads to overestimation of $\hat{\alpha}$ and $\hat{K}_s$ in the presence of observation errors. Data with $\hat{Q}_1 \leq \hat{Q}_2$ are rejected because they yield an unreasonable result, that is negative values of $\hat{\alpha}$. A large FPD is therefore an indicator of potential bias in tension infiltrometer results.

It is important to recognize, however, that a small FPD does not necessarily imply a small spatial bias. Three possible explanations can account for a small FPD in field studies. Measurement errors could be very small, the mean value of the sampled K_s could be large and the mean α could be small, or inversion-model errors could reduce the FPD. Recall that our contact error reduces the FPD across parameter space, yet causes much more bias in spatial statistics than observation errors. Other inversion-model errors, including viscosity errors, could cause a similar effect.

43

Our results also indicate that measurement errors can introduce false cross-correlation between $\hat{\alpha}$ and $\hat{K}_s$. Because $\hat{K}_s$ is proportional to $\hat{\alpha}$, correlation coefficients will show a positive bias, and very large positive correlation coefficients are a possible indicator of error. Negative correlation coefficients, however, do not indicate the absence of measurement error bias.

The other spatial statistics (mean, variance, and variogram) offer few diagnostic indicators of measurement bias. In fact, spatial statistics can appear realistic, but still be strongly biased. Nugget variograms could indicate either strong bias or lack of spatial correlation. Similarly a nugget effect in the variogram, a positive difference between the variance and model variance, could indicate bias but may also indicate uncorrelated random errors, sub-sample scale heterogeneity, or non-ideal sample location (e.g., Journel and Huijbregts, 1978).

Unfortunately, we find no unique indicators of bias in tension infiltrometer data. Certain results (e.g., large FPD, large positive correlation coefficients, and nugget variograms) can strongly suggest the presence of bias, but indicators of little or no bias are not obvious from our results. Investigators should take care to minimize observation errors, thereby reducing observation error bias. In addition, workers should diligently attempt to identify, quantify, and treat, possibly with error analyses, inversion-model errors that are likely to affect their measurements. Finally, spatial statistics should be considered with skepticism unless they are validated through an error analysis or independent metric.

2.5.4 The Bias Problem

Bias in property measurements is a critical problem in groundwater hydrology that potentially affects many hydraulic property measurements. For most measurement systems in physics and engineering, calibration is used to quantify and remove measurement bias (e.g., Mandel, 1964; Doebelin, 1966). Although the individual components of many devices used for measuring hydraulic properties are calibrated (e.g., Ankeny, 1988), calibration of device components does not insure the elimination of measurement bias. Unbiased errors in the device response can still lead to bias in measurements that use a non-linear inversion model (e.g., Mandel, 1964). Calibration standards are available and incorporated into some field hydraulic property measurement procedures (e.g., Davis, et al., 1994). Using calibration standards, bias can be effectively quantified and eliminated from measured hydraulic properties only when the physical processes, including process time and length scales, in the standard and the sample are similar.

For many field methods used to estimate porous media hydraulic properties, like the tension infiltrometer, whole instrument field calibration standards are not feasible or practical, and the exact nature of the bias induced by property-measurement errors cannot be directly quantified or removed. For these methods, bias can only be quantified using indirect approaches such as a Monte Carlo error analysis. Given the wide range of types of error that may affect measurements of properties, however, it may be impossible to identify and model their effects for every property estimation technique.

2.6 SUMMARY AND CONCLUDING REMARKS

In this paper, we show that small observation and inversion-model errors bias unsaturated hydraulic properties estimated with the tension infiltrometer and that this bias can preclude accurate estimation of spatial statistics. For this analysis, we develop Monte Carlo models to evaluate the effects of small, simple observation and inversion-model errors on estimated spatial statistics for the saturated hydraulic conductivity, K_s, and the single parameter for an exponential relative permeability, α. Observation errors consist of simple errors in infiltrometer flux-rates and applied tension at the infiltrometer source. Only one type of inversion-model error is modeled, a simple contact error. We generate spatially correlated random fields of α and K_s, simulate tension infiltrometer measurements with errors, and estimate α and K_s from the resulting tension infiltrometer data. When tension infiltrometer errors are due to observations only, spatial statistics of estimated hydraulic properties are most biased when the field mean α is high or the mean K_s is low, because flux rates are dominated by errors. When simple contact errors are included, the nature of the bias changes dramatically, and spatial statistics are most biased at low mean α. False cross-correlation between estimated parameters occurs because estimates of K_s depend on estimates of α and because both parameters are estimated from the same data.

Our results have broad implications for all other types of instruments used for characterizing spatial variability. All hydraulic properties are experimentally estimated using an instrument that observes the response of the hydrologic system to a transient or steady perturbation. Observed system states (e.g., pressure and flux-rates) are used in a

46

mathematical inversion of the governing equations to infer the hydraulic property values. Observation and inversion-model errors lead to biased property estimates because most inversion models are non-linear. As a result, estimated hydraulic properties and their spatial statistics are biased. The extent of this bias depends on the non-linearity, the true values of the sampled hydraulic properties, and the nature of measurement and inversion-model errors present. Strong bias can produce or eliminate cross-correlation between parameters and preclude accurate estimation of the mean, variance, and variogram. The effects of observation and inversion-model error can be insidious, as hydraulic property estimates may appear reasonable and generate realistic-looking spatial statistics, which are, however, inaccurate and misleading. The geostatistical approaches used in spatial variability studies offer no formal approaches for detecting and treating measurement bias.

Robust field-estimation of hydraulic properties for spatial variability studies may not be possible with many current instruments and inversion models, because multiple parameters are estimated using a single, nonlinear model. In addition, bias in spatial statistics of estimated hydraulic properties is extremely sensitive to different inversion-model errors, and it is not possible to identify *a priori* all types of inversion-model error that may affect a particular property estimation method. Therefore, error analyses cannot be used to uniquely identify all material types or conditions under which a particular instrument or inversion model will perform best or to remove bias caused by measurement errors. For spatial variability studies, hydraulic properties are best estimated using direct measurements of the property or an essentially linear inversion

model. If non-linear inversion-models are required, only one parameter should be estimated from a single model and data set.

Despite the difficulty and added cost, laboratory-estimated hydraulic properties may be preferable to field-estimated properties, because some properties are directly measured, measurement errors are smaller, and inversion-model errors can, to some extent, be controlled. However, this suggestion must be tested by studies of bias in estimated spatial statistics of laboratory-estimated hydraulic properties. Finally, the impact of bias in spatial statistics on stochastic models of flow and transport remains to be assessed.

2.7 REFERENCES CITED

Ankeny, M. D., T. C. Kaspar, and R. Horton, 1988, Design for an automated tension infiltrometer, *Soil Science Society of America Journal*, v. 52, p. 893-896.

Ankeny, M. D., M. Ahmed, T. C. Kaspar, and R. Horton, 1991, Simple field method for determining unsaturated hydraulic conductivity, *Soil Science Society of America Journal*, v. 55, p. 467-470.

Beckie, R., 1996, Measurement scale, network sampling scale, and groundwater model parameters, *Water Resources Research*, v. 32, p. 65-76.

Bresler, E., 1978, Analysis of trickle irrigation systems with application to design problems, *Irrigation Science*, v. 1, p. 3-17.

Brooks, R. H., and A. T. Corey, 1964, Hydraulic properties of porous media, *Hydrol. Pap. 3,* Colorado State University, Fort Collins.

Clothier, B. E., D. Scotter, and E. Harper, 1985, Three-dimensional infiltration and trickle irrigation, *Transactions of the American Society of Agricultural Engineers*, v. 28, p. 497-501.

Davis, J.M., J.L. Wilson, and F.M. Phillips, 1994. A portable air-minipermeameter for in-situ field measurements, *Ground Water*, v. 32, p. 258-266

Deutsch, C. V., and A. G. Journel, 1992, GSLIB: *Geostatistical software library and user's guide*, 2nd ed., Oxford University Press, New York, NY, 369 pp.

Doebelin, E. O., 1966, *Measurement Systems: Application & Design*, McGraw Hill, NY, NY, 1966, 743 pp.

DOE, 1993, *Hydrogeologic data for existing excavations at the Area 5 Radioactive Waste Management site, Nevada Test Site, Nye County, Nevada*, DOE/NV/11432-40, U. S. Department of Energy Nevada Operations Office, Las Vegas, NV.

Freeze, R. A., and J. A. Cherry, 1979, *Groundwater*, Prentice Hall, Englewood Cliffs, N.J., 604 pp.

Harter, T., and T. –C. Jim Yeh, 1996, Stochastic analysis of solute transport in heterogeneous, variably saturated soils, *Water Resources Research*, v. 32, p. 1585-1595.

Hussen A. A., and A. W. Warrick, 1993, Alternative analyses of hydraulic data from disc tension infiltrometers, *Water Resources Research*, v. 29, p. 4103-4108.

Indelman, P., D. Or, and Y. Rubin, 1993, Stochastic analysis of unsatured steady state flow through bounded heterogeneous formations, *Water Resources Research*, v. 29, p. 1141-1148.

Istok, J. D., D. O. Blout, L. Barker, K. R. Johnejack, and D. P. Hammermeister, 1994, Spatial variability in alluvium properties at a low-level nuclear waste site, *Soil Science Society of America Journal*, v. 58, p. 1040-1051.

Jarvis, N. J., and I. Messing, 1995, Near-saturated hydraulic conductivity in soils of contrasting texture measured by tension infiltrometers, *Soil Science Society of America Journal*, v. 59, p. 27-34.

Journel, A. G., and Ch. J. Huijbregts, 1978, *Mining Geostatistics*, Academic Press, Inc., New York, N.Y., 600 pp.

Kempthorne, O. and R. R. Allmaras, 1986, Errors and variability of observations, in A. Klute, Ed., *Methods of Soil Analysis, Part 1, Physical and Mineralogical*

Methods, 2nd ed., American Society of Agronomy and Soil Science Society of America, Madison, WI, p. 1-31.

Mandel, J., 1964, *The Statistical Analysis of Experimental Data*, Dover Publications, New York, NY, pp. 410.

Mantoglou, A. and L. W. Gelhar, 1987a, Capillary tension head variance, mean soil moisture content, and effective specific soil moisture capacity of transient unsaturated flow in stratified soils, *Water Resources Research*, v. 23, p. 47-56.

Mantoglou, A. and L. W. Gelhar, 1987b, Effective hydraulic conductivities of transient unsaturated flow in stratified soils, *Water Resources Research*, v. 23, p. 57-67.

Mohanty, B. P., M. D. Ankeny, R. Horton, and R. S. Kanwar, 1994, Spatial analysis of hydraulic conductivity measured using disc infiltrometers, *Water Resources Research*, v. 30, p. 2489-2498.

Parlange, J. –Y., and W. L. Hogarth, 1985, Steady state infiltration: Consequences of α dependent on moisture content, *Water Resources Research*, v. 21, p. 1283-1284.

Philip, J. R., 1969, Theory of infiltration, *Advances in Hydroscience*, v. 5, p. 215-296.

Polmann, D. J., D. McLaughlin, S. Luis, L. W. Gelhar, and R. Ababou, 1991, Stochastic modeling of large-scale flow in heterogeneous unsaturated soils, *Water Resources Research*, v. 27, p. 1447-1458.

Reynolds, W. D., and D. W. Elrick, 1991, Determination of hydraulic conductivity using a tension infiltrometer, *Soil Science Society of America Journal*, v. 55, p. 633-639.

Reynolds, W. D., and D. W. Elrick, 1987, A laboratory and numerical assessment of the Guelph permeameter method, *Soil Science*, v. 144, p. 282-299.

Reynolds, W. D., and D. W. Elrick, 1987, In situ measurement of field saturated

hydraulic conductivity, sorptivity, and the α-parameter using the Guelph

permeameter, *Soil Science*, v. 140, p. 292-302.

Robin, M. J. L., A. L. Gutjahr, E. A. Sudicky, and J. L. Wilson, 1993, Cross-correlated

random field generation with the direct Fourier transform method, *Water*

Resources Research, v. 29, p. 2385-2397.

Russo, D., 1984, Design of an optimal sampling network for estimating the variogram,

Soil Science Society of America Journal, v. 48, p. 708-716.

Russo, D., 1995, Stochastic analysis of the velocity covariance and the displacement

covariance tensors in partially saturated heterogeneous anisotropic porous

formations, *Water Resources Research*, v. 31, p. 1647-1658.

Russo, D., and W. A. Jury, 1987a, A theoretical study of the estimation of the correlation

scale in spatially variable fields: 1. Stationary fields, *Water Resources Research*,

v. 23, p. 1259-1269.

Russo, D., and W. A. Jury, 1987b, A theoretical study of the estimation of the correlation

scale in spatially variable fields: 1. Nonstationary fields, *Water Resources*

Research, v. 23, p. 1269-1279.

Russo, D., and M. Bouton, 1992, Statistical analysis of spatial variability in unsaturated

flow parameters, *Water Resources Research*, v. 28, p. 1911-1925.

Russo, D., I. Russo, and A. Laufer, 1997, On the spatial variability of parameters of the

unsaturated hydraulic conductivity, *Water Resources Research*, v. 33, p. 947-956.

Shouse, P. J., and B. P. Mohanty, 1998, Scaling of near-saturated hydraulic conductivity measured using disc infiltrometers, *Water Resources Research*, v. 23, p. 1195-1205.

Simunek, J, O. Wendroth, M. T. van Genuchten, 1999, Estimating unsaturated soil hydraulic properties from laboratory tension disc infiltrometer experiments, *Water Resources Research*, v. 35, p. 2965-2979.

Simunek, J, and M. T. van Genuchten, 1996, Estimating unsaturated soil hydraulic properties from tension disc infiltrometer data by numerical inversion, *Water Resources Research*, v. 32, p. 2683-2696.

Soil Measurement Systems, 1992, *Tension Infiltrometer Users Manual*, Soil Measurement Systems, Tucson, AZ.

van Genuchten, M. Th., 1980, A closed–form equation for predicting the hydraulic conductivity of unsaturated soils, *Soil Science Society of America Journal*, v. 44, p. 892-898.

Warrick, A. W., and D. E. Myers, 1987, Optimization of sampling locations for variogram calculations, *Water Resources Research*, v. 23, p. 496-500.

Weast, R. C., ed, 1972, *Handbook of Chemistry and Physics*, 53rd ed., CRC Press, Cleveland, OH, p. F-36.

White, I., and M. J. Sully, 1992, On the variability and use of the hydraulic conductivity alpha parameter in stochastic treatments of unsaturated flow, *Water Resources Research*, v. 28, p. 209-213.

Wooding, R. A., 1968, Steady infiltration from a shallow circular pond, *Water Resources Research*, v. 4, p. 1259-1273.

Wu, L., L. Pan, M. J. Roberson, and P. J. Shouse, 1997, Numerical evaluation of ring-infiltrometers under various soil conditions, *Soil Science*, v. 162, p. 771-777.

Yeh, T. –C. Jim, L. W. Gelhar, and A. L. Gutjahr, 1985a, Stochastic analysis of unsaturated flow in heterogeneous soils: 1. Statistically isotropic media, *Water Resources Research*, v. 21, p. 447-456.

Yeh, T. –C. Jim, L. W. Gelhar, and A. L. Gutjahr, 1985b, Stochastic analysis of unsaturated flow in heterogeneous soils: 2. Statistically isotropic media with variable α, *Water Resources Research*, v. 21, p. 457-464.

Yeh, T. –C. Jim, L. W. Gelhar, and A. L. Gutjahr, 1985c, Stochastic analysis of unsaturated flow in heterogeneous soils: 3. Observations and applications, *Water Resources Research*, v. 21, p. 465-471.

Zhang, D. Z., T. C. Wallstrom, and C. L. Winter, 1998, Stochastic analysis of steady-state unsaturated flow in heterogeneous media: Comparison of the Brooks-Corey and Gardner-Russo models, *Water Resources Research*, v. 34, p. 1437-1449.

CHAPTER 3 - SPATIAL BIAS IN LABORATORY-ESTIMATED UNSATURATED HYDRAULIC PROPERTIES

3.1 ABSTRACT

We use a Monte Carlo error analysis to evaluate spatial bias in the log transform of hydraulic conductivity (K_s) estimated with Darcy columns, porosity (ϕ) estimated using the saturated weight of samples, and van Genuchten (1980) parameters (α and n) estimated by fitting experimental moisture characteristic [$\theta(\psi)$] data. Estimates of $\ln(K_s)$ and $\ln(\phi)$ appear unbiased in space, because observation errors are small and their inversion models are simple. Moisture-characteristic curves are estimated in four different error scenarios across a parameter space characterized by a systematically varied geometric mean n. Measured moisture-characteristic curves are overestimated, and the average error increases with tension and geometric mean n (essentially the degree of sorting). The van Genuchten (1980) model is fit to the biased data. The spatial statistics of fitting parameters $\ln(\hat{\alpha})$ and $\ln(\hat{n})$ show modest bias that increases when equilibrium errors are considered and varies depending on the errors present and the geometric mean n. A surrogate metric for pore-water velocity shows significant errors. Under one error-scenario, variogram-model parameters for $\ln(n)$ cannot be reliably estimated from a limited number of samples. Spatial bias due to measurement error greatly increases the uncertainty due to limited sampling.

3.2 INTRODUCTION

It has long been recognized that field scale unsaturated hydraulic properties vary in space (e.g., Russo and Bresler, 1981; Wierenga et al, 1991; Shouse and Mohanty, 1998), and the impact of this heterogeneity on prediction of flow and transport has been the focus of substantial research. Theoretical and numerical stochastic models of ensemble flow and transport behavior in the unsaturated zone (e.g., Yeh et al., 1985a, b, c; Mantoglou and Gelhar, 1987a, b; Hopmans et al., 1988; Polmann, et al., 1991; Indelman, et al., 1993; Russo, 1995; Harter and Yeh, 1996; Zhang et al., 1998) require knowledge of the spatial statistics (mean, variance, and correlation length) of unsaturated hydraulic properties. We have previously shown (Chapter 2) that measurement errors bias properties estimated with the tension infiltrometer, a common field instrument employed in spatial variability studies. Biased estimates of properties result when small observation errors are propagated through a non-linear inversion model and from errors in the inversion model itself. For the tension infiltrometer, bias in property estimates precludes robust estimation of spatial statistics (Chapter 2).

Laboratory methods have also been used to estimate properties for unsaturated zone spatial variability studies (e.g., Wierenga et al, 1991, Healy and Mills, 1991; Istok, et al, 1994; Mallants et al., 1996; Shouse, et al, 1995; Bosch, and West, 1998). In the absence of sampling difficulties (e.g., alteration of properties during sampling), laboratory-estimated properties are, in principle, subject to smaller observation and fewer inversion-model errors than field measurements. In addition, many errors, particularly observation errors, are more readily quantified and controlled in a laboratory setting. If

sampling issues are resolved, laboratory measurements may be the only viable way of estimating spatial statistics of unsaturated hydraulic properties. Our objectives are to evaluate the extent of measurement error bias in spatial statistics of laboratory-estimated properties and to answer the question, "for which unsaturated zone properties can laboratory methods be used to accurately estimate spatial statistics?"

We use a Monte Carlo approach to propagate simple observation and inversion-model errors through numerically simulated laboratory measurements of properties. In particular, we consider estimates of saturated hydraulic conductivity, porosity, and parameters that describe the moisture-retention curve. We neglect sampling issues and assume that sample properties are not significantly altered from their *in situ* condition. We generate and numerically sample a series of artificial realities with known spatial statistics and estimate the properties using standard laboratory techniques subject to known errors. We use our property estimates to determine bias in the spatial statistics of laboratory-estimated unsaturated hydraulic properties.

3.3 METHODS

We investigate the impact of laboratory measurement errors on estimated spatial statistics by simulating laboratory analysis of samples in a series of different of artificial realities. We assume that the tension-saturation curve, $S(\psi)$, is a monotonic function described by the van Genuchten (1980) parametric model

$$S(\psi) = \frac{1}{\left[1 + (-\alpha\psi)^n\right]^{1-\frac{1}{n}}} \qquad (3-1)$$

where ψ is the matric potential, n is a parameter related to standard deviation of the effective pore radii, and α is a parameter that is related to an air entry pressure. The moisture-characteristic curve, $\theta(\psi)$, is described by

$$\theta(\psi) = (\phi - \theta_r)S(\psi) + \theta_r \qquad (3-2)$$

where ϕ is the porosity, and θ_r is the residual moisture content, here assumed to be zero. We assume that the relative permeability, $k_r(\psi)$, is completely described using Mualem's (1976) relationship, which for the van Genuchten model (1980) is

$$k_r(\psi) = S(\psi)^\beta \left\{ 1 - \left[1 - S(\psi)^{\frac{n}{n-1}} \right]^{1-\frac{1}{n}} \right\}^2 \qquad (3-3)$$

where β is a parameter that accounts for tortuosity and the correlation between adjacent pores. The unsaturated hydraulic conductivity, $K(\psi)$, is given by

$$K(\psi) = K_s k_r(\psi) \qquad (3-4)$$

where K_S is the saturated hydraulic conductivity.

We generate four independent random fields with known statistics for K_s, ϕ, α, and β. Each of the four random fields span properties representative of clastic materials consisting of poorly- to well consolidated, argillaceous to sandy deposits. We combine the K_s, ϕ, α, and β fields with seven different random fields of n, each with a different geometric mean representing materials with different pore-size distributions, and estimate K_s, ϕ, α, and n using simulated laboratory methods subject to simple observation and inversion-model errors.

Standard laboratory methods (e.g., Hillel, 1980; Klute, 1986; Hendrickx, 1990; Stephens, 1995) are numerically simulated to estimate properties. Porosity is estimated from the saturated and dry weight of the sample. Moisture-characteristic curves are measured directly using hanging columns and pressure chambers. The saturated hydraulic conductivity (K_s) is estimated using a Darcy column. We consider four different scenarios with progressively larger and more realistic errors.

3.3.1 Error Scenarios

We begin with a very idealistic scenario, where only observation errors are present and measurements reflect true equilibrium conditions. Observation errors are limited to mean-zero, white-noise errors associated with estimates of volume, length, weight, pressure, and time. Porosity, ϕ, and saturated hydraulic conductivity, K_S are estimated. Moisture-characteristic [$\theta(\psi)$] curves are measured and fit with van Genuchten's (1980) parametric model to estimate α and n.

Our second scenario is more realistic, because we consider both equilibrium and observation errors in estimates of the moisture characteristic curve. When estimating $\theta(\psi)$ curves, equilibrium is assumed when the sample weight changes less than a specified amount over a fixed period of time (e.g., less than 0.01 gm in 24 hours). Depending on the sample properties and history, the moisture content at this "apparent" equilibrium may be very different from the true equilibrium moisture content. We account for equilibrium errors by generating moisture-characteristic data with a transient, 1D, finite-difference model. Observation errors are added to the results, and moisture-

59

characteristic data are fit with the van Genuchten (1980) parametric model to generate a second estimate of α and n.

In the boundary error scenario, moisture characteristic data are affected by heterogeneity in α at the base of the sample, to account for disturbance and errors in the sample apparatus, and by errors in observations and equilibrium time. The boundary error diminishes the connection of the sample with the porous plates in hanging columns and pressure pots at higher tensions and can substantially lengthen equilibrium times, resulting in non-equilibrium observations of moisture content. Moisture-characteristic curves with these boundary errors are used to generate a third set of van Genuchten parameters, α and n.

In our final scenario, we examine moisture-characteristic curves generated from repacked or disturbed samples, while also including observation, equilibrium, and boundary errors. We develop simple models for modifying α and n based upon the Haverkamp and Parlange (1986) empirical mapping of cumulative grain-size distributions to pressure-saturation curves using bulk density data. We assume that the sample is repacked to its original bulk density, but the sample properties are altered because the bulk density of the repacked sample is erroneous. These curves provide a fourth set of estimated α and n.

For each reality, the mean, variance, and variogram for each estimated property is then determined, and variograms are fit with the exponential model (eliminating error in the choice of variogram model), yielding estimates of correlation length, variance, and nugget variance. Relative errors in the statistics and variogram-model (VM) parameters

60

are calculated by comparing "estimated" versus "true" values. Bias affecting the spatial statistics is revealed by the relative error. Details are discussed below.

3.3.2 Random Fields

In this study the parameters K_s, ϕ, α, n, and β are considered spatially correlated random fields, where the first four parameters are log-normally distributed and β is normally distributed. Although all five parameters can be related conceptually to the pore-size distribution, the exact nature of the cross-correlation between parameters is unknown, and we assume no specific cross-correlation between the parameters for this study.

The zero-mean random fields of all five properties are generated using an the FFT method (e.g., Robin et al., 1993) with an isotropic, exponential variogram model

$$\gamma^e(\mathbf{h}) = \sigma^2 \left[1 - \exp\left(-\frac{3\mathbf{h}}{\lambda_c} \right) \right] \tag{3-5}$$

where σ^2 is the variance of the random process, $\mathbf{h}$ is a separation vector, and λ_c is the correlation length. Final random fields are constructed by adding the mean to the zero-mean field. Each random field consists of 16,384 points located on a square lattice (128 by 128), spaced one unit apart. Required input spatial statistics for all parameters are summarized in Table 3-1. For convenience (e.g., Yeh et al., 1985a, b, c; Mantoglou and Gelhar, 1987a, b), the correlation lengths for all parameters are the same, 10.0 length units.

61

	$\ln(K_s)$ $\ln(cm/s)$	$\ln(\phi)$	$\ln(\alpha)$ $\ln(1/cm)$	$\ln(n)$	β
Mean	-9.2 (-9.1)	-1.4 (-1.33)	-4.6 (-4.5)	Variable	0.5 (0.48)
Variance	1.0 (0.90)	0.05 (0.047)	0.5 (0.37)	0.02 (0.018)	0.1 (0.094)
Correlation Length	10.0 (9.5)	10.0 (14.4)	10.0 (6.7)	10.0 (9.5)	10.0 (9.0)

Table 3-1. Input and calculated, in parentheses, spatial statistics for generated random fields.

We generate only one random field each for K_s, ϕ, α, and β. The ranges of K_s (5×10^{-6} to 3×10^{-3} cm/s), ϕ (0.13 to 0.50), and α (0.001 to 0.1 1/cm) are representative of mixed clastic materials containing poorly- to well-consolidated, argillaceous to sandy deposits. Because there is little information about the range of β in nature, we assume that its range is –0.7 to 1.7 with a mean of 0.5. The parameter n is inversely related to the width of the pore-size distribution and controls the slope of both the moisture characteristic and unsaturated hydraulic conductivity curves. A small n indicates a wide pore-size distribution and poor sorting of grain sizes (e.g., a paleosol deposit), while a large n signifies a narrow range of pore sizes and a high degree of sorting (e.g., an eolian sandstone). We generate seven different random fields for n, with the geometric mean n varying from 1.5 (e.g., argillaceous sand) to 7.0 (well-sorted sand). The four random

fields for other properties are combined with each random field of n to create seven different realities, which are then completely sampled for each of our scenarios, allowing us to assess bias in spatial statistics as a function of n and the type of error considered.

The random fields used in this study differ from those used in Chapter 2 because the domain size is much smaller, 128×128 versus 512×512. We elected to use a smaller domain because our error calculations are computationally expensive. Although our fields are not strictly ergodic, our results with a 128×128 field differ from those of a 512×512 field by only a few percent. As a result of the smaller domain, actual correlation lengths and model variances differ from theoretical values (Table 1), and minor amounts of cross correlation are observed between $\ln(\alpha)$ and $\ln(n)$, correlation coefficient of ~0.08. Because the objective of any spatial variability study is to characterize the local variogram rather than the theoretical variogram (Journel and Huijbregts, 1978), the smaller domain size is acceptable for this study

3.3.3   Observation Errors

Errors affecting laboratory hydraulic property estimates occur during the observation of weight, length, volume, time, and pressure. We assume that all observation errors are mean-zero, derived from a normal distribution, and have a constant variance. Our error estimates were obtained for typical instruments and methods used in our two laboratories (New Mexico Institute of Mining and Technology and Sandia National Laboratories) for these kinds of measurements. Observed weights for an object l are determined using

63

$$\hat{W}_l = W_l + \varepsilon_l \qquad\qquad (3\text{-}6)$$

where W_l is the true weight of the object l and ε_l is the error in the balance which is characterized by a variance of $\sigma_\varepsilon^2 = 1.4 \times 10^{-4} \, gm^2$. Similarly, an estimated length of an object l is calculated using

$$\hat{L}_l = L_l + \xi_l \qquad\qquad (3\text{-}7)$$

where L_l is the true length of the object l and ξ_l is the error in the observation which has a variance of $\sigma_\xi^2 = 2.5 \times 10^{-3} \, cm^2$.

For hanging column observations of the moisture-characteristic curve, we assume that pressure is estimated using the height of the Buchner funnel. We consider only white-noise errors in the estimate of the height, such that for an observation l the observed pressure is

$$\hat{\psi}_l = \psi_l + \xi_l \qquad\qquad (3\text{-}8)$$

where ψ_l is the true height and ξ_l is an error in length. When pressure chambers are used, pressures are determined by reading a pressure gauge. Based upon the reported precision of pressure gauges in our laboratories, the variance of pressure-gauge readings is estimated to be 111 cm^2.

We assume that all sample containers are cylinders. The estimated volume of a cylinder l is given by

$$\hat{V}_l = \hat{L}_h \left(\frac{\hat{L}_d}{2} \right)^2 \pi \qquad\qquad (3\text{-}9)$$

64

where $\hat{L}_h$ is the estimated height of the cylinder and $\hat{L}_d$ is the estimated diameter of the cylinder. Errors are common in the estimate of the original volume of a field sample. We assume that the volume of the field-sample container (V_s) is equal to 102 cm^3 and that the true sample volume is equal to

$$\hat{V}_s = V_s + v_s \qquad (3\text{-}10)$$

where v_s is the error in the estimate of the volume of sampled material. Because highly porous, granular materials are typically more friable and less cohesive than similar materials with low porosity and clay-rich materials are likely to be readily deformed, we assume that sample volume errors increase in materials with a high porosity. We use an arbitrary relationship to calculate the variance of v_s (σ_v^2)

$$\sigma_v^2(\phi) = \left(30\,\phi^2 + 1\right)^2 \qquad (3\text{-}11)$$

Using this relationship (3-11), the estimated volumes to 95% confidence are

$\hat{V}_s = V_s \pm 2.5\%$ at $\phi = 0.1$ and $\hat{V}_s = V_s \pm 16.7\%$ at $\phi = 0.5$.

Estimates of time are calculated using $\hat{t}_Q = t_Q + \tau_Q$, where t_Q is the true time and τ_Q is the error in a time observation, which has a variance of $\sigma_\tau^2 = 1.0\ s^2$.

3.3.4 Equilibrium Error

True equilibrium conditions are difficult to achieve in unsaturated materials. During measurements of moisture characteristic curves, equilibrium is often assumed when the sample weight changes less than a specified amount over a fixed period of time. With this procedure, "apparent" equilibrium is reached when the flux rate from the

sample falls below a critical value. Depending on the sample properties, the moisture content at an apparent equilibrium may be much larger or smaller than the "true" equilibrium moisture content, because the sample has not completely drained or wetted. Equilibrium errors are a type of inversion model error, because moisture characteristic data are fit with a parametric model that implicitly assumes equilibrium conditions.

We account for equilibrium errors by simulating the transient drainage of each sample using a block centered finite difference model of Richard's equation. The change in weight of our samples over 24 hours is monitored, and the "apparent" equilibrium moisture content is determined when the sample weight changes less than a 0.01 gm (the resolution of our scale) in a 24 hour period. Once apparent equilibrium is reached, the weight of the sample is determined and used to estimate moisture content. This is the standard procedure in our laboratories and many others. We begin with a fully saturated sample and measure a drainage curve by allowing the sample to reach an apparent equilibrium at a series of increasing tensions. For each measurement, the final moisture content profile at apparent equilibrium is used as the initial condition for the subsequent measurement.

3.3.5 Boundary Error

In our experience samples used for measuring moisture characteristic curves can be heterogeneous at their base. This heterogeneity results from disturbance of the lower part of the sample itself and apparatus used to contain the sample. At the top and bottom of the sample, grains may be plucked from the sample, and pores may dilate due to vibrations and other disturbances. Pores deep within the sample are less likely to be

disturbed, because the sample ring confines grains. We assume that the base of a sample is covered with a porous cloth to prevent the sample from falling out of the ring. The cloth can not completely conform to the individual grains present at the lower edge of the sample, and it may bridge irregularities on the sample surface. These small heterogeneities can drastically increase the sample equilibrium time. Larger pores at the base of the sample drain at lower tensions, decreasing the hydraulic conductivity of the lower part of the sample and increasing the time required to drain the portion of the sample above the heterogeneity. When boundary error is significant, equilibrium errors increase.

We are not interested in exploring this type of error in detail but only in its impact on estimated spatial statistics, and employ a simple model for altering the properties of the lower 1.0 mm of the sample. In the van Genuchten parametric model (3-1) effective pore radii are scaled by the parameter α. We allow the parameter α to be randomly increased by a scaling factor to simulate a dilation of pores in the lower 1mm of the sample and larger pores between the sample and the cloth. The scaling factor is drawn from a uniform distribution between of 1.0 to 2.0. The properties within the rest of the sample remain unchanged. The sample weight at apparent equilibrium is determined using the finite difference approach described above.

3.3.6 Repacking Errors

Field samples are often disturbed or repacked prior to laboratory analysis for $S(\psi)$. The repacking of samples, while convenient, may alter the sample hydraulic properties,

creating a form of inversion-model error. Repacking destroys the original sample pore-structure and it is not possible, due to observation errors, to repack a sample to its original bulk density. These dissimilarities between the original and repacked samples lead to errors in estimates of the field properties and their parameters. We develop simple models to describe how parameters α and n are altered when samples are repacked.

Models for modifying α and n are based upon the Haverkamp and Parlange (1986) empirical mapping of cumulative grain-size distributions to pressure-saturation curves using bulk density data. The derivation of these models is presented in Appendix A. We assume that the pore structure of intact samples is truly homogeneous and that all modifications to the parameters α and n occur because the repacked-sample bulk density is not equal to the intact-sample bulk density. Repacked samples do not retain the bulk density of the original sample. In a container of known volume, samples are typically repacked to a target weight. The target sample weight is

$$W_T = \hat{\rho}_b \hat{V}_r \qquad (3\text{-}12)$$

where $\hat{V}_r$ is the estimated volume of the sample ring determined using equation (3-9) and $\hat{\rho}_b$ is the estimated intact-sample bulk density given by

$$\hat{\rho}_b = \frac{\rho_b V_s + \varepsilon_1 - \varepsilon_2}{V_s + v_s} \qquad (3\text{-}13)$$

in which ε_1 is the error in the weight of the sample and its container, ε_2 is the error in the weight of the container, and ρ_b is the true intact-sample bulk density. The intact-sample bulk density is calculated from

$$\rho_b = \rho_d(1 - \phi) \qquad (3\text{-}14)$$

68

where ρ_d is the sample grain density and ϕ is the sample porosity. Prior to repacking the samples into a ring, the ring is weighed and the volume of the sample ring is estimated. The ring is filled until the estimated weight of the dry sample and the sample ring is equal to the target weight. The true dry weight of the sample is determined using

$$W_b = W_T - \varepsilon_3 + \varepsilon_4 \qquad (3\text{-}15)$$

where ε_3 is the error in the estimated weight of the ring and sample material and ε_4 is the error in the estimated weight of the ring. The true bulk density of the sample in the ring is calculated by

$$\rho_m = \frac{W_b}{V_r} \qquad (3\text{-}16)$$

where V_r is the true volume of the sample ring. The true bulk density of the sample in the ring (ρ_m) provides the basis for altering the parameters α and n due to repacking. For a known value of n, we calculate a modified n parameter (Appendix A)

$$n_m = \left(\frac{\rho_m}{\rho_b}\right)^{a_2} (n-1)+1 \qquad (3\text{-}17)$$

where a_2 is a constant equal to 3.8408. We calculate an α parameter that is modified due to repacking using

$$\alpha_m = \alpha \frac{b_1 + b_2(n-1) + b_3(n-1)^2}{b_1 + b_2(n_m-1) + b_3(n_m-1)^2} \qquad (3\text{-}18)$$

where $b_1 = 17.1736$, $b_2 = -4.7043$, and $b_3 = 0.4$. Note that b_3 differs from that of Haverkamp and Parlange (1986), because their value yields physically implausible results at high n.

We assume that the saturated hydraulic conductivity can be described by a bundle of capillary tubes model, with a series of effective hydraulic radii. In addition, we

assume that, at any matric potential, the effective hydraulic radius scales like the effective pore radius. We determine a scaling factor for the effective pore radius using

$$f = \frac{\alpha_m}{\alpha} \qquad (3\text{-}19)$$

The true saturated hydraulic conductivity of the repacked sample is determined using

$$K_m = f^2 K_s \qquad (3\text{-}20)$$

We also develop a simple model for altering β in (3-3) due to repacking. Mualem (1976) evaluated the "best" value of the parameter β, using 45 sets of $S(\psi)$ and $K(\psi)$ or $K(\theta)$ data and concluded that the "best" value for β is 0.5. The majority of samples used in Mualem's study, however, were repacked, suggesting that for repacked samples the optimal value of β is 0.5. When a sample is repacked, we determine the repacked β with $\beta_{repacked} = \beta \pm g|\beta - 0.5|$, where g is a random number uniformly distributed between 0 and 0.9 and the rightmost term is added when $\beta < 0.5$ and subtracted when $\beta > 0.5$.

3.3.7   Hydraulic Property Estimates

Moisture content observations are determined using simulations of hanging column and pressure-chamber devices. Nine different tensions (25, 50, 75, 100, 125, 200, 330, 1000, and 3000 cm) are selected to capture the air-entry pressure and the slope of the moisture characteristic curve for most samples. Moisture content measurements at tensions at and below 200 cm are made in hanging columns, while measurements at higher tensions are made in pressure chambers. For equilibrium conditions (the observation error scenario), errors arise from observations of weight, estimates of the

70

applied pressure, and averaging of moisture content through the sample. We assume that all moisture content observations reflect drainage. The average moisture content at the applied tension is determined using equation (3-2) in

$$\overline{\theta}(\psi_i) = \frac{1}{H_r} \int_{\psi_i + \upsilon - H_r/2}^{\psi_i + \upsilon + H_r/2} \theta(\psi) \, d\psi \tag{3-21}$$

where ψ_i is the ith applied tension, $i = 1, \ldots, 9$ for each of the tensions used to measure the moisture content, H_r is the height of the sample ring and υ is the error in pressure at the center of the sample ring. The error in pressure υ is considered an error in length, ε, for moisture-content observations made in hanging columns and an error in pressure, ζ, for moisture-content observations made in pressure-chamber devices. For non-equilibrium conditions (equilibrium, boundary, and repacking error scenarios), errors arise from observations of weight, estimates of the applied pressure, averaging of moisture content through the sample, and incomplete drainage of the sample. $\overline{\theta}$ is determined by numerically simulating drainage from the sample with a lower boundary condition set equal to $\psi_i + \upsilon - H_r/2$. The sample is allowed to drain until the sample weight changes less than 0.01 gm in 24 hours, and the resulting moisture content profile is averaged over the entire sample to derive $\overline{\theta}$. Assuming that the density of water is equal to 1 gm/cm^3, the estimated moisture content at tension ψ_i is

$$\hat{\theta}(\psi_i) = \frac{\overline{\theta}(\psi_i) V_r + \varepsilon_5 - \varepsilon_6}{\hat{V}_r} \tag{3-22}$$

where ε_5 is the error in the combined weight of the wet sample and container and ε_6 is the error in the combined weight of the container and dry sample. This procedure is

71

repeated for the predetermined ψ_i, providing a $\hat{\theta}(\hat{\psi}_i)$ data set which is fit with equations (3-1) and (3-2) using a Levenberg-Marquardt algorithm, resulting in estimates of the van Genuchten (1980) parameters α and n, represented by the symbols $\hat{\alpha}$ and $\hat{n}$. The estimated porosity ($\hat{\phi}$) is determined by substituting the porosity (ϕ) for the average moisture content ($\overline{\theta}$) in equation (3-22).

The saturated hydraulic conductivity is estimated using a Darcy column. A constant head is applied to the inlet, the outlet is open to the atmosphere, and a steady flux rate is measured. The true flux through the column is determined from

$$Q_s = K_s \frac{L_H}{L_L} \pi \left(\frac{L_D}{2}\right)^2 \tag{3-23}$$

where L_H is the height between the constant head reservoir and the inlet, L_L is the length of the column, and L_D is the diameter of the column. The saturated hydraulic conductivity is estimated using

$$\hat{K}_s = \frac{\hat{V}_Q}{\hat{t}_Q} \frac{4\hat{L}_L}{\hat{L}_H \pi \hat{L}_D{}^2} \tag{3-24}$$

where the flux rate is estimated using the observed volume of water ($\hat{V}_Q$) eluted as a function of observed time ($\hat{t}_Q$).

We only determine only one set of porosity and saturated hydraulic conductivity estimates, $\hat{\phi}$ and $\hat{K}_s$, because they are independent of n. Multiple estimates of van Genuchten (1980) parameters α and n are made because their errors vary with the geometric mean n and with each of the four the error scenarios considered. The parameters $\hat{\alpha}$ and $\hat{n}$ are determined by fitting the van Genuchten, (3-1) and (3-2)

72

parametric model to the estimated moisture characteristic data. $\hat{\theta}(\psi)$ data that fall below

the detection limit for moisture content $(1.7 \times 10^{-4} \text{ cm}^3/\text{cm}^3)$ are not fit. The residual

moisture content, θ_r, is considered to be zero for the observation error scenario. For all

other scenarios, however, the best estimates of α and n are achieved when the residual

moisture content is included in the fit. All fits are performed using a Levenberg-

Marquardt algorithm. For each of the 16,384 sampled points in our seven realities, the

four sets of $\hat{\theta}(\psi)$ data, corresponding to the observation, equilibrium, boundary, and

repacking error scenarios, are fit yielding four sets of $\hat{\alpha}$ and $\hat{n}$, and three sets of

estimated residual moisture contents, $\hat{\theta}_r$.

3.3.8 Statistics and Variogram-Model (VM) Parameters

The mean and variance of all "true" and "estimated" parameters are determined,

and local variograms are calculated using the GSLIB subroutines gam2 (Deutsch and

Journel, 1998)

$$\gamma(\mathbf{h}) = \frac{1}{2N(\mathbf{h})} \sum_{i=1}^{N(\mathbf{h})} [U(\mathbf{x}_i + \mathbf{h}) - U(\mathbf{x}_i)]^2 \qquad (3\text{-}25)$$

where N($\mathbf{h}$) is the number of samples in lag interval $\mathbf{h}$ and U(x) is the random field. All

of the resulting variograms are fit, using a Levenberg-Marquardt algorithm, with the

exponential variogram model

$$\hat{\gamma}^m(\mathbf{h}) = \sigma_m^2 \left[1 - \exp\left(-\frac{3\mathbf{h}}{\hat{\lambda}_c} \right) \right] + \sigma_n^2 \qquad (3\text{-}26)$$

where $\hat{\lambda}_c$ is the estimated "correlation length", $\hat{\sigma}_m^2$ is the "model variance", and $\hat{\sigma}_n^2$ is the

nugget variance. It is important to note that the model variance differs from the variance

in that it is a fitting parameter while the variance is a directly calculated statistic. The

variance of the fitted data is the sum of model and nugget variances. When a variogram is

flat for all lag distances, we refer to it as a "nugget variogram" in which $\hat{\sigma}_m^2 = 0.0$ and $\hat{\lambda}_c$

$= 0.0$. In classical geostatistics nugget variograms represent white noise processes that

have no spatial correlation. Bias for each statistical parameter is shown using a ratio

$\hat{P}_E / \hat{P}_T$ where $\hat{P}_E$ is the statistical parameter (e.g., mean, variance, or variogram model

parameters) for a random field of estimates and $\hat{P}_T$ is the statistical parameter determined

for the true random field. The ratio equals 1.0 for an unbiased statistic.

3.4   BIAS DUE TO MEASUREMENT ERROR

This section errors presents errors in the spatial statistics of our estimated

parameters. We first show that observation errors introduce little bias in the spatial

statistics for the log transform of the saturated hydraulic conductivity and porosity,

$\ln(\hat{K}_s)$ and $\ln(\hat{\phi})$. We then examine errors in the estimated moisture-characteristic

curves, $\hat{\theta}(\psi)$, to provide the basis for diagnosing bias in estimates of van Genucthen

parameters $\hat{\alpha}$ and $\hat{n}$. We present the bias affecting the spatial statistics of $\ln(\hat{\alpha})$ and

$\ln(\hat{n})$. Because we must include the residual moisture content to achieve good estimates

of $\hat{\alpha}$ and $\hat{n}$ in the equilibrium, boundary, and repacking error scenarios, we show the

spatial statistics of $\hat{\theta}_r$ and discuss the relationship between $\hat{\theta}_r$ and estimates of the

74

parameters K_s, ϕ, α, n, and β. Recall that true parameters α and n are uncorrelated. Because the errors in $\hat{\theta}(\psi)$ are propagated through the non-linear van Genuchten model, (3-1) and (3-2), apparent cross-correlation develops between $\ln(\hat{\alpha})$ and $\ln(\hat{n})$. We show this cross-correlation and discuss its relationship to the geometric mean n in our random fields.

3.4.1 Hydraulic Conductivity (K_s) and Porosity (ϕ)

Measurement errors affecting the hydraulic conductivity, $\ln(\hat{K}_s)$, and the porosity, $\ln(\hat{\phi})$, are small and minimally impact spatial statistics. On average, measurement errors cause a bias in $\ln(\hat{K}_s)$ and $\ln(\hat{\phi})$ of less than a tenth of a percent in these simulations. Estimated statistics (mean and variance) and variogram-model parameters for the log-transformed parameters $\ln(\hat{K}_s)$ and $\ln(\hat{\phi})$ show no significant bias (Table 3-2).

	Mean	Variance	Model Variance	Correlation Length
$\ln(\hat{K}_s)/\ln(K_s)$	1.000	1.001	1.005	0.993
$\ln(\hat{\phi})/\ln(\phi)$	0.999	1.011	1.262	0.994

Table 3-2. Bias in $\ln(\hat{K}_s)$ and $\ln(\hat{\phi})$

These results illustrate that spatial statistics can be estimated for parameters with inversion models that are linear, or nearly linear, with respect to small observation errors. Although $\ln(\hat{K}_s)$ and $\ln(\hat{\phi})$ are not strictly linear functions of observation error, their measurement errors appear unbiased in space because observation errors are small and their inversion models are simple. On the other hand, we have not considered inversion-model errors for these two measurements; their presence, especially in determining $\ln(\hat{K}_s)$, could well produce spatial bias in estimated parameters.

3.4.2 Moisture Content $\theta(\psi)$ Data

We explore errors in $\hat{\theta}(\psi)$ data to provide the necessary background for interpreting bias in the spatial statistics of van Genuchten (1980) parameters $\hat{\alpha}$ and $\hat{n}$. Figure 3-1 shows arithmetic mean of $\hat{\theta}(\psi)$ for all scenarios, at three geometric mean n. In general, moisture-characteristic curves are overestimated, and the average error increases with tension, geometric mean n (as the pore-size distribution narrows), and additional types of error.

For the observation error scenario, average errors in $\hat{\theta}(\psi)$ are relatively small across all tensions, except when the moisture content approaches its detection limit $(\pm 1.7 \times 10^{-4} \, cm^3/ \, cm^3)$. When equilibrium errors are considered, errors in $\hat{\theta}(\psi)$ increase significantly, especially at high tension. At high tension and large geometric mean n, average $\hat{\theta}(\psi)$ abruptly flattens to an apparent residual moisture content. When boundary
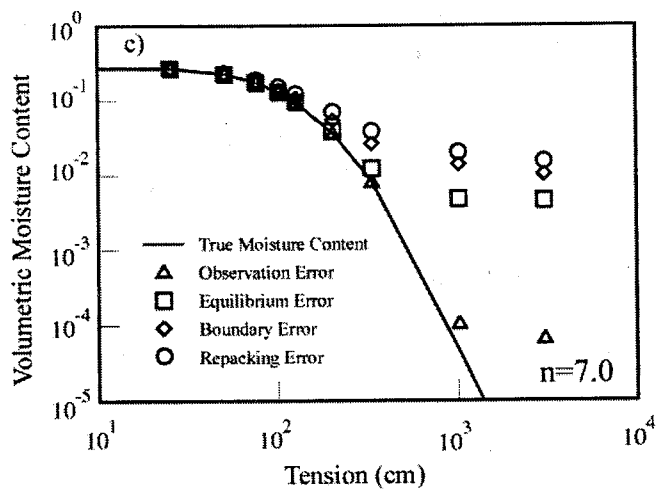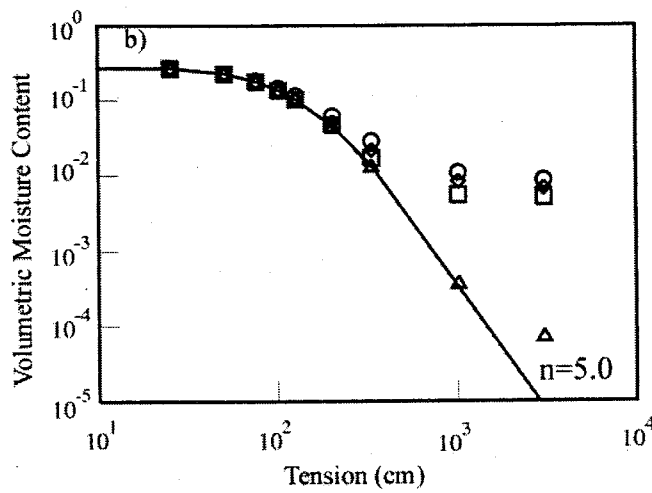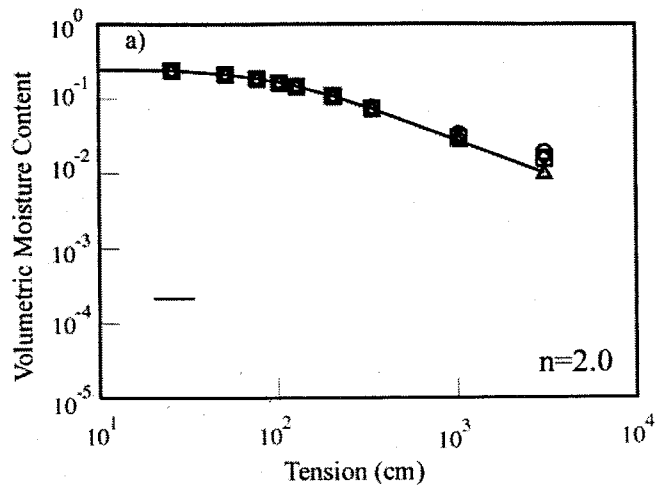
Figure 3-1. Average moisture contents for a) $n = 2.0$, b) $n = 5.0$, and c) $n = 7.0$. Points

represent the arithmetic mean moisture content for the entire sampled field.

errors are added, average $\hat{\theta}(\psi)$ increases further but does not flatten as quickly at high tension. This behavior is most evident in Figure 3-1c. When repacking errors are included, average $\hat{\theta}(\psi)$ shows the most error, the highest apparent residual moisture content, and the shallowest slope across intermediate tensions.

In the observation error scenario, errors in $\hat{\theta}(\psi)$ arise from errors in the sampled tension, estimates of sample weights, and estimates of container volume (3-9). At low tension, relative errors affecting $\hat{\theta}(\psi)$ are small and essentially unbiased with respect to ψ and constitutive parameters. These errors cause a bias of under 1% and measurement uncertainty of no more than $\sim \pm 4\%$. At low tension, errors in $\hat{\theta}(\psi)$ are dominated by pressure and container volume errors, because relative errors in $\hat{\theta}(\psi)$ due to weight are mean-zero with an uncertainty, to 95%, of $\pm 1.7 \times 10^{-4}\%$ of $\theta(\psi)$. As $\hat{\theta}(\psi)$ decreases, however, relative errors in $\hat{\theta}(\psi)$ become increasingly larger, due to the errors in weight. When the change in $\hat{\theta}(\psi)$ between consecutive tensions approaches the detection limit for moisture content ($\pm 1.7 \times 10^{-4}\, cm^3/\, cm^3$), errors in weight generate a large, up to orders of magnitude, positive bias in $\hat{\theta}(\psi)$.

In the equilibrium error scenario, both errors in observations and equilibrium times cause errors in $\hat{\theta}(\psi)$ data. Equilibrium errors in $\hat{\theta}(\psi)$ depend on the flux rate from the sample and are, therefore, a function of $K(\psi)$. As $K(\psi)$ decreases, flux rates decrease, and equilibrium errors increase. Consider a series of apparent equilibrium moisture contents for three different values of K_S, but where all other parameters are the
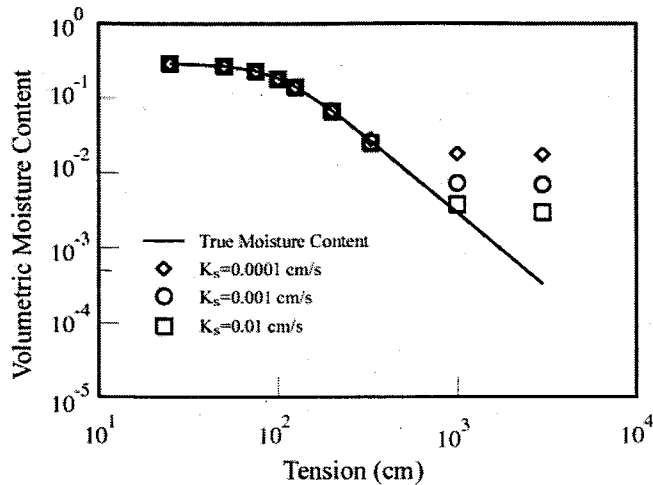
Figure 3-2. Illustration of the effects of equilibrium time errors on observed moisture contents for three different K_s.

same (Figure 3-2). $K(\psi)$ is proportional to K_S (3-4). As K_S decreases, equilibrium errors increase and become significant at progressively lower tensions. Equilibrium errors are greatest at higher tensions and cause the measured moisture characteristic curves to flatten abruptly (Figures 3-1 and 3-2). Similar behavior results when either α, n, or β is large, because the unsaturated hydraulic conductivity decreases. Equilibrium errors also depend on porosity. When porosity increases, the volume of fluid drained from or added to the sample at equilibrium increases, but the hydraulic conductivity does not change. The equilibrium time increases, causing larger equilibrium errors.

We find that equilibrium errors also depend on the drainage or wetting history of the sample. Incomplete drainage or wetting at apparent equilibrium increases the error in subsequent measurements. If the number of measurements or the tensions were changed,

a different measured moisture characteristic curve would result. Although we do not specifically address hysteresis in this study, it is important to note that equilibrium errors can profoundly affect the measurement of hysteretic moisture characteristic curves, and hysteretic moisture characteristic curves can result from equilibrium errors, even if the true moisture characteristic function is monotonic.

In the boundary error scenario, $\hat{\theta}(\psi)$ is affected by both errors in observations, equilibrium time, and heterogeneity in α at the base of the sample. We randomly alter α in the lower 1mm of the sample to account for larger pores due to sample disturbance and the sample apparatus. At moderate to high tensions, the hydraulic conductivity in the lower part of the sample decreases significantly relative to the remainder of the sample, and flow from the sample is restricted. Because sample flux rates are reduced, equilibrium time errors are enhanced, and $\hat{\theta}(\psi)$ curves tend to flatten and become more sigmoidal (Figure 3-1), especially at high n (e.g., well-sorted materials).

When repacking errors are included with the other errors, $\hat{\theta}(\psi)$ is consistently overestimated, especially at high tensions (Figure 3-1). Because our repacking model tends to decrease n and increase α, and equilibrium errors increase with α, $\hat{\theta}(\psi)$ for the repacking error scenario tends to be larger than that for the boundary error scenario. This difference increases with the geometric mean n (e.g., sorting).

3.4.3   van Genuchten Parameters (α and n)

In the following, we present and discuss errors in the spatial statistics for $\ln(\hat{\alpha})$ and $\ln(\hat{n})$ as a function of the geometric mean n for each of our four error scenarios.

Because $\hat{\alpha}$ and $\hat{n}$ are determined by fitting $\hat{\theta}(\psi)$ data, we emphasize the connection

between errors in $\hat{\theta}(\psi)$ and the spatial statistics of $\ln(\hat{\alpha})$ and $\ln(\hat{n})$. Finally, we discuss

several important concepts illustrated by our results.

The spatial statistics of $\ln(\hat{\alpha})$ and $\ln(\hat{n})$ show the least bias in the observation

error scenario (Figure 3-3) and are best estimated at smaller values of geometric mean n

(e.g., poorly sorted materials). Observed trends reflect errors in $\hat{\theta}(\psi)$, which increase
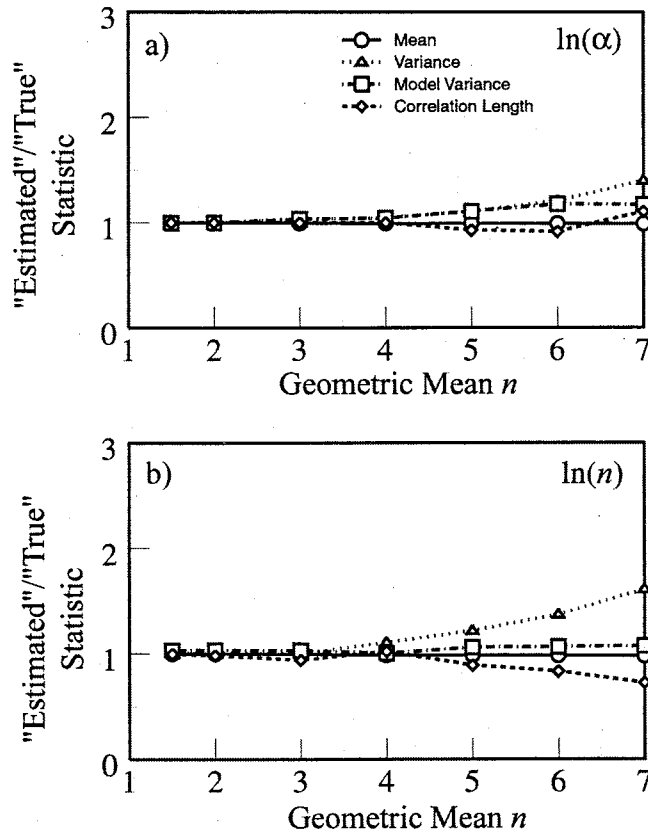

Figure 3-3. Bias in spatial statistics of a) $\ln(\hat{\alpha})$ and b) $\ln(\hat{n})$ for the observation-error

scenario.

with tension and n. Errors in the means of $\ln(\hat{\alpha})$ and $\ln(\hat{n})$ are very small, because $\hat{\theta}(\psi)$ values below the detection limit are excluded from the van Genuchten model fitting and average errors in the remaining $\hat{\theta}(\psi)$ data are very small. At high geometric mean n, errors in $\hat{\theta}(\psi)$ are potentially larger and more variable. This variability causes larger errors in the variance (ie, the sum of model and nugget variances), the model variance, and the correlation length of $\ln(\hat{\alpha})$ and $\ln(\hat{n})$. Errors are generally worse for $\ln(\hat{n})$, because $\hat{n}$ depends on the slope of $\hat{\theta}(\psi)$ at high tensions, where $\hat{\theta}(\psi)$ errors are the greatest. Errors for $\ln(\hat{\alpha})$ are smaller, because $\hat{\alpha}$ is most sensitive to $\hat{\theta}(\psi)$ at low tensions.

When equilibrium errors are included, they minimally alter the spatial statistics of $\ln(\hat{\alpha})$ from the observation error scenario (Figure 3-4a). The spatial statistics of $\ln(\hat{\alpha})$ show slightly more error at lower geometric mean n (e.g., poorly sorted materials) and slightly less error in the variance at high geometric mean n (e.g., well-sorted materials). Errors in spatial statistics for $\ln(\hat{n})$ increase significantly, especially when the geometric mean n is small (Figure 3-4b), as in poorly sorted materials. The mean, variance and model variance for $\ln(\hat{n})$ overestimate those for $\ln(n)$, while the correlation length of $\ln(\hat{n})$ consistently underestimates that of $\ln(n)$. For the equilibrium error scenario, the spatial statistics of both $\ln(\hat{\alpha})$ and $\ln(\hat{n})$ are best estimated when the true geometric mean n is between 3.0 and 4.0.

Equilibrium errors in $\hat{\theta}(\psi)$ tend to increase with n (e.g., sorting) and tension. Because $\hat{\theta}(\psi)$ errors are small at low tensions, the spatial statistics of $\ln(\hat{\alpha})$ change little

82

Figure 3-4. Bias in spatial statistics of a) $\ln(\hat{\alpha})$ and b) $\ln(\hat{n})$ for the equilibrium-error

scenario. Observation errors also affect results.

from the observation error scenario. Because equilibrium errors cause $\hat{\theta}(\psi)$ to abruptly

flatten to an apparent residual moisture content, the best estimates of $\hat{\alpha}$ and $\hat{n}$ are

achieved when a non-zero residual moisture content is included in (3-2) during the fitting.

A larger value of $\hat{n}$ is required to accommodate the residual moisture content ($\hat{\theta}_r$),

leading to consistent overestimation by the mean $\ln(\hat{n})$. When the geometric mean n is

small, equilibrium errors affect fewer samples, but the differences between the affected

and unaffected samples increases, causing the variance and model variance of $\ln(\hat{n})$ to be

greatly overestimated. At a larger geometric mean n, most samples are affected by

83

Figure 3-5. Bias in spatial statistics of a) $\ln(\hat{\alpha})$ and b) $\ln(\hat{n})$ for the boundary-error scenario. Observation and equilibrium errors also affect results.

equilibrium errors and the variability of $\ln(\hat{n})$ is less. Because of distortion in the $\ln(\hat{n})$ field, correlation lengths for $\ln(\hat{n})$ underestimate the true correlation length of $\ln(n)$, particularly at high geometric mean n (e.g., well-sorted materials).

Spatial statistics for $\ln(\hat{\alpha})$ and $\ln(\hat{n})$ change significantly when boundary errors are included (Figure 3-5). Below a geometric mean n of 3.0, the spatial statistics of $\ln(\hat{\alpha})$ and $\ln(\hat{n})$ differ little from the equilibrium error scenario. Above that, the variance and model variance for $\ln(\hat{\alpha})$ markedly increases, while the mean and correlation length change very little. The mean $\ln(\hat{n})$ decreases and underestimates the mean $\ln(n)$. The

variance of $\ln(\hat{n})$ increases dramatically and overestimates the variance of $\ln(n)$, by a factor of 12 at a geometric mean n of 7.0. Between a geometric mean n of 3.0 and 6.0, the model variance of $\ln(\hat{n})$ underestimates that of $\ln(n)$ by as much as 38%. At a geometric mean n of 7.0, the model variance of $\ln(n)$ is overestimated by 72%. Above a geometric mean n of 3.0, the correlation length of $\ln(\hat{n})$ underestimates that of $\ln(n)$ by as much as 34%.

The boundary error causes $\hat{\theta}(\psi)$ to gradually flatten to a residual moisture content and these effects increase with n. Because of the more gradual approach to the apparent residual moisture content, a smaller value of $\hat{n}$ is required to fit the $\hat{\theta}(\psi)$ data. As a result, $\hat{n}$ tends to be underestimated at high geometric mean n. Because the boundary errors are a random variable, they add significant noise to the $\ln(\hat{n})$ field, especially at large geometric mean n. This noise results in an increase of the variance of $\ln(\hat{n})$ and a decrease of the model variance and correlation length.

When repacking errors are also included, errors in some spatial statistics show another significant change (Figure 3-6). The variance of $\ln(\hat{\alpha})$ increases, while estimates of the mean, model variance, and correlation length change little from the boundary error scenario. The mean of $\ln(\hat{n})$ also changes little from the boundary error scenario, but errors in the variance, model-variance, and correlation length of $\ln(\hat{n})$ increase, yet still follow the same pattern as the boundary error scenario. The variance of $\ln(\hat{n})$ is significantly overestimated, while the model variance and the correlation length is underestimated.
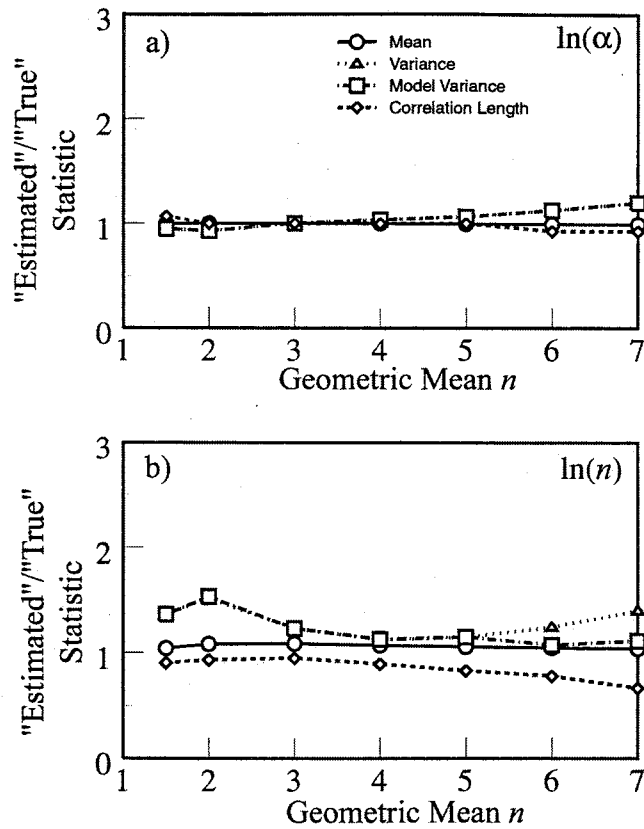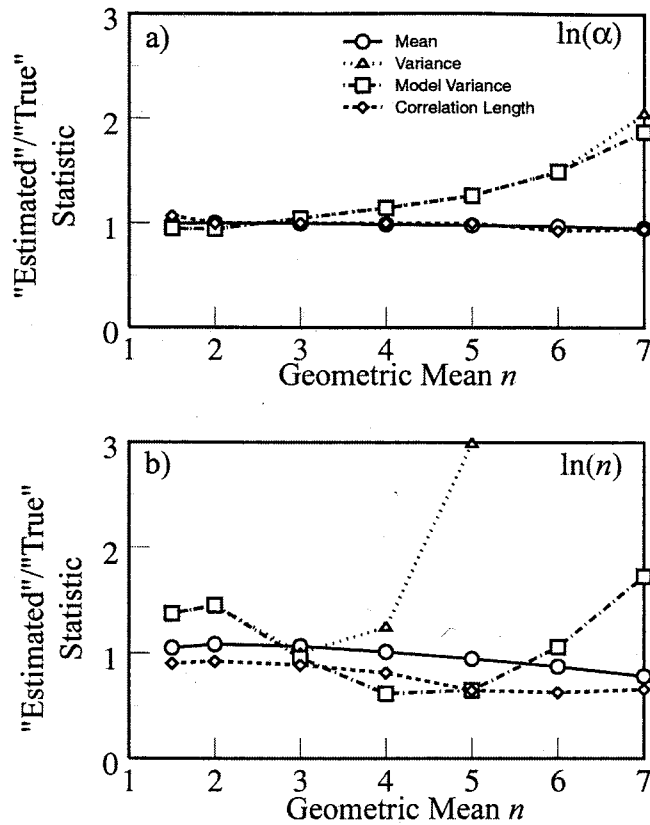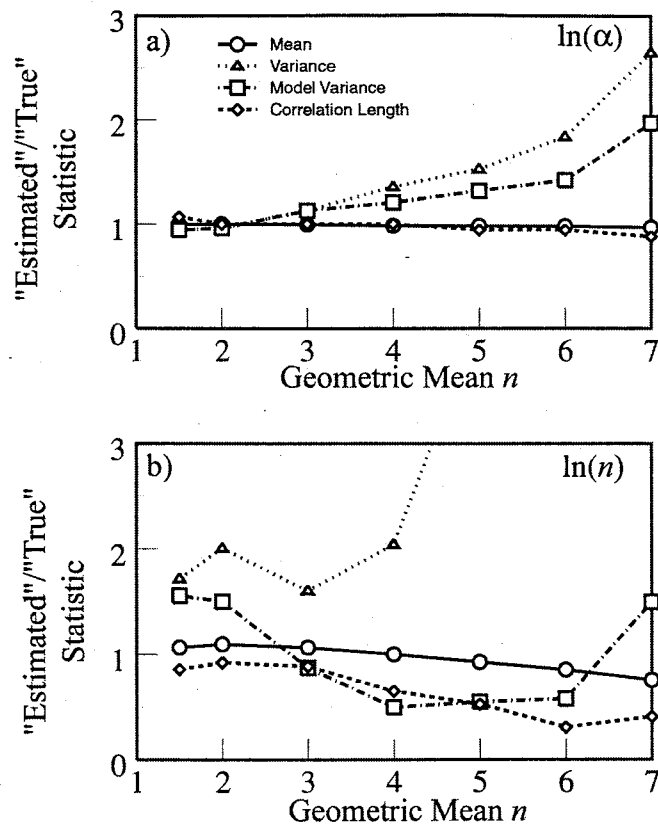
Figure 3-6. Bias in spatial statistics of a) $\ln(\hat{\alpha})$ and b) $\ln(\hat{n})$ for the repacking-error

scenario. Observation, equilibrium, and boundary errors also affect results.

Because repacking errors tend to increase with n, they affect the spatial statistics

of $\ln(\hat{n})$ more as the geometric mean n increases. As with the boundary errors, repacking

errors are random functions, and they increase the noise in the $\ln(\hat{n})$ field. As a result,

variance, model variance, and correlation length errors increase.

Our results show that the character of spatial bias in estimated parameters changes

with the type of error affecting measurements. Spatial bias may either increase or

decrease when a different kind of error affects measurements. Consider estimates of

variance of $\ln(\hat{n})$ between the observation error scenario (Figure 3-3b) and the

equilibrium error scenario (Figure 3-4b). When equilibrium errors are added, the amount

of overestimation in the variance of $\ln(\hat{n})$ increases at low geometric mean n and

decreases at high geometric mean n. Overestimation of the variance increases

significantly at high geometric mean n, when heterogeneity is present at the lower sample

boundary (Figure 3-5b). Because significant changes in spatial bias occur with different

types of error, *a priori* knowledge of all errors is required for a complete error analysis.

Bias in spatial statistics is most sensitive to inversion-model errors. The

magnitude and potential effect of inversion-model errors is unconstrained compared to

those of observation errors, which are minimized by design and limited by the inversion

model. Inversion-model errors may be either systematic functions of the hydraulic

properties of the medium (e.g., equilibrium errors) or random errors that depend on

sample-specific conditions (e.g., boundary or repacking error). Systematic inversion-

model errors act as filters, whose response depends on media properties, and affect all

measurements to some degree. They distort the underlying spatial pattern in estimated

parameter fields, but introduce little noise. Inversion-model errors with a random

component add noise to estimated parameter fields, which tends to obscure spatial

correlation. In the boundary and repacking error scenarios, large differences between the

variance and model variance (i.e. a large nugget) reflect the addition of noise to $\ln(\hat{\alpha})$

and $\ln(\hat{n})$ fields.

The degree of spatial bias in multiple parameters, estimated from a single set of

observations, varies with parameter sensitivity to observations. Our observations of

$\hat{\theta}(\psi)$ are biased with respect to tension, and this leads to differences between errors in statistics for $\ln(\hat{\alpha})$ and $\ln(\hat{n})$. The parameter $\hat{\alpha}$ is most sensitive to $\hat{\theta}(\psi)$ at low tensions, while the parameter n is related to the slope of $\hat{\theta}(\psi)$ at high tensions. Because errors in $\hat{\theta}(\psi)$ increase with tension, the spatial statistics of $\ln(\hat{n})$ generally show more error than those of $\ln(\hat{\alpha})$, regardless of geometric mean n.

It is important to recall that our results are presented for log-transformed variables and small differences in the statistics between our estimated and true values, say $\ln(\hat{n})$ and $\ln(n)$, reflect much larger differences in non-transformed variables, $\hat{n}$ and n. When the geometric mean $n = 7.0$ in our repacking error scenario, the ratio of $\ln(\hat{n})$ to $\ln(n)$ is 0.79 while the ratio of $\hat{n}$ to n is 0.67. Although these differences may seem small, they can cause orders of magnitude difference in the moisture content and unsaturated hydraulic conductivity. Using the values of $\hat{n}$ and n with $\alpha = 0.01$ cm^{-1}, the moisture content would be overestimated by a factor of 87 at -500 cm tension.

3.4.4 Residual Moisture Content

While we recognize that there are many physical reasons to have non-zero residual moisture contents in most porous media, we have chosen to fix the "real" residual moisture content to 0.0 for this study. When only observation errors are present, good estimates of $\hat{\alpha}$ and $\hat{n}$ can be achieved with zero residual moisture content. When equilibrium errors are present (the equilibrium, boundary, and repacking error scenarios),

88

we must include a non-zero residual moisture content ($\hat{\theta}_r$) to achieve the best estimates of $\hat{\alpha}$ and $\hat{n}$ from $\hat{\theta}(\psi)$ data.

The spatial statistics of $\hat{\theta}_r$ reflect errors in $\hat{\theta}(\psi)$. Trends in the mean $\hat{\theta}_r$ (Figure 3-7) reflect average errors in $\hat{\theta}(\psi)$ at high tensions (Figure 3-1). The coefficient of variation (CV) (Figure 3-7) reflects the hydraulic property variability in the sampled field and the type of measurement error present. For geometric mean n less than 3.0, the CV decreases with increasing geometric mean n and added measurement errors. Fewer points in the sampled field have small n values (large $\hat{\theta}_r$) as the geometric mean n increases, so the variability of $\hat{\theta}_r$ decreases. When boundary and repacking errors are added, $\hat{\theta}_r$ becomes less sensitive to n, and the CV decreases. For geometric mean n greater than 3.0, the CV increases with the geometric mean n and added errors. In the equilibrium error scenario, the CV gently rises with increasing geometric mean n, because $\hat{\theta}_r$ becomes more sensitive to n. When boundary and repacking errors are included, the additional noise from these random inversion-model errors causes the CV to increase significantly at high geometric mean n.

Variograms of $\hat{\theta}_r$ are readily fit with the exponential model, with the exception of geometric mean n of 1.5 where all variograms show a trend. Correlation lengths for $\hat{\theta}_r$ are roughly equivalent to the correlation lengths of $\ln(K_s)$, $\ln(\alpha)$, $\ln(n)$, $\ln(\phi)$, or β and range from ~ 22 to ~29 length units. The model variance closely follows the variance, except at high geometric mean n when random inversion-model errors generate
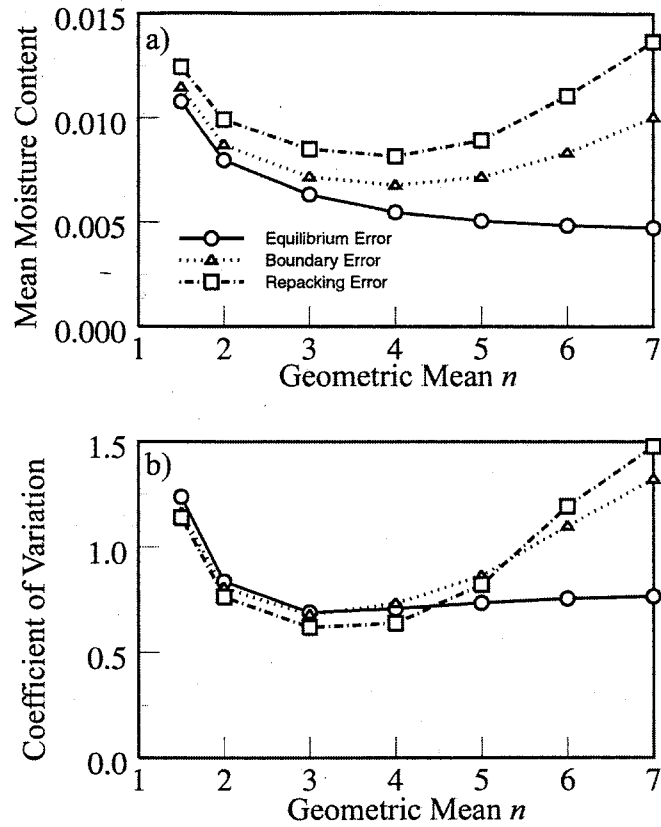
Figure 3-7. Mean (a) and coefficient of variation (b) for the estimated residual moisture content.

substantial nugget variance. Variogram results suggest a strong relationship between the estimated residual moisture content $\hat{\theta}_r$ and the true hydraulic properties in our fields.

The residual moisture content shows cross-correlation with other, real parameters (Figure 3-8), because the measurement errors depend on those parameters. In the equilibrium error scenario (Figure 3-8a), cross-correlation with $\hat{\theta}_r$ is strongest with β and $\ln(K_s)$, followed by $\ln(\alpha)$, $\ln(\phi)$, and $\ln(n)$. At a geometric mean n of 1.5, the correlation with $\ln(n)$ is negative, because $\hat{\theta}(\psi)$ increases with decreasing n for n below

~2.0. In the boundary and repacking error scenarios (Figure 3-8b and 3-8c), correlation between $\hat{\theta}_r$ and the hydraulic properties changes significantly. Correlation with $\ln(\alpha)$ decreases at high geometric mean n, because α is randomly altered in the lower 1 mm of the sample. Because $\hat{\theta}(\psi)$ errors are controlled by the heterogeneity at the base of the sample, the magnitude of the negative correlation between $\hat{\theta}_r$ with $\ln(K_s)$ decreases at high geometric mean n. In the boundary error scenario, correlation with β decreases at high geometric mean n for similar reasons. In the repacking error scenario, correlation between $\hat{\theta}_r$ and β decreases significantly, while correlation with $\ln(\phi)$ increases, because β is randomly altered and repacked parameters are independent of β.

These results suggest that accuracy of residual moisture content data is questionable. Because $\hat{\theta}_r$ results appear realistic, it is virtually impossible to determine from the data whether or not the residual moisture content is uniquely describing physical characteristics of the medium. Estimates of residual moisture contents can be determined by measurement errors, which are functions of the hydraulic properties of the medium. For field data, it may not be possible to unravel the relationship between the residual moisture content and hydraulic parameters. In two of our error scenarios, the residual moisture content shows the strongest correlation with the parameter β, which is an unmeasured parameter. Artifactual parameters, like $\hat{\theta}_r$, are an insidious byproduct of estimating multiple parameters from a single data set subject to observation or inversion model errors.
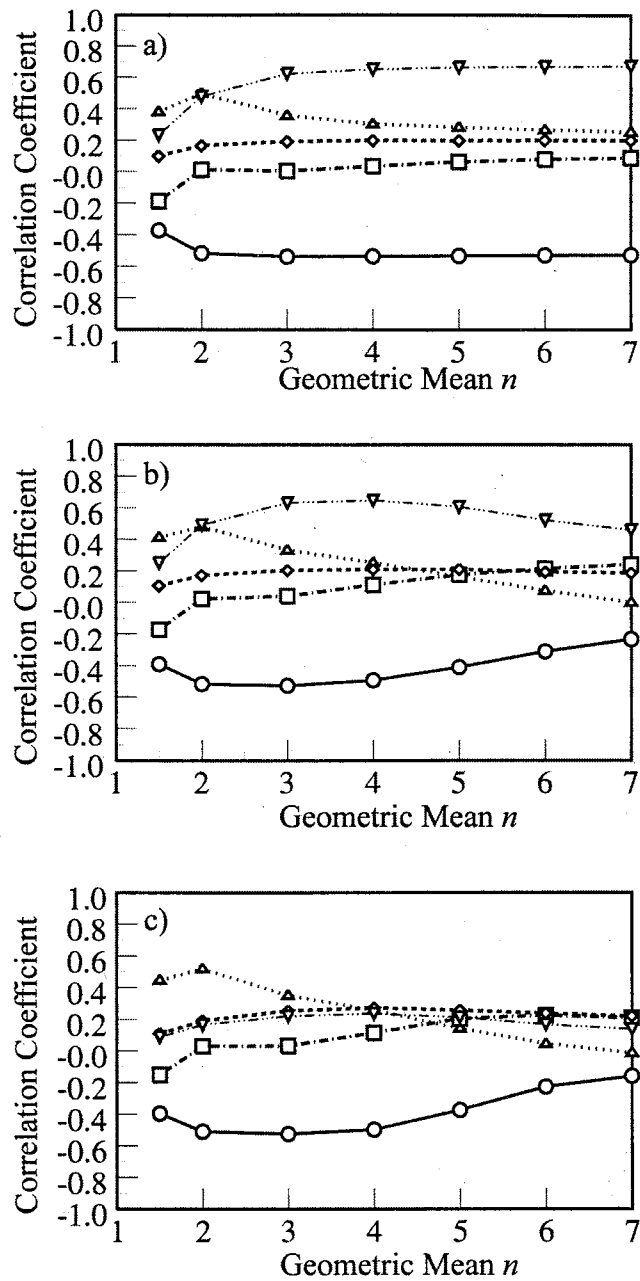
Figure 3-8   Correlation coefficients between $\hat{\theta}_r$ and $\ln(K_s)$ (—o—), $\ln(\alpha)$ (⋯▲⋯),

$\ln(n)$ (--□--), $\ln(\phi)$ (⋯◇⋯), and β (--▽⋯) for the a) equilibrium-error scenario, b)

boundary-error scenario, and c) repacking-error scenario.

3.4.5 Induced Cross-Correlation

Estimated fields of $\ln(\hat{\alpha})$ and $\ln(\hat{n})$ show cross-correlation that depends on the type of errors present and the geometric mean n (Figure 3-9). Although the original random fields of $\ln(\alpha)$ and $\ln(n)$ were generated with zero specified cross-correlation, some cross-correlation occurs between $\ln(\alpha)$ and $\ln(n)$ because our random fields are relatively small (only ~ 4 correlation lengths across). However, the observed cross-correlation between estimated values, $\ln(\hat{\alpha})$ and $\ln(\hat{n})$, is significantly different, because they were estimated using a non-linear model (the van Genuchten model) from a single data set containing errors [$\hat{\theta}(\psi)$].

Generally, the strength of the cross-correlation between $\ln(\hat{\alpha})$ and $\ln(\hat{n})$ increases as more errors are added (Figure 3-9). In the observation error scenario, $\ln(\hat{\alpha})$ and $\ln(\hat{n})$ are negatively correlated, because $\hat{\theta}(\psi)$ is overestimated, leading to a smaller $\hat{n}$, when α is large. When equilibrium errors are present, $\ln(\hat{\alpha})$ and $\ln(\hat{n})$ are positively correlated at small geometric mean n, because $\hat{\theta}_r$ increases with large α and accommodation of $\hat{\theta}_r$ requires a larger $\hat{n}$. At large geometric mean n and large α, $\hat{\theta}(\psi)$ tends to be overestimated at moderate tensions, leading to smaller $\hat{n}$. As a result, $\ln(\hat{\alpha})$ and $\ln(\hat{n})$ are negatively correlated.

When multiple parameters are estimated through a single inversion model from a biased data set, strong, but false, cross-correlation between the estimated parameters can develop. Cross-correlation due to measurement errors can completely obscure the "true"

cross-correlation between parameters. Using single-parameter inversion models with

independent data sets may alleviate this problem.
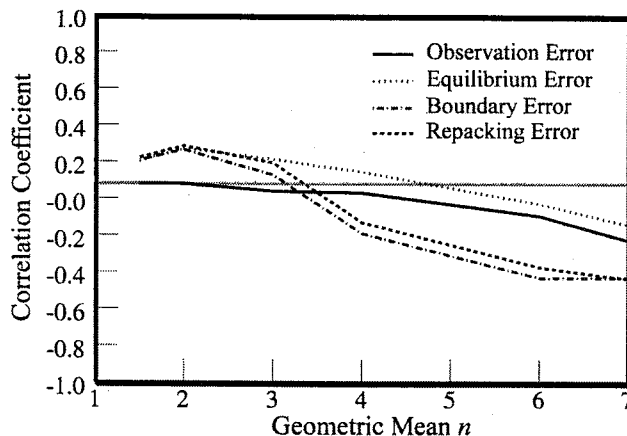
Figure 3-9. Correlation coefficients between $\ln(\hat{\alpha})$ and $\ln(\hat{n})$. Horizontal gray line

represents the true correlation coefficient in the sampled field (0.08).

3.5 POTENTIAL IMPACT OF MEASUREMENT ERROR BIAS ON FLOW AND TRANSPORT PREDICTIONS

The geometric mean of the unsaturated hydraulic conductivity, $K^G(\psi)$ and the

arithmetic mean moisture content, $\langle \theta(\psi) \rangle$, are two parameters commonly used in

probabilistic models of contaminant transport. The ratio of these parameters is a

surrogate for the mean velocity under unit gradient conditions, and for some constitutive

relationships, like the Gardner-Russo models for unsaturated hydraulic conductivity and

moisture retention, this ratio is exactly a first order approximation to the mean velocity

(e.g., Zhang et al., 1998).

94

To illustrate the potential impact of measurement errors on flow and transport predictions, we compare $K^G(\psi)$, $\langle\theta(\psi)\rangle$, and the ratio $K^g(\psi)/\langle\theta(\psi)\rangle$ calculated using our estimates and the true values of K_s, n, α, ϕ, and θ_r. We arbitrarily chose $\psi = -500$ cm for this comparison, typical of a semi-arid vadose zone. It is important to recall that the true residual moisture content is zero. The results of our comparison are shown in Figure 3-10. In the following discussion, we refer to the geometric mean $K(\psi)$ and the mean moisture content determined from our estimates as $\hat{K}^G(\psi)$ and $\langle\hat{\theta}(\psi)\rangle$, respectively.

When only observation errors are present, $\hat{K}^G(\psi)$, $\langle\hat{\theta}(\psi)\rangle$, and their ratio is relatively accurate, suggesting that flow and transport predictions would also be accurate. When equilibrium errors are considered, $\hat{n}$ tends to be overestimated leading to underestimation of $\hat{K}^G(\psi)$ by up to an order of magnitude at high geometric mean n (e.g., well-sorted material), and the addition of an artifactual residual moisture content causes overestimation of $\langle\hat{\theta}(\psi)\rangle$. The ratio $\hat{K}^g(\psi)/\langle\hat{\theta}(\psi)\rangle$ is consistently underestimated, implying that the velocity could be underestimated by nearly two orders of magnitude. When the boundary error is included, $\hat{K}^G(\psi)$ is underestimated at low geometric mean n (e.g., poorly sorted materials) and overestimated by over three orders of magnitude at high geometric mean n. Not unexpectedly, these trends are the opposite of the mean $\ln(\hat{n})$. The overestimation of $\langle\hat{\theta}(\psi)\rangle$ is greater than that for the equilibrium scenario because $\hat{\theta}_r$ increases. $\hat{K}^g(\psi)/\langle\hat{\theta}(\psi)\rangle$ mimics $\hat{K}^G(\psi)$, indicating that velocities

95
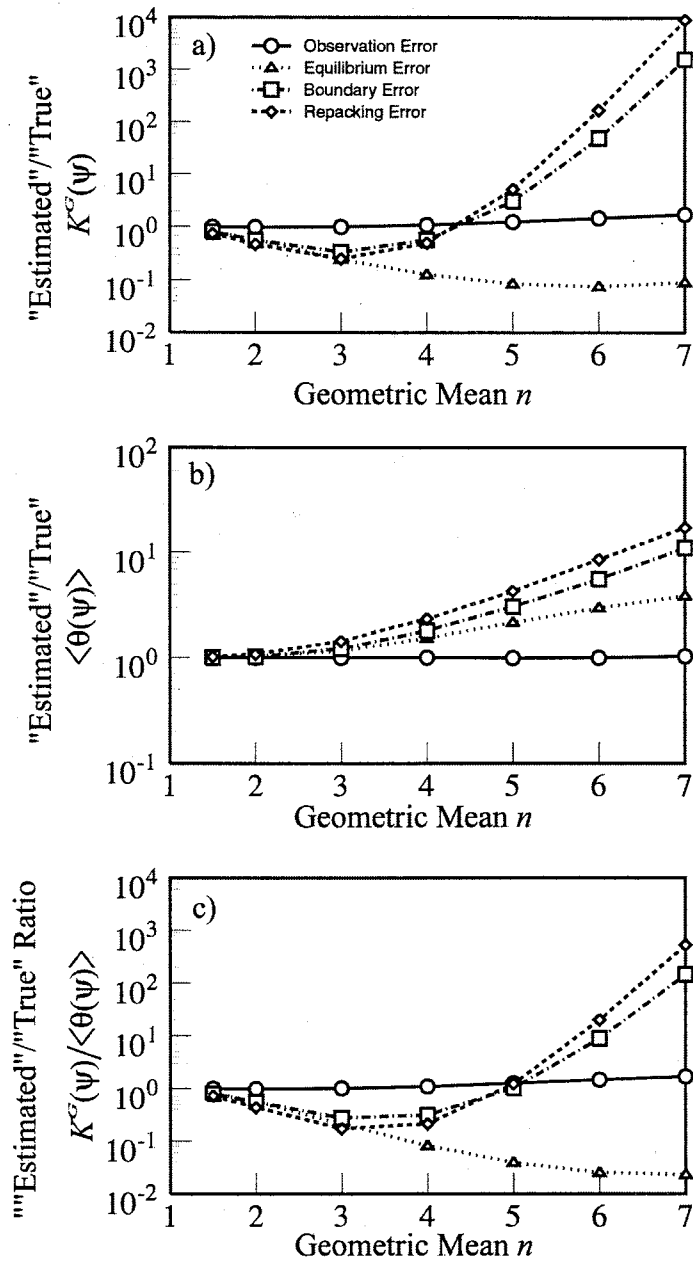
Figure 3-10. a) The geometric mean conductivity $\hat{K}^G(\psi)$, b) the mean moisture content $\langle \hat{\theta}(\psi) \rangle$, and c) the ratio $\hat{K}^g(\psi) / \langle \hat{\theta}(\psi) \rangle$, for $\psi = -500$ cm.

could be underestimated by nearly an order of magnitude at low to moderate geometric mean n and overestimated by over two orders of magnitude at high geometric mean n. When samples are repacked, the magnitude of these errors increases.

These results mainly reflect errors in $\hat{n}$ and $\hat{\theta}_r$. The magnitude of error decreases under wetter conditions (lower tension) and increases significantly for drier conditions (higher tension). Although the magnitude of bias in the spatial statistics of $\ln(\hat{n})$ appears small in Figures 3-3 to 3-6, this bias has the potential to generate large errors in transport calculations. In our case, a parameter, $\hat{\theta}_r$, that is simply an artifact of measurement errors exerts a strong influence on the calculation of transport times. These results suggest that accurate flow and transport models should not be based only on laboratory estimates of hydraulic properties.

3.6   UNCERTAINTY IN ESTIMATED SPATIAL STATISTICS

We have used every point in our random fields to estimate spatial statistics, and our results reveal the bias caused by measurement errors. In most spatial variability studies, however, it is not possible to sample everywhere, and estimates of spatial statistics are uncertain because of incomplete sampling and non-ideal sample locations, so-called structural errors (e.g., Journel and Huijbregts, 1978). We show that structural errors increase the effects of bias significantly and can preclude reliable estimation of spatial statistics when measurement bias is present.

Consider the fields of true $\ln(n)$ and estimated $\ln(\hat{n})$ from the boundary-error scenario, when the geometric mean n is 5.0. We define a subset consisting of 100 sample

points randomly selected from the 16,384 points in the field and then determine the model variance and correlation length for $\ln(n)$ and $\ln(\hat{n})$ from these data. We repeat this 500 times with different points, yielding 500 sets of variogram-model parameters for $\ln(n)$ and $\ln(\hat{n})$ each estimated from 100 measurements. We then increase the subset sample size to 200 points and repeat the entire procedure, generating another 500 sets of spatial statistics. The procedure is repeated with 300, 400,..., and 1000 point subsets, giving a distribution of 500 estimates of spatial statistics for $\ln(n)$ and $\ln(\hat{n})$ which we then plot as a function of the number of samples in a subset. We normalize estimates of the model variance and correlation length with the values from the complete $\ln(n)$ field and show the median and 5 and 95 percentiles in Figure 3-11. Journel and Huijbregts (1978) suggest that the number of pairs at each variogram point exceed between 30 and 50 points. Even with only 100 samples, we satisfy this criterion within our sampled fields.

Uncertainty due to structural errors is revealed by the results for the true $\ln(n)$ field (Figure 3-11a). The normalized medians for the correlation length and the model variance approach one as the subset sample size increases. The uncertainty (illustrated by the normalized 5 and 95 percentiles) decreases significantly as the number of samples in a subset increases. When a limited number of true $\ln(n)$ data are used to estimate the variogram, the uncertainty due to structural errors may be within the acceptable range for many applications.

When we include measurement errors and use estimated $\ln(\hat{n})$ data, however, estimates of spatial statistics are very uncertain and biased (Figure 3-11b). Until the

98
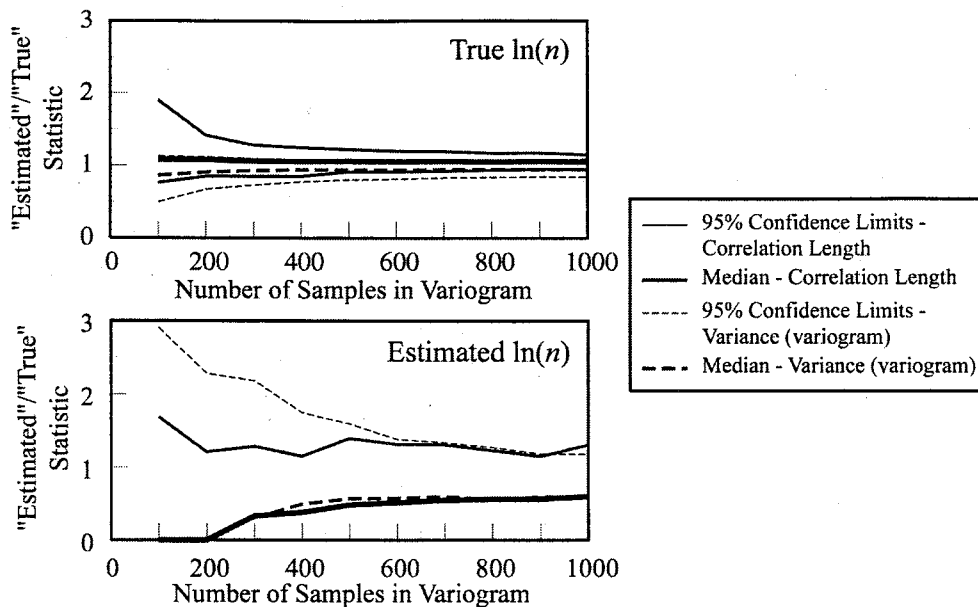
Figure 3-11. Median and 95% confidence limits of the correlation length (solid lines) and model variance (dashed lines) determined from 500 variograms for $\ln(\hat{n})$, as a function of the number of samples. Results for true values are shown in a) and estimated values are shown in b). For the sampled field, the geometric mean $n = 5.0$.

subset sample size increases beyond 200 points, over 50% of the variograms are nugget variograms showing no spatial structure. Even with a subset sample size of 1,000 locations over 10% of the variograms are nugget variograms. Because of the large number of nugget variograms, the spatial statistics of $\ln(n)$ cannot be reliably estimated with a limited number of estimated $\ln(\hat{n})$ data. These results suggest that methods for optimizing variogram sample locations may need to include the effects of measurement error bias.

3.7   NEGLECTED ERRORS

In this study, we have not attempted to fully characterize the effects of all types of measurement errors on estimates of spatial statistics for unsaturated hydraulic properties. Instead, we have focused on examining the impact of only a limited number of errors. In this context, we believe that the results presented here are overly favorable, because we have neglected a variety of errors that are likely to affect estimated spatial statistics. These errors can be subdivided into to several classes, including model errors, methodological errors, errors due to sample damage, and errors due to non-equilibrium conditions.

In our study, we have eliminated several sources of model error. We have assumed that $\theta(\psi)$ is monotonic and completely described by the van Genuchten constitutive model. While convenient and popular, this model is not appropriate for all materials and flow conditions. With its use, it is implicitly assumed that pore sizes are distributed unimodally and the materials are non-hysteretic. In addition, we assume that the correct variogram model is known, thereby eliminating uncertainty due to choice of a variogram model.

Methodological errors can result from inadequate sample assemblies and flaws within measurement procedures. In the following, we provide some examples based on our experience. It is common to find that measurement uncertainty results from idiosyncrasies associated with holding the sample in a measurement apparatus. For example, an annulus or region of larger pores exists between the sample and sample ring. This annulus drains rapidly, and affects estimates of the porosity, $\hat{\phi}$, and saturated

hydraulic conductivity, $\hat{K}_s$. These errors mask the air-entry pressure, cause difficulties in

fitting $\hat{\theta}(\psi)$ data and, if uncorrected, cause $\hat{\alpha}$ and $\hat{n}$ to be underestimated. Parts of the

sample assembly required for holding the sample in the ring also affect estimates of

$\hat{\theta}(\psi)$. For example, filter paper is often used to hold poorly consolidated samples in a

ring during measurement of $\hat{\theta}(\psi)$. Under typical conditions, the filter paper may hold up

to 1 gm of water and will wet and drain differently than the sample. This produces a bias

in $\hat{\theta}(\psi)$ that becomes most important at low moisture contents. The impact of this bias

on estimates of $\hat{\alpha}$ and $\hat{n}$ depends on the drainage characteristics of both the sample and

the filter paper. In addition, contact material, such as diatomaceous earth, is typically

used to provide contact between the sample and porous plates. For estimating $\theta(\psi)$, the

sample weight is determined by removing the sample from the porous plate, and some of

the contact material usually adheres to the sample apparatus causing additional errors in

$\hat{\theta}(\psi)$.

We assume that intact samples are removed undamaged from the field and that

sample hydraulic properties remain unchanged throughout measurement procedures. In

our experience, it is virtually impossible to remove samples from the field without some

alteration of hydraulic properties. Poorly consolidated samples suffer the most alteration.

During sampling, the pore structure along sample edges is disturbed, and vibration during

transport can loosen weak grain cements and cause settling. Also, sample properties are

often altered by the measurements themselves. In poorly consolidated materials, grains

can be displaced during sample saturation. Drainage may cause compaction, and fine

materials may be transported from the sample. It is not unusual to find that the final sample weight is less than the initial sample weight. Transported fines can clog pores and contact materials reducing effectively reducing hydraulic conductivity of the sample or boundary materials. In addition, sample properties are also altered by vibrations during sample removal or handling, as sample cohesion changes with moisture content.

We neglected a number of errors that can affect equilibrium time, such as sub-sample-scale heterogeneity. The simple heterogeneity used in the boundary error scenario caused significant equilibrium time errors, and other horizontally oriented heterogeneities will increase equilibrium times significantly. Evaporation from the experimental apparatus will also affect equilibrium time. In addition, differences between equilibrium-time scales of the sampled medium and equipment components can cause equilibrium errors.

The number of errors that may affect any one estimate of a hydraulic property is very large, and the magnitude of these errors is likely to vary significantly between measurements. It is, therefore, not possible to determine *a priori* all of the errors affecting a single measurement or a group of measurements, and for the standard laboratory methods considered here, it is not possible to remove the bias introduced by measurement errors.

3.8   SUMMARY

We investigate the influence of measurement errors on the spatial statistics of laboratory-estimated saturated and unsaturated hydraulic properties with a Monte Carlo

approach. Using an exponential-variogram model, we construct a series of artificial realities consisting of independent, random fields of $\ln(K_s)$, $\ln(\phi)$, $\ln(\alpha)$, $\ln(n)$, and β. Between realities, the geometric mean of the van Genuchten parameter n was systematically varied. Each point in the reality is sampled, and we estimate the porosity, $\hat{\phi}$, saturated hydraulic conductivity, $\hat{K}_s$, and the moisture-characteristic curve, $\hat{\theta}(\psi)$, using numerical simulations of standard laboratory procedures subject to error. The van Genuchten model is fit to $\hat{\theta}(\psi)$ data yielding estimates of its parameters $\hat{\alpha}$ and $\hat{n}$. The spatial statistics of $\ln(\hat{\phi})$, $\ln(\hat{K}_s)$, $\ln(\hat{\alpha})$, and $\ln(\hat{n})$ are determined, and their bias is assessed.

We incorporate only simple errors into simulated laboratory measurements. Only observation errors are considered when determining $\hat{\phi}$ and $\hat{K}_s$. Four different error scenarios are considered when determining $\hat{\theta}(\psi)$, each with an increasing number of different types of errors. In the observation error scenario, only errors in weight, length, volume, and time are considered, and $\hat{\theta}(\psi)$ observations are truly at equilibrium. In the equilibrium error scenario, transient drainage of the sample is considered along with observation errors. The boundary error scenario adds to this a small, random heterogeneity at the base of the sample. In the repacking error scenario, the sample hydraulic properties are also modified using a simple model based on the Haverkamp and Parlange (1986) mapping of cumulative grain-size distributions to pressure-saturation curves using bulk density data. Moisture characteristic curves, subject to observation, equilibrium, and boundary errors, are then measured on the repacked samples.

103

We found that measurement errors cause no significant bias in spatial statistics of K_s and ϕ, because inversion-models are simple and observation errors are small. In general, $\hat{\theta}(\psi)$ is overestimated, and the amount of overestimation increases with tension (drier soils) and geometric mean n (sorting). Equilibrium error causes $\hat{\theta}(\psi)$ curves to abruptly flatten at high tensions, leading to errors of up to several orders of magnitude. Errors are increased when a simple heterogeneity is included at the lower sample boundary, and the $\hat{\theta}(\psi)$ curve assumes a sigmoidal shape. When repacking errors are also included, $\hat{\theta}(\psi)$ shows the greatest overestimation.

The parameters, $\hat{\alpha}$ and $\hat{n}$, are estimated by fitting the van Genuchten model to experimental $\hat{\theta}(\psi)$ curves. The spatial statistics of $\ln(\hat{\alpha})$ and $\ln(\hat{n})$ are least biased in the observation scenario and are best estimated for small geometric mean n. When equilibrium errors are added, the spatial statistics of $\ln(\hat{\alpha})$ change little from the observation error scenario, but the spatial statistics of $\ln(\hat{n})$ change significantly, especially when the geometric mean n is small. When boundary errors are also present, $\ln(\hat{\alpha})$ shows much more spatial bias, especially at high geometric mean n, and the spatial statistics of $\ln(\hat{n})$ show significant bias regardless of geometric mean n. Finally, when repacking errors are added, bias in spatial statistics increases further.

Although the "true" residual moisture content is zero for all of our simulated realities, we estimate a non-zero residual moisture content in order to achieve the best estimates of $\hat{\alpha}$ and $\hat{n}$ when equilibrium errors are present (equilibrium, boundary, and repacking error scenarios). Despite the fact that it is an artifact of the measurement

method, the residual moisture content shows realistic spatial statistics, including variograms that are readily fit with an exponential variogram model.

Parameters $\ln(\hat{\alpha})$ and $\ln(\hat{n})$ show strong apparent cross-correlation, which increases with added error and the non-linearity of the true moisture-characteristic curve. The apparent cross-correlation is a byproduct of using biased data in a non-linear inversion model to estimate multiple parameters. This problem might be eliminated through the use of single-parameter inversion models with independent data sets.

We examine the potential impact of measurement errors on flow and transport calculations by comparing the geometric mean unsaturated hydraulic conductivity, the mean moisture content, and their ratio (a surrogate for mean velocity) determined using our estimated parameters and the true parameters. At a tension of 500 cm, we find that the ratio may be either underestimated by up to two orders of magnitude or overestimated by over three orders of magnitude, depending on the error scenario and geometric mean n (material sorting). This suggests that robust modeling of flow and transport may not be possible using only laboratory-estimated data to parameterize the model.

Because most spatial variability studies rely on a limited number of samples, we examined the uncertainty in variogram-model parameters for $\ln(\hat{n})$, as a function of the number of variogram samples. We considered the case where the geometric mean n is 5.0. We found that errors due to a limited number of samples preclude reliable estimation of the model variance and correlation length, even when variograms are based on 1,000 samples.

In the absence of significant inversion-model errors, spatial statistics can be accurately estimated for parameters that are directly measured or have simple inversion models (e.g., porosity or hydraulic conductivity estimated from a Darcy column). When inversion models are highly non-linear, like the van Genuchten (1980) model, spatial bias caused by property-measurement error can become significant. Spatial bias in properties increases significantly in the presence of inversion-model errors, because their effect is unconstrained. Systematic inversion-model errors (e.g., equilibrium error) are insidious, because they cause spatial distortion without introducing significant noise. Random inversion-model errors (e.g., sample repacking) add noise to the property field and obscure spatial correlation. Alone, either of these types of error can cause significant bias in estimated spatial statistics. When combined, their effects can multiply. Because the number and nature of inversion-model errors is highly variable and often unknown, it may be impossible to remove their effects from the data using data processing tools.

3.9 REFERENCES CITED

Bosch, D. D., and L. T. West, 1998, Hydraulic conductivity variability for two sandy soils, *Soil Science Society of America Journal*, v. 62, p. 90-98.

Deutsch, C. V., and A. G. Journel, 1998, GSLIB: *Geostatistical Software Library and User's Guide*, 2nd ed., Oxford University Press, New York, NY, 369 pp.

Harter, T., and T. –C. Jim Yeh, 1996, Stochastic analysis of solute transport in heterogeneous, variably saturated soils, *Water Resources Research*, v. 32, p. 1585-1595.

Haverkamp, R., and J. –Y. Parlange, 1986, Predicting the water-retention curve from particle-size distribution: 1. Sandy soils without organic matter, *Soil Science*, v. 142, p. 325-339.

Healy, R. W., and P. C. Mills, 1991, Variability of an unsaturated sand unit underlying a radioactive-waste trench, *Soil Science Society of America Journal*, v. 55, p. 899-907

Hendrickx, J. M. H., 1990, Determination of hydraulic soil properties, in Process Studies in Hillslope Hydrology, M. G. Anderson and T. P. Burt eds., John Wiley and Sons, New York, NY, p. 43-86.

Hillel, D., 1980, *Fundamentals of Soil Physics*, Acdemic Press, New York, N.Y., 385 p.

Hopmans, J. W., H. Schukking, and P. J. J. F. Torfs, 1988, Two-dimensional steady state unsaturated water flow in heterogeneous soils with autocorrelated soil hydraulic properties, *Water Resources Research*, v. 24, p. 2005-2017.

Indelman, P., D. Or, and Y. Rubin, 1993, Stochastic analysis of unsaturated steady state

flow through bounded heterogeneous formations, *Water Resources Research*, v.

29, p. 1141-1148.

Istok, J. D., D. O. Blout, L. Barker, K. R. Johnejack, and D. P. Hammermeister, 1994,

Spatial variability in alluvium propertties at a low-level nuclear waste site, *Soil

Science Society of America Journal*, v. 58, p. 1040-1051.

Journel, A. G., and Ch. J. Huijbregts, 1978, *Mining Geostatistics*, Academic Press, Inc.,

New York, N.Y., 600 pp.

Klute A., 1986, , *Methods of Soil Analysis, Part 1, Physical and Mineralogical Methods*,

2nd ed., American Society of Agronomy, Agronomy Report 9 , Madision, WI.,

1188 p.

Mallants, D., B. P. Mohanty, D. Jacques, and J. Feyen, 1996, Spatial variability of

hydraulic properties in a multi-layered soil profile, *Soil Science*, v. 161, p. 167-

181.

Mantoglou, A. and L. W. Gelhar, 1987a, Capillary tension head variance, mean soil

moisture content, and effective specific soil moisture capacity of transient

unsaturated flow in stratified soils, *Water Resources Research*, v. 23, p. 47-56.

Mantoglou, A. and L. W. Gelhar, 1987b, Effective hydraulic conductivities of transient

unsaturated flow in stratified soils, *Water Resources Research*, v. 23, p. 57-67.

Mualem, Y., 1976, A new model for predictting the hydraulic conductivity of unsaturated

porous media, *Water Resources Research*, v. 12, p. 513-522.

Polmann, D. J., D. McLaughlin, S. Luis, L. W. Gelhar, and R. Ababou, 1991, Stochastic modeling of large-scale flow in heterogeneous unsaturated soils, *Water Resources Research*, v. 27, p. 1447-1458.

Robin, M. J. L., A. L. Gutjahr, E. A. Sudicky, and J. L. Wilson, Cross-correlated random field generation with the direct Fourier transform method, *Water Resources Research*, v. 29, p. 2385-2397.

Russo, D., 1995, Stochastic analysis of the velocity covariance and the displacement covariance tensors in partially saturated heterogeneous anisotropic porous formations, *Water Resources Research*, v. 31, p. 1647-1658.

Russo, D., and E. Bresler, 1981, Soil hydraulic properties as stochastic processes: I. An analysis of field spatial variability, *Soil Science Society of America Journal*, v. 45, p. 682-687.

Shouse, P. J., W. B. Russell, D. S. Burden, H. M. Selim, J. B. Sisson, and M. Th. van Genuchten, 1995, Spatial variability of soil water retention functions in a silt loam soil, *Soil Science*, v. 160, p. 1-12.

Shouse, P. J., and B. P. Mohanty, 1998, Scaling of near-saturated hydraulic conductivity measured using disc infiltrometers, *Water Resources Research*, v. 23, p. 1195-1205.

Stephens, D. B., 1995, *Vadose Zone Hydrology*, Lewis Publishers, Boca Raton, L.A. 347 p.

van Genuchten, M. Th., 1980, A closed –form equation for predicting the hydraulic conductivity of unsaturated soils, *Soil Science Society of America Journal*, v. 44, p. 892-898.

Wierenga, P. J., R. G. Hills, and D. B. Hudson, 1991, The Las Cruses Trench site: characterization, experimental Results, and one-dimensional flow predictions, *Water Resources Research*, v. 27, p. 2695-2705.

Yeh, T. –C. Jim, L. W. Gelhar, and A. L. Gutjahr, 1985a, Stochastic analysis of unsaturated flow in heterogeneous soils: 1. Statistically isotropic media, *Water Resources Research*, v. 21, p. 447-456.

Yeh, T. –C. Jim, L. W. Gelhar, and A. L. Gutjahr, 1985b, Stochastic analysis of unsaturated flow in heterogeneous soils: 2. Statistically isotropic media with variable α, *Water Resources Research*, v. 21, p. 457-464.

Yeh, T. –C. Jim, L. W. Gelhar, and A. L. Gutjahr, 1985c, Stochastic analysis of unsaturated flow in heterogeneous soils: 3. Observations and applications, *Water Resources Research*, v. 21, p. 465-471.

Zhang, D. Z., T. C. Wallstrom, and C. L. Winter, 1998, Stochastic analysis of steady-state unsaturated flow in heterogeneous media: Comparison of the Brooks-Corey and Gardner-Russo models, *Water Resources Research*, v. 34, p. 1437-1449.

CHAPTER 4 - ERROR IN UNSATURATED STOCHASTIC-MODELS PARAMETERIZED WITH FIELD DATA

4.1 ABSTRACT

We use Monte Carlo error analysis to evaluate the impact of measurement errors in field-estimated hydraulic properties on 1D and 3D unconditional unsaturated stochastic model results. Hydraulic properties are determined by simulating tension-infiltrometer measurements across a parameter space representative of poorly- to well-sorted, sandy silt to coarse sand. Two types of observation error are considered, along with one inversion-model error resulting from poor contact between the instrument and the medium. Errors in the spatial statistics of hydraulic properties cause critical stochastic model assumptions to be violated, limiting the parameter space usable in the model. Even where critical assumptions are valid, stochastic-model results show significant error, and the magnitude and pattern of error changes with mean tension and the type of measurement error considered. Mean velocities may show errors up to an order of magnitude. The velocity variance is overestimated by up to three orders of magnitude during 3D flow and eight orders of magnitude during 1D flow. The 1D velocity integral scale is underestimated by as much as five orders of magnitude. The estimates for 1D longitudinal macrodispersivity are surprisingly robust and show relatively small error across most of the parameter space.

4.2 INTRODUCTION

Since the landmark work of Freeze (1975), stochastic theory for flow and transport in permeable media has advanced and matured, but the application of stochastic models in risk-based decision processes has been disappointing, especially for unsaturated media. The under-use of unsaturated stochastic models can be partly attributed to difficulties in collecting the required unsaturated hydraulic property data. For example, samples are difficult to remove intact and many field instruments employ observations of capillary pressure that rely on direct hydraulic contact with the medium. Furthermore, unsaturated hydraulic properties are not directly observed, but are estimated indirectly. Typically, a hydrologic system is perturbed, the system response to the perturbation is observed, and the observed response is then used in a non-linear inversion model to infer property values. "Measurement errors" in hydraulic properties arise from errors in both the observations and the inversion model and are correlated with the "true" hydraulic properties (Chapters 2 and 3). As a result, the spatial statistics of estimated hydraulic properties are biased, even when very small observation or inversion-model errors affect measurements (Chapters 2 and 3), and it is likely that this bias will affect stochastic-model results. When used in risk-based decision processes, for example at contaminated sites, errors in stochastic models can have serious consequences, in the form of ineffective monitoring, poor remedial designs, and increased cost and risk to the public.

We believe that measurement errors in field-estimated hydraulic properties can cause significant bias, or systematic distortion, of stochastic model results. Our objective

is to quantify the effects of measurement errors on unconditional stochastic flow and transport models. We use Monte Carlo error analysis to evaluate error in unsaturated stochastic model results, specifically stochastic estimates of the mean, variance, and integral scale of the fluid velocity and the longitudinal macrodispersivity. We focus on the ensemble statistics for the velocity, because velocity fields or moments are required input for contaminant transport calculations. The mean velocity is inversely proportional to mean travel time. The ensemble velocity variance measures the point variability in velocity over all possible realizations and is, therefore, a metric for the uncertainty in travel time over short travel distances. The integral scale of the velocity is a measure of the continuity of the ensemble flow field. The longitudinal macrodispersivity can be related to the uncertainty in mean travel times, especially over large travel distances.

We chose two different stochastic models for our analysis, each representing end-members in the style of heterogeneity. The first is based on the seminal work of Yeh et al. (1985a, b), where it is assumed that hydraulic parameters are statistically isotropic. The second model is that of Zhang et al. (1998), where the hydraulic parameters are perfectly layered. Geologic materials lie between these two extremes, with most materials showing distinct layering.

We use the tension-infiltrometer (Reynolds and Elrick, 1991), which can provide the hydraulic property data required by the stochastic models. Required properties include the saturated hydraulic conductivity and the pore-size distribution parameter for the exponential unsaturated hydraulic conductivity model. Two types of observation error are used in the analysis, along with one inversion-model error resulting from poor contact between the instrument and the medium. We follow the approach of Chapter 2 to

113

estimate spatial statistics of unsaturated hydraulic properties from the tension infiltrometer, which are then used to estimate the mean, variance, and integral scale of velocity and the longitudinal macrodispersivity. We then assess the errors in these stochastic model results.

4.3   BACKGROUND

For calculating the mean, variance, and integral scale of velocity and the longitudinal macrodispersivity, we modify steady flow stochastic models presented by Yeh et al. (1985a, b) and Zhang et al. (1998). We extend the work of Yeh et al. (1985a, b) and derive a mean and variance of the velocity for three-dimensional unsaturated flow through statistically isotropic media under mean unit-gradient conditions with spatially varying effective moisture content. Zhang et al. (1998) developed models for unit-gradient flow through perfectly stratified media (one-dimensional flow), including expressions for the mean and variance of velocity. For the model of Zhang et al., we derive additional expressions for the velocity integral scale and the longitudinal macrodispersivity. We review critical components of these models and their extensions below.

These steady flow models satisfy continuity

$$\nabla \cdot \mathbf{q}(\mathbf{x}) = 0 \qquad\qquad (4\text{-}1)$$

and Darcy's law

$$q_i(\mathbf{x}) = -K(\mathbf{x})\left[-\frac{\partial h(\mathbf{x})}{\partial x_i} - \delta_{i1}\right] \qquad (4\text{-}2)$$

where $\mathbf{q}$ is the specific discharge vector, $h(\mathbf{x})$ is the absolute value of the tension head, $K(\mathbf{x})$ is the unsaturated hydraulic conductivity scalar which is a random space function, and $\delta_{i1} = 1$ when i equals 1, representing the vertical direction, and $\delta_{i1} = 0$ otherwise. We assume that $K(\mathbf{x})$ is log-normally distributed and that $Y(\mathbf{x}) = \ln[K(\mathbf{x})]$, which may be decomposed into a mean and perturbation, $Y(\mathbf{x}) = \langle Y(\mathbf{x})\rangle + Y'(\mathbf{x})$. Similarly, we have $q_i(\mathbf{x}) = \langle q_i(\mathbf{x})\rangle + q'_i(\mathbf{x})$ and $h(\mathbf{x}) = \langle h(\mathbf{x})\rangle + h'(\mathbf{x})$, and (4-2) can be re-written as

$$\langle q_i(\mathbf{x})\rangle + q'_i(\mathbf{x}) = K^G(\mathbf{x})\left[1 + Y'(\mathbf{x}) + \frac{Y'^2}{2} + \ldots\right]\left[\frac{\partial\langle h(\mathbf{x})\rangle}{\partial x_i} + \frac{\partial h'(\mathbf{x})}{\partial x_i} + \delta_{i1}\right] \qquad (4\text{-}3)$$

where $K^G(\mathbf{x}) = \exp[\langle Y(\mathbf{x})\rangle]$ is the geometric mean of $K(\mathbf{x})$. Taking the expected value of (4-3) and retaining terms up to first order gives

$$\langle q_i(\mathbf{x})\rangle = K^G(\mathbf{x})J_i(\mathbf{x}) \qquad (4\text{-}4)$$

where $J_i(\mathbf{x}) = \left(\partial\langle h(x)\rangle/\partial x_i\right) + \delta_{i1}$ is the mean hydraulic gradient in the direction x_i. Following most stochastic models (e.g., Yeh et al., 1985a, b; Russo, 1993, 1995; Harter and Yeh, 1996; Yang et al., 1996; Zhang et al., 1998), we assume that flow is dominated by gravity and that $J_i(\mathbf{x}) = \delta_{i1}$. Subtracting (4-4) from (4-3) and retaining terms up to first order yields

$$q'_i(\mathbf{x}) = K^G \left[j_i(\mathbf{x}) + \delta_{i1} Y'(\mathbf{x}) \right] \qquad (4\text{-}5)$$

where $j_i(\mathbf{x}) = -\partial h'(\mathbf{x})/\partial x_i$ is the perturbation in the gradient. The single point

covariance of the specific discharge $\sigma^2_{q_{i,j}} = \langle q'_i(\mathbf{x}) q'_j(\mathbf{x}) \rangle$ is

$$\sigma^2_{q_{ij}} = K^{G^2} \left[\sigma^2_{j_{ji}} + \delta_{i1} \sigma^2_{Y'j_i} + \delta_{j1} \sigma^2_{Y'j_j} + \delta_{i1} \delta_{j1} \sigma^2_{Y'} \right] \qquad (4\text{-}6)$$

where $\sigma^2_{j_{i,j}}$ is the single point covariance of the gradient in the i and j directions, $\sigma^2_{Y'j_i}$ is

the single point covariance between $Y'(\mathbf{x})$ and $j_i(\mathbf{x})$, and $\sigma^2_{Y'}$ is the variance of $Y'(\mathbf{x})$.

The seepage velocity, u_i is related to the specific discharge, q_i, by

$$u_i(\mathbf{x}) = \frac{q_i(\mathbf{x})}{\theta_e(\mathbf{x})} \qquad (4\text{-}7)$$

where $\theta_e = \theta - \theta_{im}$ is the effective volumetric moisture content, θ is the volumetric

moisture content, and θ_{im} is the immobile moisture content. We follow Zhang et al.

(1998) and assume that immobile moisture does not affect advective transport. With

$\theta_e = \langle \theta_e \rangle + \theta'_e$, the velocity (4-7) can be written as

$$u_i(\mathbf{x}) = \frac{\langle q_i \rangle + q'_i(\mathbf{x})}{\langle \theta_e \rangle} \left[1 - \frac{\theta'_e(\mathbf{x})}{\langle \theta_e \rangle} + \frac{\theta'^2_e(\mathbf{x})}{\langle \theta_e \rangle^2} + \cdots \right] \qquad (4\text{-}8)$$

To the first order, the mean velocity is

$$\langle u_i \rangle = \frac{\langle q_i \rangle}{\langle \theta_e \rangle} , \qquad (4\text{-}9)$$

The perturbation in velocity is

116

$$u'_i(\mathbf{x}) = \frac{q'_i(\mathbf{x})}{\langle \theta_e \rangle} - \frac{\langle q_i \rangle \theta'_e(\mathbf{x})}{\langle \theta_e \rangle^2} , \tag{4-10}$$

and the variance of the velocity is

$$\sigma^2_{u_{ij}} = \frac{1}{\langle \theta_e \rangle^2}\left(\sigma^2_{q_{ij}} - \langle u_i \rangle \sigma^2_{q_j \theta_e} - \langle u_j \rangle \sigma^2_{q_i \theta_e} + \langle u_i \rangle \langle u_j \rangle \sigma^2_{\theta_e}\right) , \tag{4-11}$$

where $\sigma^2_{q_i \theta_e}$ is the single point covariance between the specific discharge, q_i, and the

effective moisture content, θ_e, and $\sigma^2_{\theta_e}$ is the variance of the effective moisture content.

In deriving (4-9), it is assumed that $\sigma^2_{\theta_e}/\langle \theta_e \rangle^2$ is small ($<< 1$).

In order to derive the statistical moments required for parameterizing (4-9) and (4-11), we must specify constitutive models for K and θ_e as functions of tension h. Because of its mathematical simplicity, the Gardner-Russo (Gardner, 1958; Russo, 1988) model is commonly used for analytical modeling of stochastic unsaturated flow and transport (e.g., Yeh et al., 1985a, b; Russo, 1993, 1995; Indelman et al., 1993; Yang et al., 1996; Zhang et al., 1998). The Gardner (1958) model for unsaturated hydraulic conductivity is

$$K(\mathbf{x}) = K_s(\mathbf{x}) \exp\left[- \alpha(\mathbf{x}) h(\mathbf{x})\right] \tag{4-12}$$

where $\alpha(\mathbf{x})$ is the slope of $\ln[K(\mathbf{x})]/h(\mathbf{x})$, and $K_s(\mathbf{x})$ is the saturated hydraulic conductivity. The Russo (1988) moisture content function is

$$\theta_e = (\theta_s - \theta_r)\{[1 + 0.5\alpha(\mathbf{x})h(\mathbf{x})]\exp[- 0.5\alpha(\mathbf{x})h(\mathbf{x})]\}^{2/(m+2)} \tag{4-13}$$

where m is a parameter related to media tortuosity and θ_s is the saturated moisture content. We assume that $\alpha(\mathbf{x})$ and the log transform of the saturated hydraulic conductivity $f(\mathbf{x}) = \ln[K_s(\mathbf{x})]$ are normally distributed, second-order stationary random

117

space functions, each consisting of a constant mean and a spatially varying perturbation:

$f(\mathbf{x}) = \langle f \rangle + f'(\mathbf{x})$ and $\alpha(\mathbf{x}) = \langle \alpha \rangle + \alpha'(\mathbf{x})$. Our previous studies (Chapter 2.0 and

Chapter 3.0) suggest that measurement errors can induce an apparent correlation between

estimates of $\alpha(\mathbf{x})$ and $f(\mathbf{x})$ even when there is none. Nevertheless, we assume that the

spatial covariance between $\alpha(\mathbf{x})$ and $f(\mathbf{x})$ is zero, because it is difficult to define a

physically meaningful positive semi-definite cross-covariance function. The log

transform of (4-12) is

$$Y(\mathbf{x}) = \langle f \rangle + f'(\mathbf{x}) - \left[\langle \alpha \rangle + \alpha'(\mathbf{x}) \right]\left[\langle h \rangle + h'(\mathbf{x}) \right] \qquad (4\text{-}14)$$

with, to the first order

$$\langle Y \rangle = \langle f \rangle - \langle \alpha \rangle \langle h \rangle \qquad (4\text{-}15)$$

$$Y'(\mathbf{x}) = f'(\mathbf{x}) - \langle h \rangle \alpha'(\mathbf{x}) - \langle \alpha \rangle h'(\mathbf{x}) \qquad (4\text{-}16)$$

$$\sigma_{Y'}^2 = \sigma_f^2 + \langle h \rangle^2 \sigma_\alpha^2 + \langle \alpha \rangle^2 \sigma_h^2 - 2\langle \alpha \rangle \sigma_{fh}^2 + 2\langle h \rangle \langle \alpha \rangle \sigma_{\alpha h}^2 \qquad (4\text{-}17)$$

where σ_f^2 is the variance of $\ln[K_s(\mathbf{x})]$, σ_α^2 is the variance of $\alpha(\mathbf{x})$, σ_h^2 is the tension

head variance, σ_{fh}^2 is the point covariance between $f(\mathbf{x})$ and $h(\mathbf{x})$, and $\sigma_{\alpha h}^2$ is the point

covariance between $\alpha(\mathbf{x})$ and $h(\mathbf{x})$. In deriving (4-15), we assumed that $\sigma_{\alpha h}^2$ is small

(<<1). Because we assume that the hydraulic head is a stationary random process,

therefore the point covariance between the head perturbation and its gradient $\sigma_{hj_i}^2$ is

identically equal to zero, and the point covariance between $Y'(\mathbf{x})$ and $j_i(\mathbf{x})$ is then

$$\sigma^2_{Y'j_i} = \sigma^2_{f j_i} - \langle h \rangle \sigma^2_{\alpha j_i} \qquad (4\text{-}18)$$

where $\sigma^2_{f j_i}$ is the point covariance between $f(\mathbf{x})$ and $j_i(\mathbf{x})$ and $\sigma^2_{\alpha j_i}$ is the point

covariance between $\alpha(\mathbf{x})$ and $j_i(\mathbf{x})$. The first-order mean, perturbation, and variance of

the effective water content are (Zhang et al., 1998)

$$\langle \theta_e \rangle = (\theta_s - \theta_r) \exp\left[-\langle \alpha \rangle \langle h \rangle / (m+2)\right]\left[1 + 0.5 \langle \alpha \rangle \langle h \rangle\right]^{2/(m+2)} \qquad (4\text{-}19)$$

$$\theta'_e(\mathbf{x}) = \frac{\langle \theta_e \rangle}{(2 + \langle \alpha \rangle \langle h \rangle)(m+2)}\left(\langle \alpha \rangle \langle h \rangle^2 \alpha'(\mathbf{x}) + \langle \alpha \rangle^2 \langle h \rangle h'(\mathbf{x})\right) \qquad (4\text{-}20)$$

$$\sigma^2_{\theta_e} = \frac{\langle \theta_e \rangle^2}{(2 + \langle \alpha \rangle \langle h \rangle)^2 (m+2)^2}\left(\langle \alpha \rangle^2 \langle h \rangle^4 \sigma^2_\alpha + 2\langle \alpha \rangle^3 \langle h \rangle^3 \sigma^2_{\alpha h} + \langle \alpha \rangle^4 \langle h \rangle^2 \sigma^2_h\right) \qquad (4\text{-}21)$$

The point covariance between q_i and θ_e is

$$\sigma^2_{q_i \theta_e} = \frac{\langle \theta_e \rangle K^G}{(2 + \langle \alpha \rangle \langle h \rangle)(m+2)}\left(\begin{array}{c} \delta_{i1}\langle \alpha \rangle^2 \langle h \rangle \sigma^2_{fh} + \langle \alpha \rangle \langle h \rangle^2 \sigma^2_{\alpha j_i} - 2\delta_{i1}\langle \alpha \rangle^2 \langle h \rangle^2 \sigma^2_{\alpha h} \\ -\delta_{i1}\langle \alpha \rangle \langle h \rangle^3 \sigma^2_\alpha - \delta_{i1}\langle \alpha \rangle^3 \langle h \rangle \sigma^2_h \end{array}\right) \quad (4\text{-}22)$$

We assume that the spatial structure of $f(\mathbf{x})$ and $\alpha(\mathbf{x})$ is completely described

by an exponential covariance function

$$C_p(\mathbf{r}) = \sigma_p^{\ 2} \exp\left(-\frac{|\mathbf{r}|}{\lambda_p}\right) \qquad (4\text{-}23)$$

where $C_p(\mathbf{r})$ is the covariance function as a function of separation distance $\mathbf{r}$, σ_p^2 is the

variance, and λ_p is the correlation length of parameter p. With this covariance function

we are able to derive relationships for σ^2_h, σ^2_{fh}, $\sigma^2_{\alpha h}$, $\sigma^2_{f j_i}$, $\sigma^2_{\alpha j_i}$, and $\sigma^2_{j_i}$ (Table 1 with

equation numbers 4-24 to 4-37) and determine the ensemble mean and variance of the

velocity, which can be related to contaminant transport times.

119

Statistic	3D Isotropic [1]	1D/3D Perfectly Stratified [2]
σ_h^2	$\dfrac{\sigma_f^2}{\langle\alpha\rangle^2}F_1(\lambda_f)+\dfrac{\langle h\rangle^2\sigma_\alpha^2}{\langle\alpha\rangle^2}F_1(\lambda_\alpha)$ (4-24)	$\dfrac{\sigma_f^2\lambda_f}{(1+\langle\alpha\rangle\lambda_f)\langle\alpha\rangle}+\dfrac{\langle h\rangle^2\sigma_\alpha^2\lambda_\alpha}{(1+\langle\alpha\rangle\lambda_\alpha)\langle\alpha\rangle}$ (4-25)
σ_{fh}^2	$\dfrac{\sigma_f^2}{\langle\alpha\rangle}F_1(\lambda_f)$ (4-26)	$\dfrac{\sigma_f^2\lambda_f}{(1+\langle\alpha\rangle\lambda_f)}$ (4-27)
$\sigma_{\alpha h}^2$	$-\dfrac{\langle h\rangle\sigma_\alpha^2}{\langle\alpha\rangle}F_1(\lambda_\alpha)$ (4-28)	$-\dfrac{\langle h\rangle\sigma_\alpha^2\lambda_\alpha}{(1+\langle\alpha\rangle\lambda_\alpha)}$ (4-29)
σ_{fj}^2	$-\dfrac{\langle h\rangle\sigma_\alpha^2}{\langle\alpha\rangle}F_2(\lambda_\alpha)$ (4-30)	$\dfrac{\sigma_f^2}{(1+\langle\alpha\rangle\lambda_f)}$ (4-31)
$\sigma_{\alpha j}^2$	$-\langle h\rangle\sigma_\alpha^2 F_2(\lambda_\alpha)$ (4-32)	$-\dfrac{\langle h\rangle\sigma_\alpha^2}{(1+\langle\alpha\rangle\lambda_\alpha)}$ (4-33)
σ_j^2	$\sigma_f^2 F_3(\lambda_f)+\langle h\rangle^2\sigma_\alpha^2 F_3(\lambda_\alpha)$ (4-34)	**N/A**
$F_1(\lambda_p)$ [1]	$1-\dfrac{2\ln(1+\langle\alpha\rangle\lambda_p)}{\langle\alpha\rangle\lambda_p}+\dfrac{1}{1+\langle\alpha\rangle\lambda_p}$ (4-35)	
$F_2(\lambda_p)$ [1]	$\dfrac{2}{\langle\alpha\rangle^2\lambda_p^2}\left[1-\dfrac{2\ln(1+\langle\alpha\rangle\lambda_p)}{\langle\alpha\rangle\lambda_p}+\dfrac{1}{1+\langle\alpha\rangle\lambda_p}\right]-\dfrac{1}{1+\langle\alpha\rangle\lambda_p}$ (4-36)	
$F_3(\lambda_p)$ [1]	$\dfrac{1}{2\langle\alpha\rangle\lambda_p}-\dfrac{1}{\langle\alpha\rangle^2\lambda_p^2}+\dfrac{2}{\langle\alpha\rangle^3\lambda_p^3}-\dfrac{5}{\langle\alpha\rangle^4\lambda_p^4}$ $-\dfrac{1}{\langle\alpha\rangle^5\lambda_p^5}\left(\dfrac{\langle\alpha\rangle\lambda_p}{1+\langle\alpha\rangle\lambda_p}-6\ln\left|1+\langle\alpha\rangle\lambda_p\right|\right)$ (4-37)	

Table 4-1. Required stochastic functions for the Gardner-Russo model, [1] From Yeh et al. (1985) and [2] from Zhang et al. (1998).

The integral scale of the vertical velocity in the vertical direction is

$$I_{u_1} = \frac{1}{\sigma_{u_1}^2} \int_0^\infty C_{u_1}(\mathbf{r}) \, d\mathbf{r} \qquad (4\text{-}38)$$

$C_{u_1}(\mathbf{r})$

where $C_{u_1}(\mathbf{r})$ is the vertical velocity covariance. Using the Zhang et al.'s (1998)

expression for $C_{u_1}(\mathbf{r})$ (their Equation 61) for (4-11), the integral scale for the velocity

during 1D vertical flow can be shown to be

$$I_{u_1} = \frac{\langle u_1 \rangle^2 \langle \alpha \rangle^2 \langle h \rangle^2 \sigma_f^2 \lambda_f}{\left(2 + \langle \alpha \rangle \langle h \rangle\right)^2 (m+2) \sigma_{u_1}^2} \qquad (4\text{-}39)$$

The longitudinal macrodispersivity can be defined as

$$A_1 = \frac{1}{\langle u_1 \rangle} \int_0^t C_{u_1}\left(\langle u_1 \rangle t'\right) dt' = \frac{1}{\langle u_1 \rangle^2} \int_0^z C_{u_1}(r) \, dr \qquad (4\text{-}40)$$

where $z = \langle u_1 \rangle t$ is the mean travel distance of a solute plume. For very large mean travel

distances ($z \to \infty$), A_1 approaches a constant value given by

$$A_1 = \frac{\sigma_{u_1}^2}{\langle u_1 \rangle^2} I_{u_1} \qquad (4\text{-}41)$$

4.4 METHODS

The tension infiltrometer is commonly used for determining the spatial statistics

of the log saturated conductivity f and the slope parameter α (e.g., DOE, 1993; Mohanty,

et al., 1994; Jarvis and Messing, 1995; Shouse and Mohanty, 1998), which are needed to

estimate the ensemble statistics of the velocity and the macrodispersivity. It is a simple

121

device for applying a constant (negative) pressure boundary condition to unsaturated soil (Figure 4-1). The design and operation of the tension infiltrometer is described by Ankeny et al. (1988). With knowledge of two applied pressures and corresponding observed steady-state flux rates, parameters f and α can be estimated using the analytical approximation of Wooding (1968).
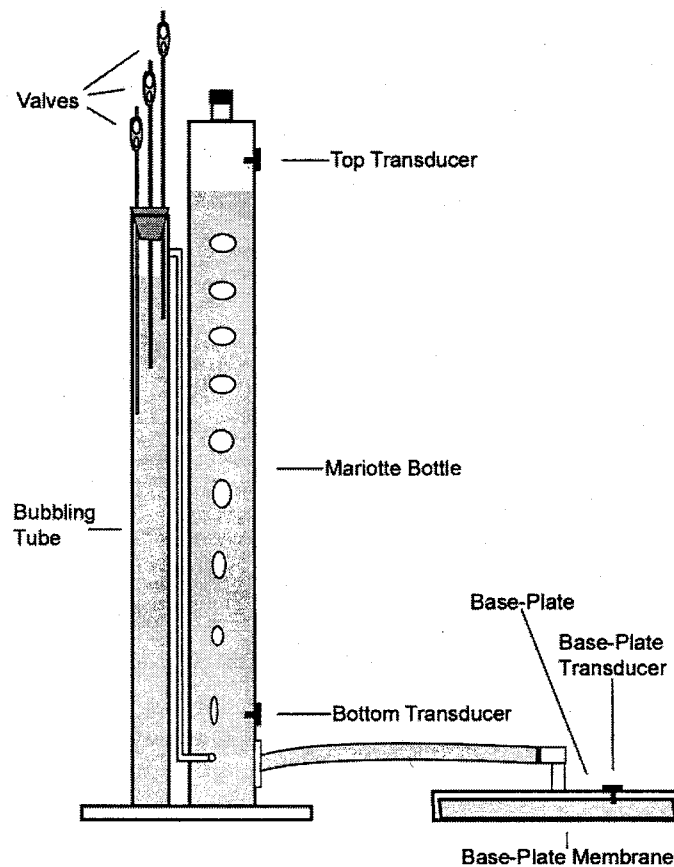

Figure 4-1. Schematic of the tension infiltrometer. Observation errors are due to unbiased noise in the three transducers used to measure the flow rate and applied tension. The base plate membrane is in contact with the soil "sample".

We employ a Monte Carlo approach to conduct our analysis, following the approach in Chapter 2. We generate 221 pairs of statistically homogeneous Gaussian random fields of the log saturated hydraulic conductivity $f(\mathbf{x})$ and the exponential parameter $\alpha(\mathbf{x})$, with $\text{cov}[f(\mathbf{x}), \alpha(\mathbf{x})] = 0$. Each combined field of $f(\mathbf{x})$ and $\alpha(\mathbf{x})$ constitutes an artificial reality. At every spatial location in a Monte Carlo simulation, we estimate the true flux and applied tension, add observation error to these values, and re-estimate $f(\mathbf{x})$ and $\alpha(\mathbf{x})$. We assume that (4-12) describes the unsaturated hydraulic conductivity, (4-13) describes the moisture-characteristic function, and the parameter m in (4-13) is known and equal to 0. We also assume that Wooding's (1968) approximation is exact, and that sub-sample-scale heterogeneity does not exist. As in Chapter 2, we consider only two error scenarios. In the first, transducer errors yield errors in observations of flux-rates and applied pressures. The second includes the observation errors but adds an error in the contact between the disk and the medium. As in practice, physically implausible results are rejected during the re-estimation. We calculate the spatial statistics (mean, variance, and correlation length) for the estimated fields of $f(\mathbf{x})$ and $\alpha(\mathbf{x})$. These spatial statistics along with the true spatial statistics of the fields are used to determine error in the ensemble statistics of velocity and the macrodispersion coefficient. Relevant details are discussed below.

For each Monte Carlo simulation, we generate over 26,000 pairs (a 512 by 512 random field) of $f(\mathbf{x})$ and $\alpha(\mathbf{x})$, with a fixed mean and variance. The means of $f(\mathbf{x})$ and $\alpha(\mathbf{x})$ are varied between simulations, while the variance of $f(\mathbf{x})$ remains fixed at 1.0 and the coefficient of variation (CV) for $\alpha(\mathbf{x})$ is fixed at 0.1. Mean values vary across

a parameter space representative of poorly to well-sorted silty sand to very coarse sand.
We vary the mean of α from 10^{-4} cm^{-1} (poorly sorted) to 0.1 cm^{-1} (well sorted), and we
vary the geometric mean of the unsaturated hydraulic conductivity $K_s^G = \exp(\langle f(\mathbf{x}) \rangle)$
from 10^{-5} cm/s (sandy silt) to 0.1 cm/s (coarse sand). Our treatment of $\alpha(\mathbf{x})$ differs from
that of Chapter 2 where $\alpha(\mathbf{x})$ was log-normally distributed with a variance of $\ln(\alpha)$ equal
to 1.0.

Random fields are generated using the FFT method (e.g., Robin et al., 1993). We
employ a 2D, isotropic, exponential variogram model

$$\gamma(\mathbf{r}) = \sigma^2 \left[1 - \exp\left(-\frac{\mathbf{r}}{\lambda} \right) \right] \qquad (4\text{-}42)$$

where σ^2 is the variance of the random process and λ is the correlation length. In
stochastic models, it is often assumed that the correlation lengths of unsaturated
parameters are the same (e.g., Yeh et al., 1985a, b, c; Mantoglou and Gelhar, 1987a, b),
and for convenience, we set all correlation lengths equal to 10 length units (grid
increments). Across our entire parameter space, we conduct $13 \times 17 = 221$ Monte Carlo
simulations, in which the mean of $f(\mathbf{x})$ is incremented by steps of size 0.576 and the
mean of $\alpha(\mathbf{x})$ is multiplied by 1.78 between simulations.

We follow the procedures described in Chapter 2 for determining the spatial
statistics of hydraulic properties estimated with the tension infiltrometer. The procedures
are summarized below, but the reader is referred to Chapter 2 for details. Using the
tension infiltrometer, $f(\mathbf{x})$ and $\alpha(\mathbf{x})$ can be estimated from two observed steady-state
flux rates, $\hat{Q}_1$ and $\hat{Q}_2$, at the applied tensions $\hat{h}_1$ and $\hat{h}_2$. We assume that the tension

values employed for each observation are estimated to be $\hat{h}_1 = 2.0$ cm and $\hat{h}_2 = 7.0$ cm and that $\hat{h} = h + \xi$, where ξ is a random error. The true tensions (h_n) are calculated by subtracting ξ from $\hat{h}_n$, for $n = 1,2$. For each observation, the value of ξ is determined by randomly sampling a mean-zero normal distribution with $\sigma_\xi^2 = 0.4$ cm^2 (see Chapter 2). Given h_n, α, and $K_s = \exp(f)$, we calculate the true flux from the tension infiltrometer using (Wooding, 1968)

$$Q_n = \frac{K_s}{\alpha} e^{-\alpha h_n} \left(\alpha + \frac{4}{\pi r_d} \right) \pi r_d^2 \qquad (4\text{-}43)$$

where r_d is the radius of the disk and is equal to 10 cm. Once the true flux rate is determined, we calculate the estimated flux $\hat{Q}_n$ by adding mean-zero, normally distributed error with $\sigma_Q^2 = 0.00165$ cm^4/s^2 (see Chapter 2). Sampling locations where $\hat{Q}_1 \leq \hat{Q}_2$ are discarded, as they would be in practice.

When contact errors are considered, we follow Chapter 2.0 and assume that all contact error occurs at the outside of the disk, effectively reducing the disk radius. We also assume that contact errors only occur when measurements are made at the higher tension (h_2). $\hat{Q}_1$ is estimated using the procedure outlined above, while $\hat{Q}_2$ is estimated using the same variance for σ_Q^2 but is estimated using an altered disk radius $r_d^* = r_d \sqrt{1-g}$, where g is randomly sampled from a uniform distribution over 0.0 to 0.1. This means that the disk radius may be reduced from 10 cm to a minimum of ~ 9.5 cm.

125

Once the estimated tensions ($\hat{h}_1$ and $\hat{h}_2$) and steady-state flux rates ($\hat{Q}_1$ and $\hat{Q}_2$) are determined, the relative permeability parameter, α, is then estimated with (Reynolds and Elrick, 1991)

$$\hat{\alpha} = \frac{\ln(\hat{Q}_1 / \hat{Q}_2)}{\hat{h}_2 - \hat{h}_1} \qquad (4\text{-}44)$$

and f is estimated with

$$\hat{f} = \ln\left(\frac{\hat{\alpha}\, \hat{Q}_1 e^{\hat{\alpha}\hat{h}_1}}{\hat{\alpha}\, \pi r_d^2 + 4\, r_d} \right) \qquad (4\text{-}45)$$

This procedure is repeated for all points in a reality.

The mean, variance, correlation length are determined for each of our 221 sets of true fields [$f(\mathbf{x})$ and $\alpha(\mathbf{x})$] and estimated fields [$\hat{f}(\mathbf{x})$ and $\hat{\alpha}(\mathbf{x})$]. Local variograms are calculated using the GSLIB subroutine gam2 (Deutsch and Journel, 1998)

$$\gamma(\mathbf{r}) = \frac{1}{2\,N(\mathbf{r})} \sum_{i=1}^{N(\mathbf{h})} \left[U(\mathbf{x}_i + \mathbf{r}) - U(\mathbf{x}_i)\right]^2 \qquad (4\text{-}46)$$

where $N(\mathbf{r})$ is the number of samples in lag interval $\mathbf{r}$ and $U(\mathbf{x})$ is the random field. The variograms are fit, using a Levenberg-Marquardt algorithm, with the exponential variogram model

$$\gamma(\mathbf{r}) = \sigma^2 \left[1 - \exp\left(-\frac{\mathbf{r}}{\lambda} \right) \right] + \sigma_n^2 \qquad (4\text{-}47)$$

where λ is the estimated correlation length, σ^2 is the variance (referred to as the model variance in Chapters 2 and 3), and σ_n^2 is the nugget variance. When a variogram is constant for all lag distances we refer to it as a "nugget variogram" in which $\sigma^2 = 0.0$

126

and $\lambda = 0.0$. Once the spatial statistics are determined, the mean and variance of the 3D and 1D velocity is calculated for all 221 sets of true fields and estimated fields using (4-9) and (4-11) and the appropriate subsidiary equations. Similarly, the 1D velocity integral scale and longitudinal macrodispersivity are determined from (4-39) and (4-41), respectively. Errors are quantified in contour maps of parameter space, using the ratio of the "estimated"/"true" value.

4.5   ERRORS IN SPATIAL STATISTICS

The stochastic models used in this study are parameterized with the spatial statistics for estimated saturated conductivity $\hat{f}$ and the exponential parameter $\hat{\alpha}$. Because errors in these spatial statistics directly contribute to errors in the stochastic model results, we first present and discuss errors in our input spatial statistics, which differ from those presented in Chapter 2 because we have assumed a normal distribution for α with a CV fixed at 0.1. In Chapter 2 we assumed that α was log-normally distributed, with a variance of 1.0. That translates to a $\text{var}[\alpha(\mathbf{x})] = 5 \times 10^{-8}$ cm^{-2}, at a geometric mean α of 10^{-4} cm^{-1}, and a $\text{var}[\alpha(\mathbf{x})] = 5 \times 10^{-2}$ cm^{-2}, at a geometric mean α of 0.1 cm^{-1}. In contrast, the variance of α used here is much smaller, ranging from 10^{-8} cm^{-2} at $\langle \alpha \rangle = 10^{-4}$ cm^{-1} to 10^{-4} cm^{-2} at $\langle \alpha \rangle = 0.1$ cm^{-1}.

In Chapter 2 we saw that both observation and contact errors lead to biased estimates of the exponential parameter $\langle \hat{\alpha} \rangle$, especially at small values of saturated conductivity $\langle f \rangle$ and high $\langle \alpha \rangle$. Our results here are similar, as shown in the parameter

space plots of error (Figure 4-2a and 4-2b). Errors in the log-flux ratio, $\ln\left(\hat{Q}_1/\hat{Q}_2\right)$ from

(4-44), are large at high $\langle\alpha\rangle$ (see Chapter 2) and $\hat{Q}_1$ tend to be overestimated, while $\hat{Q}_2$

is underestimated at small $\langle f\rangle$ (see Chapter 2). It is obvious from (4-44) that both of

these conditions cause overestimation of $\hat{\alpha}$. When contact errors are present (Figure 4-

2b), $\langle\hat{\alpha}\rangle$ is significantly overestimated at low $\langle\alpha\rangle$. Contact errors cause underestimation
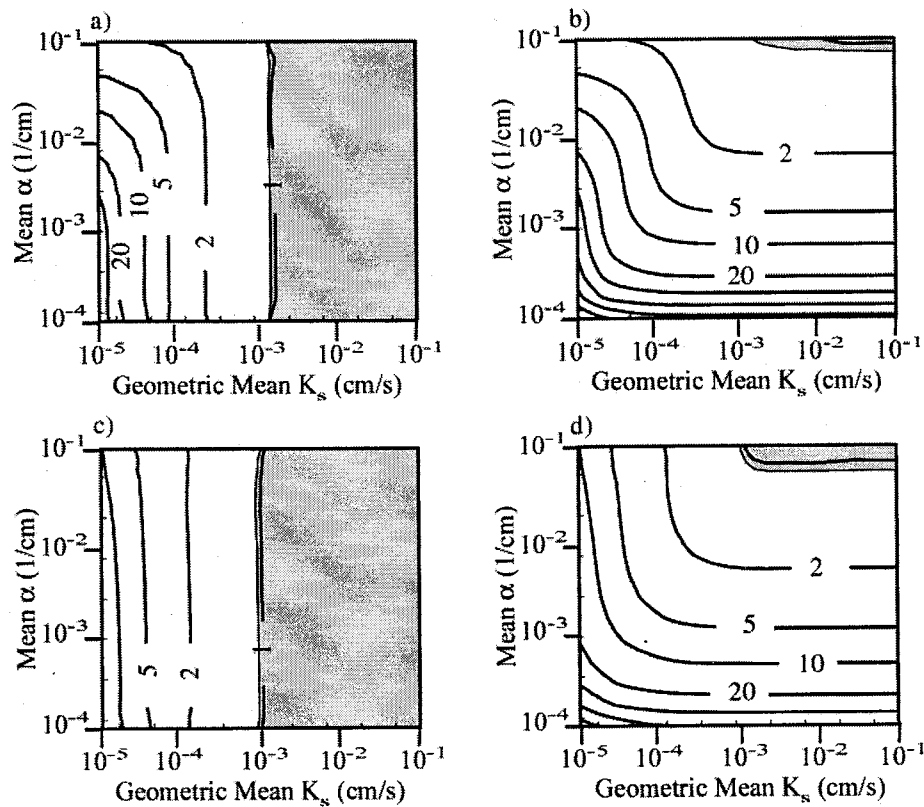

Figure 4-2. Ratio of the "estimated" to "true" geometric mean α for a) observation

scenario, b) contact-error scenario. Ratio "estimated" to "true" geometric mean K_s for c)

observation scenario, d) contact-error scenario. Accurate regions ("estimated"/"true"

between 0.95 and 1.05) are shaded.

of $\hat{Q}_2$, leading to an increase in the flux ratio and erroneously high $\hat{\alpha}$ (see Chapter 2). These effects are most pronounced at low $\langle \alpha \rangle$, where the true flux ratio tends to be very small.

Errors in the $\langle \hat{f} \rangle$ are similar to those shown in Chapter 2 and increase at small $\langle f \rangle$, on the left side of Figure 4-2c and 4-2d. From (4-45) we can see that $\hat{f}$ is proportional to $\hat{Q}_1$ and $\hat{\alpha}$. Both $\hat{Q}_1$ or $\hat{\alpha}$ tend to be overestimated at small $\langle f \rangle$, causing overestimation of $\langle \hat{f} \rangle$. When the contact error is present (Figure 4-2d), $\hat{\alpha}$ tends to be greatly overestimated at low $\langle \alpha \rangle$, leading to significant overestimation of $\langle \hat{f} \rangle$.

Errors in $\sigma_{\hat{\alpha}}^2$, the variance of $\hat{\alpha}$, follow a similar pattern to those shown in Chapter 2 and increase with decreasing $\langle f \rangle$ and $\langle \alpha \rangle$, as shown in the lower left corner of Figure 4-3a. However, the magnitude of the error in this case is much greater across most of the parameter space, because the variance of α is much smaller here. In contrast to the results of Chapter 2 $\lambda_{\hat{\alpha}}$, the correlation length of $\hat{\alpha}$, tends to underestimate the correlation length of α (Figure 4-3b), because variability due to errors in $\hat{Q}_1$ and $\hat{Q}_2$ tends to mask the true spatial structure of α due to small σ_{α}^2. As $\langle f \rangle$ decreases these effects are more pronounced. When contact errors are present error in $\hat{Q}_2$ becomes independent of the sampled hydraulic properties, especially at low $\langle \alpha \rangle$. This effectively eliminates spatial correlation in $\hat{\alpha}$, and estimated $\sigma_{\hat{\alpha}}^2$ and $\lambda_{\hat{\alpha}}$ are greatly underestimated, especially in the lower right corner of parameter space (Figure 4-3c and 4-3d).
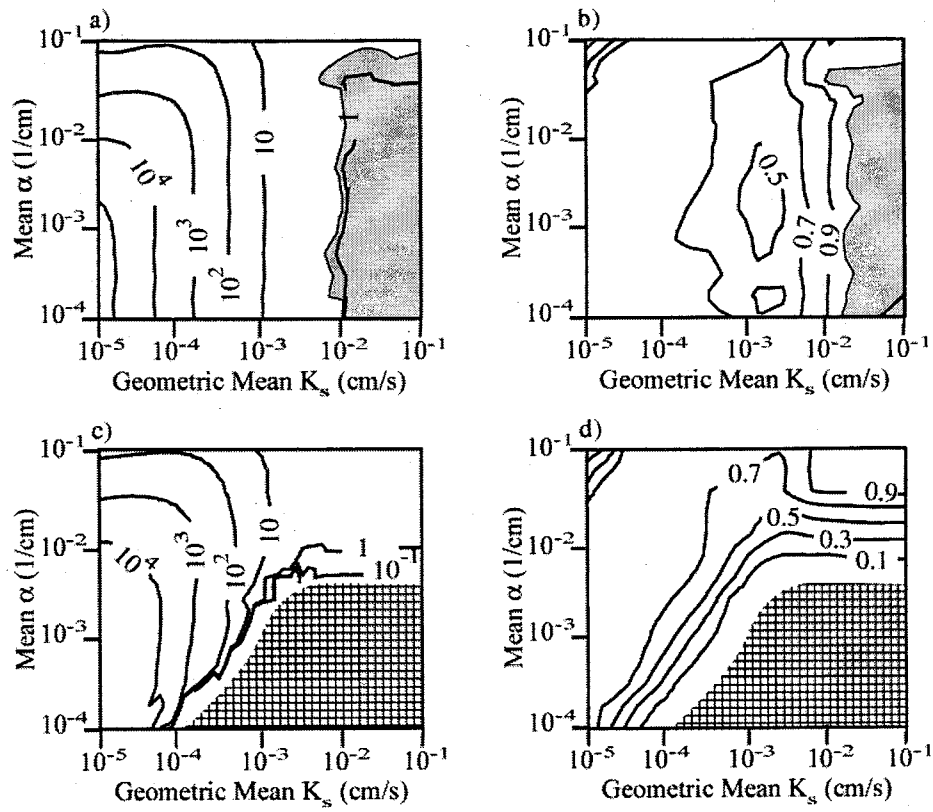
Figure 4-3. Ratio of the "estimated" to "true" variogram parameters for α. Observation error scenario: errors in a) variance and b) correlation length. Contact-error scenario: errors in c) variance and d) correlation length. Accurate regions ("estimated"/"true" between 0.95 and 1.05) are shaded, and regions where "estimated"/"true" = 0.0 are patterned. Note that c) shows no shading of the accurate region for clarity, because the accurate region is small.

When only observation errors are present, errors in $\sigma_{\hat{f}}^2$, the variance of $\hat{f}$, and the correlation length, $\lambda_{\hat{f}}$ (Figure 4-4), are very similar to those of Chapter 2. When contact errors are present, however, errors in $\sigma_{\hat{f}}^2$ are much less at low $\langle \alpha \rangle$, because the

variograms and cross-covariogram terms containing α contribute little to the estimated variance. In Chapter 2, these terms are much larger and cause significant overestimation of σ_f^2.
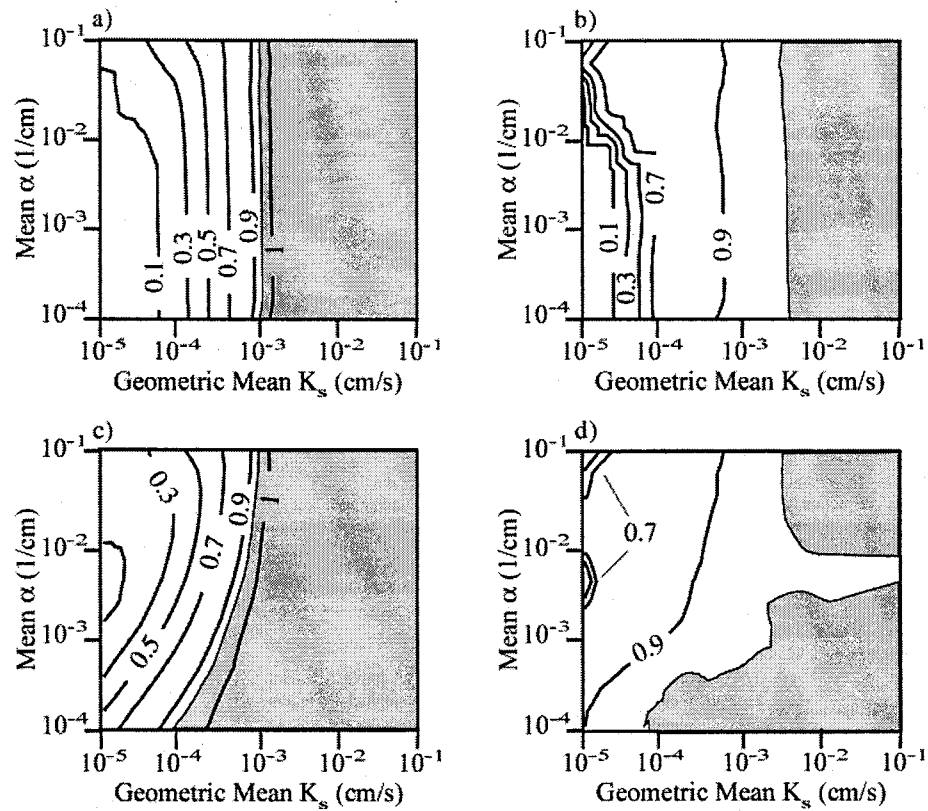

Figure 4-4. Ratio of the "estimated" to "true" variogram parameters for K_s. Observation error scenario: errors in a) variance and b) correlation length. Contact-error scenario: errors in c) variance and d) correlation length. Accurate regions ("estimated"/"true" between 0.95 and 1.05) are shaded.

4.6   STOCHASTIC MODEL ERRORS

In this section we present the results of stochastic-model error analysis for both the observation and contact error scenarios. We first consider errors affecting the mean velocity $\langle \hat{u}_1 \rangle$. Because $\langle \hat{u}_1 \rangle$ is a first-order approximation it is the same for the 3D isotropic and 1D perfectly stratified cases. We then present the errors in the velocity variance $\sigma_{\hat{u}_1}^2$ that occur for each of these two cases. Finally, we present errors in the integral scale of the velocity I_{u_1} and large-scale, longitudinal macrodispersivity for the 1D case, which has the greatest error in $\sigma_{\hat{u}_1}^2$.

The biased spatial statistics of $\hat{f}(\mathbf{x})$ and $\hat{\alpha}(\mathbf{x})$ cause stochastic-model errors in two ways. First, statistical-parameter errors also produce bias, or systematic distortion, in the model results. These errors are depicted in contour maps of our parameter space below. Second, erroneous spatial statistics may cause some of the model assumptions to be violated. For the first-order models considered here the critical assumptions are that $\sigma_{\theta_e}^2 / \langle \theta_e \rangle^2 \ll 1$, required for (4-9), and that $\sigma_{\alpha h}^2 \ll 1$, required for deriving (4-15). The $\sigma_{\theta_e}^2 / \langle \theta_e \rangle^2$ condition is more restrictive, and regions of the parameter space where $\sigma_{\hat{\theta}_e}^2 / \langle \hat{\theta}_e \rangle^2 > 1$ are excluded from the plots. The excluded area increases with mean tension $\langle h \rangle$ and, in the contact-error scenario, occupies the entire parameter space when $\langle h \rangle = 1000$ cm. Consequently, the following error plots are for mean tensions $\langle h \rangle$ of 10 cm, 100 cm, and 900 cm, representing wet to dry soils.
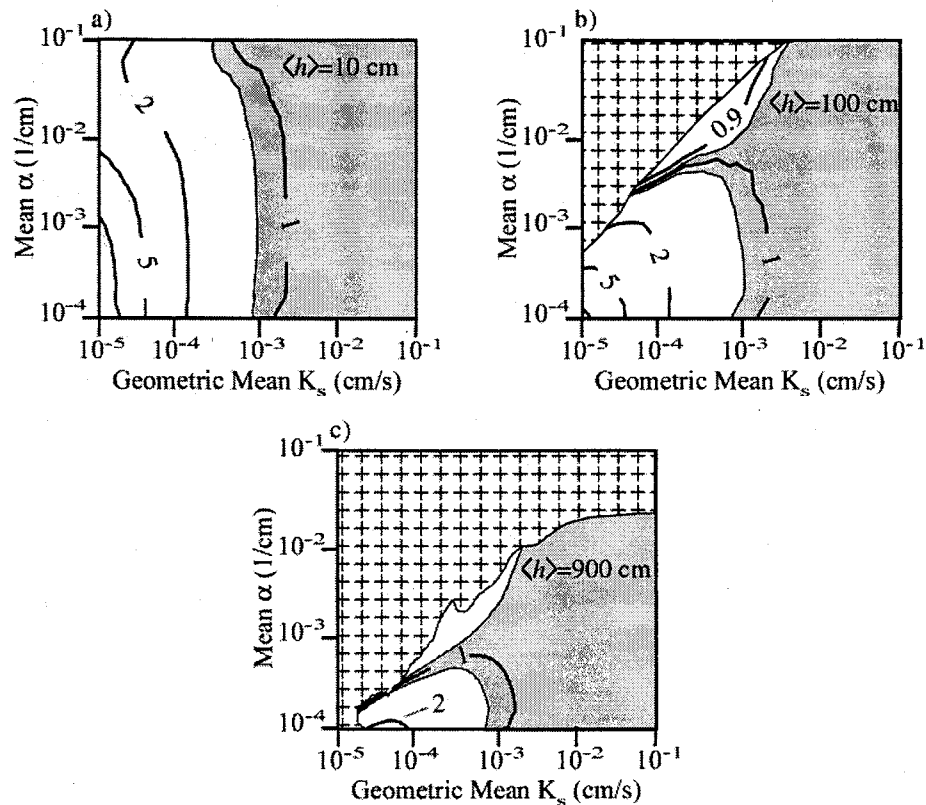
132

Figure 4-5. Ratio of the "estimated" to "true" mean velocity predicted using data from the observation-error scenario. Results are shown for three different mean tensions $\langle h \rangle$ (values shown on graphs). Accurate regions ("estimated"/"true" between 0.95 and 1.05) are shaded, and regions where $\sigma_{\hat{\theta}_e}^2 / \langle \hat{\theta}_e \rangle^2 > 1$ are patterned.

Errors in the mean velocity are shown for the three different $\langle h \rangle$ in Figure 4-5. Under very wet conditions, $\langle \hat{u}_1 \rangle$ is most sensitive to the geometric mean of saturated conductivity $\hat{K}_s$, and errors in the mean velocity (Figure 4-5a) mimic errors in $\langle \hat{f} \rangle$ (Figure 4-2c). As a result, $\langle \hat{u}_1 \rangle$ is accurately estimated at large $\langle f \rangle$ (right side of

133

parameter space) and is overestimated by more than a factor of 5.0 at small $\langle f \rangle$ (left side

of parameter space). Slight deviations occur at high $\langle \alpha \rangle$ (upper portion of parameter

space), because overestimation of $\langle \hat{\alpha} \rangle$ leads to a reduction in $\langle \hat{u}_1 \rangle$. At moderate tensions

$\langle h \rangle$ (Figure 4-4b), errors in $\langle \hat{u}_1 \rangle$ change significantly, and the excluded region,

$\sigma_{\hat{\theta}_e}^2 / \langle \hat{\theta}_e \rangle^2 > 1$, occupies roughly a third of the parameter space, concentrated in the upper

left corner of parameter space (e.g., well sorted, sandy silt). Along the boundary with

excluded region, overestimation of $\langle \hat{\alpha} \rangle$ leads to under-prediction of $\langle \hat{u}_1 \rangle$. In the lower

left corner, small $\langle f \rangle$ and $\langle \alpha \rangle$, the mean velocity $\langle \hat{u}_1 \rangle$ remains dominated by errors in

the geometric mean $\hat{K}_s$ and is overestimated. At very high tension $\langle h \rangle$ (Figure 4-5c), the

excluded region occupies much of the parameter space. Even without measurement error,

$\sigma_{\theta_e}^2 / \langle \theta_e \rangle^2$ is greater than 1 for $\langle \alpha \rangle$ exceeding 0.02 cm^{-1}. Regardless of the value of $\langle h \rangle$,

$\langle \hat{u}_1 \rangle$ is accurately estimated at large $\langle f \rangle$, because $\langle \hat{\alpha} \rangle$ and $\langle \hat{f} \rangle$ are accurately estimated.

When contact errors are present $\langle \hat{u}_1 \rangle$ errors show similar behavior (Figure 4-6).

At low tension (Figure 4-6a) $\langle \hat{u}_1 \rangle$ reflects errors in $\langle \hat{f} \rangle$ (Figure 4-2c) and is

overestimated by up to a factor 20. At progressively higher tension $\langle h \rangle$ (Figures 4-7b

and 4-7c), the magnitude of error in the mean velocity $\langle \hat{u}_1 \rangle$ decreases, and the accurate

region for $\langle \hat{u}_1 \rangle$, defined by $\langle \hat{u}_1 \rangle / \langle u_1 \rangle = 1$, sweeps across the parameter space. At very

high tension $\langle h \rangle$ (Figure 4-6c), $\langle \hat{u} \rangle$ is always underestimated, because the accurate region
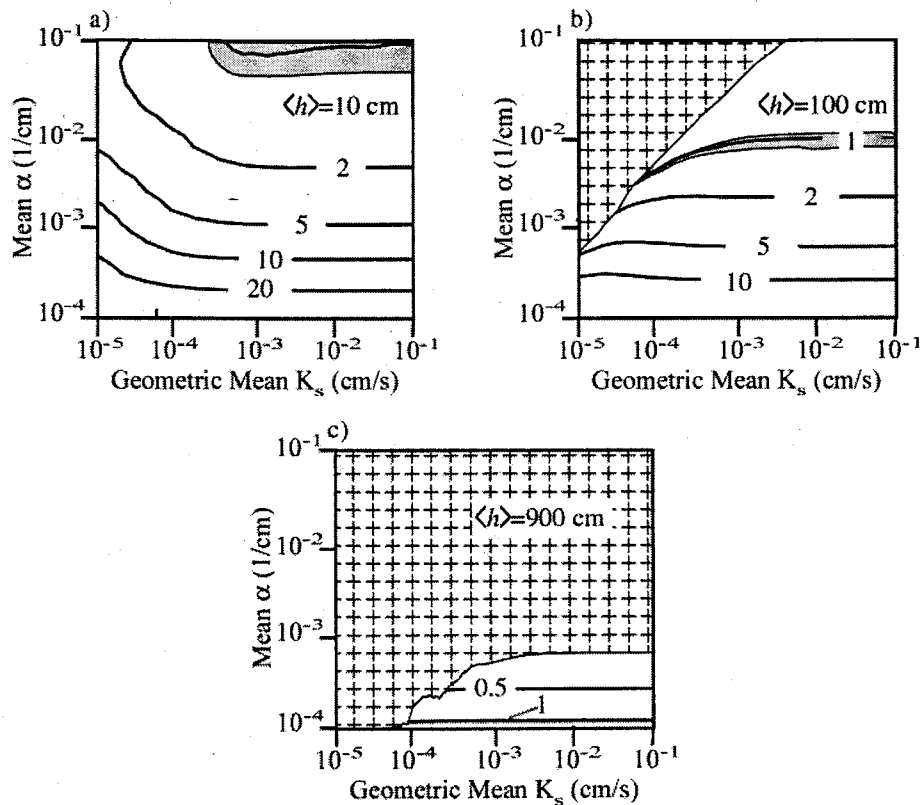
has passed out of the parameter space.

Figure 4-6. Ratio of the "estimated" to "true" mean velocity predicted using data from the contact-error scenario Results are shown for three different mean tensions $\langle h \rangle$ (values shown on graphs). Accurate regions ("estimated"/"true" between 0.95 and 1.05) are shaded, and regions where $\sigma_{\hat{\theta}_e}^2 \big/ \langle \hat{\theta}_e \rangle^2 > 1$ are patterned.

Errors in the velocity variance, $\sigma_{\hat{u}_1}^2$, are shown for the observation-error scenario in Figure 4-7 and the contact-error scenario in Figure 4-8. At low tensions, errors in the variance $\sigma_{\hat{u}_1}^2$ mimic errors in the mean velocity $\langle \hat{u}_1 \rangle$. At higher tensions, the error pattern changes and becomes more complex, reflecting errors in the correlation lengths
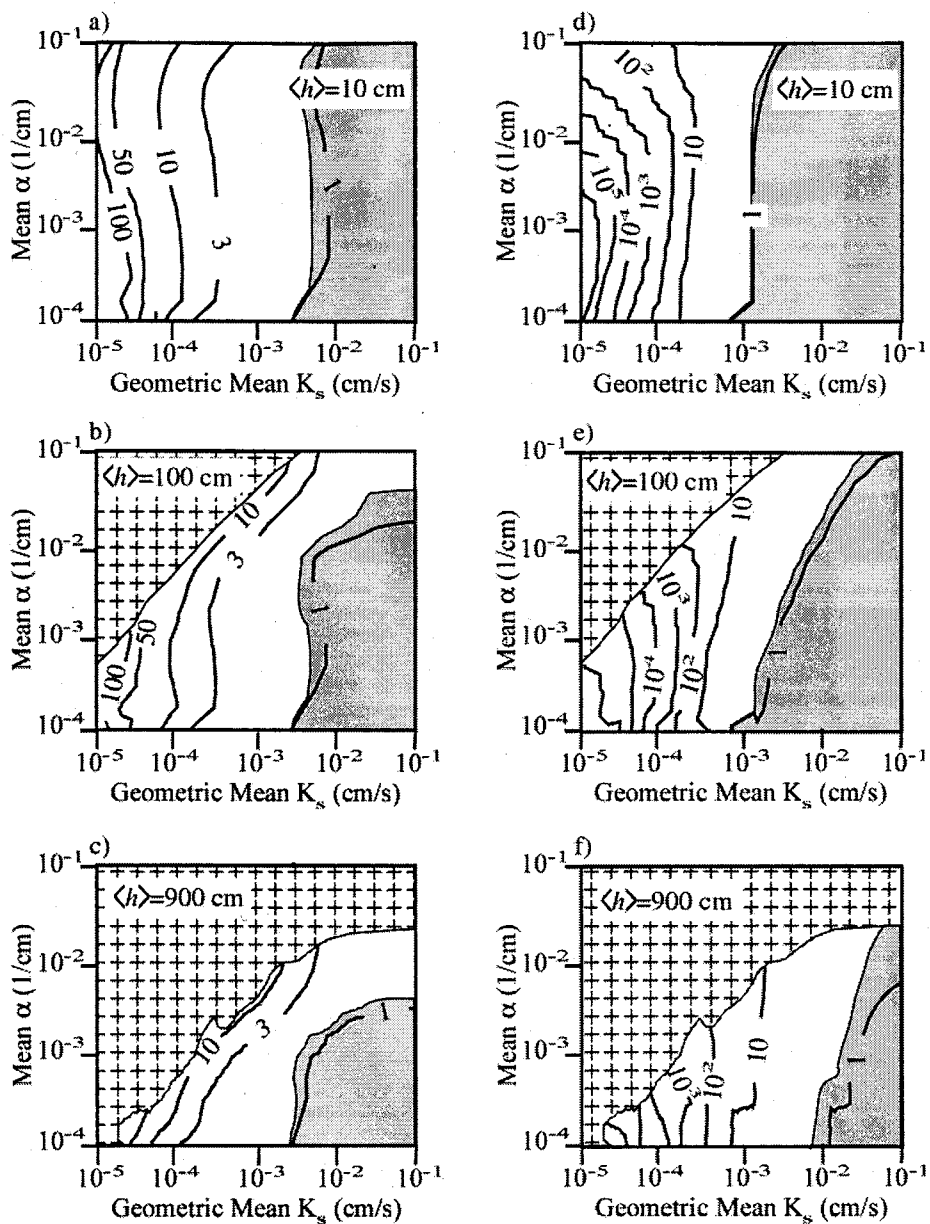
135

Figure 4-7. Ratio of the "estimated" to "true" velocity variance predicted using data from the observation-error scenario. Results for 3D isotropic flow in a), b), and c) and 1D flow in d), e), and f). Results are shown for three different mean tensions $\langle h \rangle$ (values shown on graphs). Accurate regions ("estimated"/"true" between 0.95 and 1.05) are shaded, and regions where $\sigma_{\hat{\theta}_e}^2 / \langle \hat{\theta}_e \rangle^2 > 1$ are patterned.

136

Figure 4-8. Ratio of the "estimated" to "true" velocity variance predicted using data from the contact-error scenario. Results for 3D isotropic flow in a), b), and c) and 1D flow in d), e), and f). Results are shown for three different mean tensions $\langle h \rangle$ (values shown on graphs). Accurate regions ("estimated"/"true" between 0.95 and 1.05) are shaded, and regions where $\sigma_{\hat{\theta}_e}^2 / \langle \hat{\theta}_e \rangle^2 > 1$ are patterned.
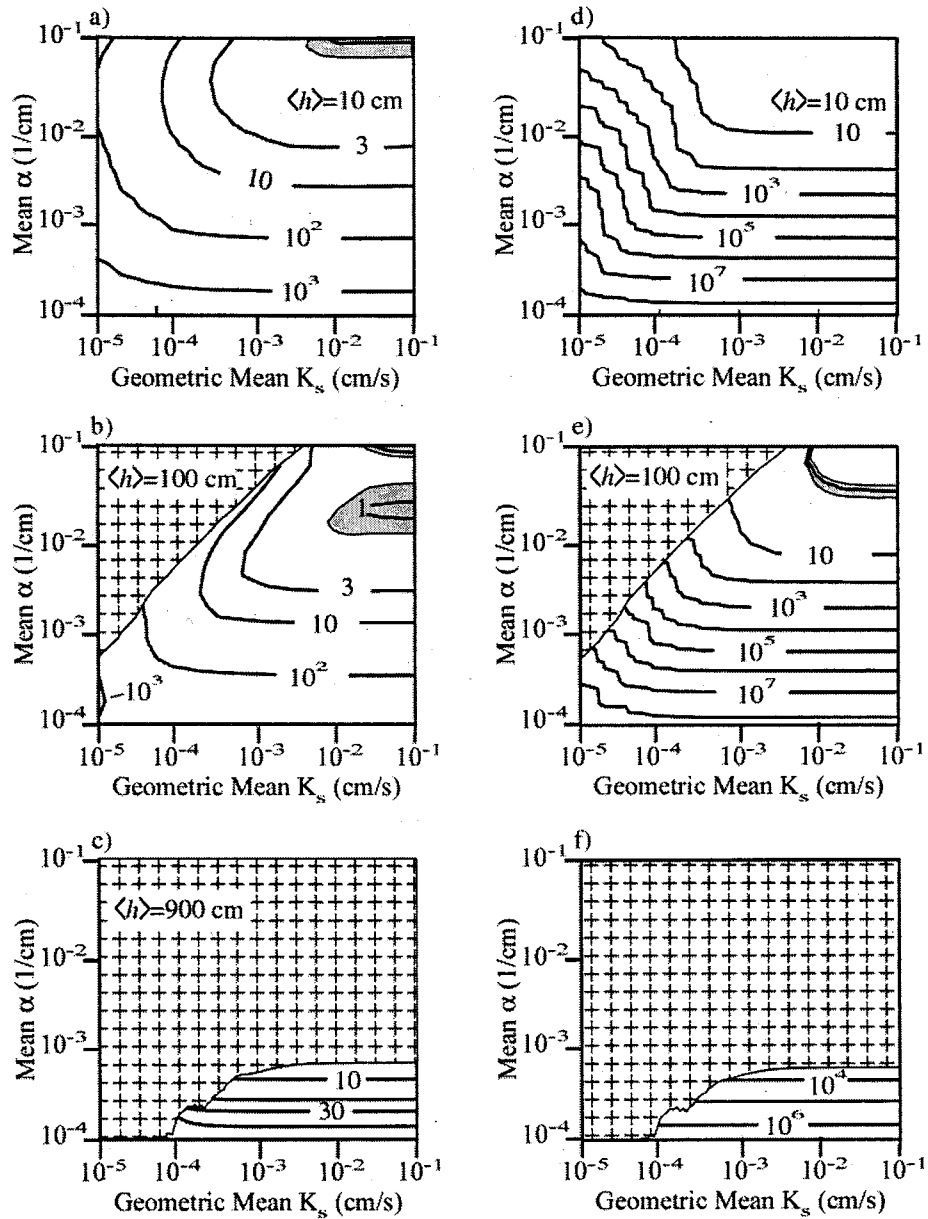
137

and variances of $\hat{\alpha}$ and $\hat{f}$. As $\langle \alpha \rangle$ increases and $\langle f \rangle$ decreases, errors in $\sigma_{\hat{u}}^2$ increase, because the cross-covariance $\sigma_{\hat{q}\hat{\theta}_e}^2$ from (4-22) is overestimated due errors in $\sigma_{\hat{\alpha}}^2$ and in the products of $\langle \hat{\alpha} \rangle$ and $\langle h \rangle$. In the observation-error scenario, $\sigma_{\hat{u}_1}^2$ is accurately estimated in a irregular region in the lower right corner, low $\langle \alpha \rangle$ and large $\langle f \rangle$ (poorly-sorted coarse sands), regardless of mean tension. In the contact-error scenario, the accurate region for $\sigma_{\hat{u}_1}^2$ sweeps across the parameter space as the mean tension increases.

While the $\sigma_{\hat{u}_1}^2$ error patterns are the same for both the 3D and 1D cases, the magnitude of the errors are strikingly different (Figures 4-7 and 4-8). During 1D flow, $\sigma_{\hat{u}_1}^2$ error may be over 4 orders of magnitude larger than during 3D flow. This result is not surprising, because measurement errors increase the apparent heterogeneity of $\hat{\alpha}$ and 1D flow samples all of the heterogeneity, while flow diverts around low permeability zones during 3D flow.

Errors in the integral scale of the 1D velocity, I_{u_1}, are presented in Figure 4-9 and tend to be inversely proportional to errors in the velocity variance $\sigma_{\hat{u}_1}^2$. In the observation-error scenario, I_{u_1} is accurately estimated in a small region in the lower right corner of parameter space, low $\langle \alpha \rangle$ and large $\langle f \rangle$, regardless of mean tension. In the contact-error scenario, the velocity integral scale is never accurately estimated. The integral scale of velocity tends to be underestimated as mean tension increases, because the velocity is increasingly sensitive to errors in $\hat{\alpha}$.
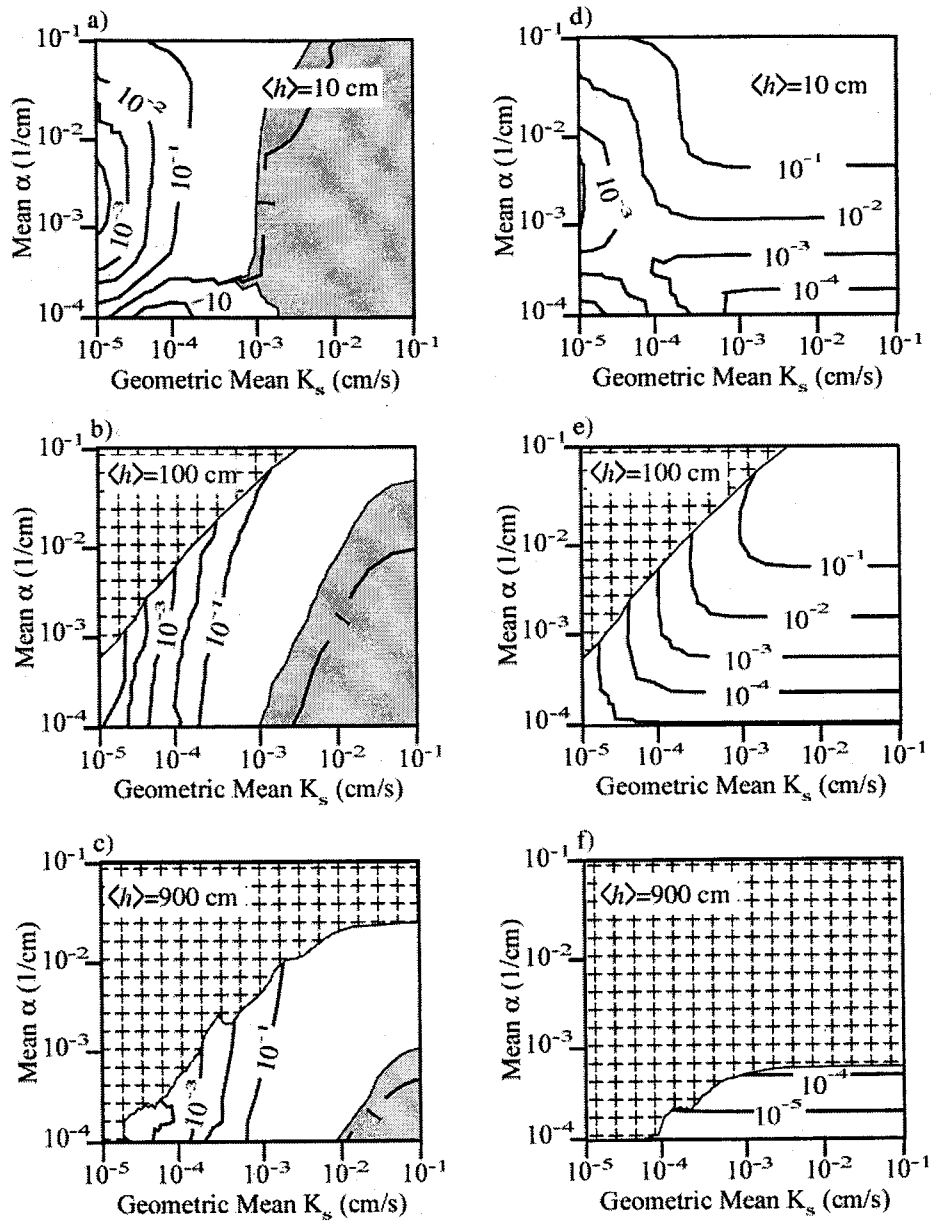
Figure 4-9. Ratio of the "estimated" to "true" 1D integral scale of the velocity predicted using data from the observation-error scenario [a), b), and c)] and the contact-error scenario [d), e), and f)]. Results are shown for three different mean tensions $\langle h \rangle$ (values shown on graphs). Accurate regions ("estimated"/"true" between 0.95 and 1.05) are shaded, and regions where $\sigma_{\hat{\theta}_e}^2 / \langle \hat{\theta}_e \rangle^2 > 1$ are patterned.

Errors in the 1D longitudinal macrodispersivity, A_1, are small (Figure 4-10), because of compensating errors in $\langle \hat{u}_1 \rangle$, $\sigma^2_{\hat{u}_1}$, and I_{u_1} (4-41). In the observation-error scenario, A_1 is accurately estimated across nearly the entire parameter space. In the contact-error scenario, however, A_1 less accurately estimated. These results suggest that the 1D macrodispersivity is a fairly robust ensemble statistic at large travel distances.

When only observation errors are present, a "sweet spot" occurs in the lower right corner of the parameter space, large $\langle f \rangle$ and moderate to low $\langle \alpha \rangle$, where estimates of ensemble velocity parameters remain accurate regardless of tension. In this region, the spatial statistics for both $\hat{\alpha}$ and $\hat{f}$ are accurate. When contact errors are present, however, the accurate regions for the spatial statistics of $\hat{\alpha}$ and $\hat{f}$ do not overlie one another in parameter space. As a result, no sweet spot occurs, and the accurate region for ensemble velocity parameters shifts through the parameter space. In general, the sweet spot is largest for macrodispersivity A_1, because of compensating errors, followed by mean velocity $\langle \hat{u}_1 \rangle$, which depends only on $\langle \hat{\alpha} \rangle$ and $\langle \hat{f} \rangle$, and smallest for the velocity variance $\sigma^2_{\hat{u}_1}$ and the velocity integral scale I_{u_1}, which depend on the variance and correlation lengths of $\hat{a}$ and $\hat{f}$.

4.7 NEGLECTED ERRORS

Because we include only very small and simple forms of error and neglect many other types of error, we believe that our results are optimistic. In Chapter 2 we explained
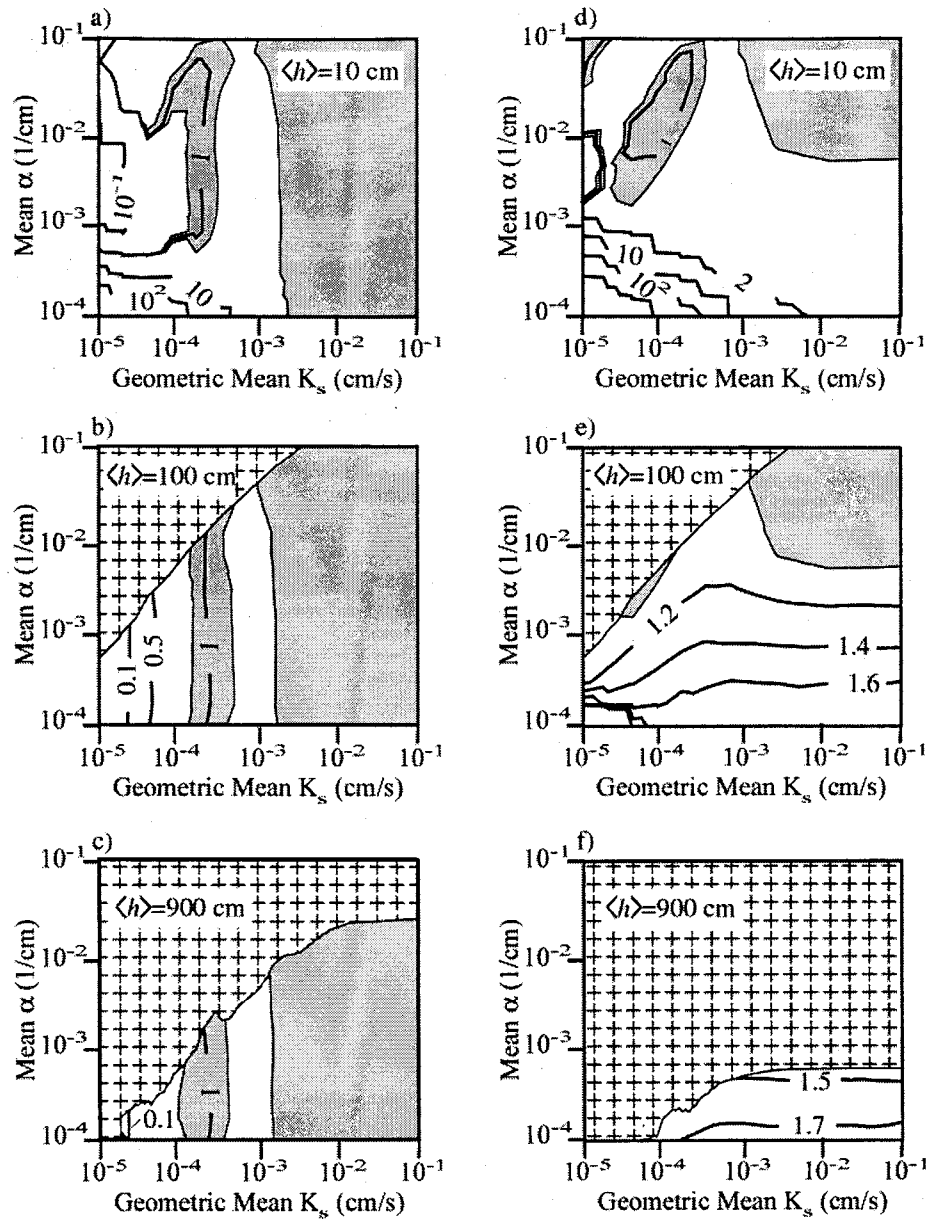
Figure 4-10. Ratio of the "estimated" to "true" longitudinal macrodispersivity (1D flow) predicted using data from the observation-error scenario [a), b), and c)] and the contact-error scenario [d), e), and f)]. Results are shown for three different mean tensions $\langle h \rangle$ (values shown on graphs). Accurate regions ("estimated"/"true" between 0.95 and 1.05) are shaded, and regions where $\sigma_{\hat{\theta}_e}^2 / \langle \hat{\theta}_e \rangle^2 > 1$ are patterned.

141

that actual tension infiltrometer flux-rate errors are likely to be higher than those considered our work, citing as one example $\sigma_Q^2 = 0.06$ cm^6/s^2, or more than an order of magnitude larger than the value $\sigma_Q^2 = 0.00165$ cm^6/s^2 used here. In addition, errors in applied tension at the disk source may be much larger than considered here, because many tension infiltrometers do not use transducers in the base plate. We have also assumed that tension infiltrometer flux rates have truly reached steady state. In the field, however, it is nearly impossible to reach true steady state.

We also considered a simple inversion-model error caused by poor contact between the tension infiltrometer and the sampled medium. Other types of inversion-model error, however, may be difficult to quantify or treat. These errors may include sub-sample heterogeneity, viscosity changes during infiltration, non-uniform wetting phase structure introduced by sub-sample scale heterogeneity or air entrapment, and incorrect parametric models for relative permeability.

Given the wide range of types of error that may affect field measurements of unsaturated hydraulic properties, it may be impossible to model all errors that affect field measurements of unsaturated hydraulic properties. Consequently it may not be possible to use error analysis to determine suitable parameter spaces for a particular field device or to remove bias from estimated spatial statistics. This suggests that under some conditions stochastic models based on these kinds of measurements may be too uncertain for use in decision-making processes.

In this study we use every point in a reality to estimate spatial statistics. However, it is not possible to sample everywhere, and estimates of spatial statistics are

uncertain because of incomplete sampling and non-ideal sample locations (structural errors). When measurement errors are present, structural errors increase significantly and the additional uncertainty can preclude reliable estimation of spatial statistics (Chapter 3).

4.8   SUMMARY AND IMPLICATIONS

We investigate impact of hydraulic property measurement errors on estimates of the ensemble mean, variance, and integral scale of velocity using a Monte Carlo error analysis. We use extensions of the unconditional stochastic flow and transport models of Yeh et al. (1985a, b) (3D statistically isotropic) and Zhang et al. (1998) (1D perfectly layered), which require input spatial statistics for the saturated hydraulic conductivity, K_s, and the exponential relative permeability parameter, α. These properties can be estimated *in situ* using the tension infiltrometer (Reynolds and Elrick, 1991).

We generate spatially correlated random fields of $\alpha(\mathbf{x})$ and $f(\mathbf{x}) = \ln[K_s(\mathbf{x})]$, sample each point in the field, and simulate tension infiltrometer measurements subject to error. We consider two error scenarios: 1) an observation-error scenario with errors in estimates of tension infiltrometer flux-rates and applied pressures and 2) a contact-error scenario which includes the effects of poor contact between the tension-infiltrometer disk and the sampled medium. We estimate $\hat{\alpha}(\mathbf{x})$ and $\hat{f}(\mathbf{x})$ using the method of Reynolds and Elrick (1991). The spatial statistics (mean, correlation length, and variance) for both the true and estimated fields are determined and used in the stochastic models of Yeh et al. (1985a, b) and Zhang et al. (1998) to determine the ensemble mean, variance, and integral scale of velocity and the longitudinal macrodispersivity. This procedure is

repeated for 221 sets of fields distributed across a parameter space representative of poorly- to well-sorted, sandy silt to coarse sand. Errors are quantified using the ratio of the "estimate" to the "true" value.

Although the general trends are similar, errors in spatial statistics differ from the results presented in Chapter 2. Major differences reflect the smaller variance of α due to our assumption here of a normal distribution for α, with fixed CV = 0.1. Because the spatial structure of $\hat{\alpha}$ is less varied, it is easily obscured by measurement errors, resulting in larger errors in the variance and smaller estimates of correlation length. In addition, variogram and cross-variogram terms containing α are smaller, leading to less error in σ_f^2 when contact errors are present.

The errors in the spatial statistics of $\hat{f}(\mathbf{x})$ and $\hat{\alpha}(\mathbf{x})$ cause errors in stochastic flow and transport models in two ways: 1) critical model assumptions may be violated, limiting the parameter space usable in the model and 2) model results become biased or systematic distorted. In our study, an assumption required for the first order approximations, $\sigma_{\hat{\theta}_e}^2 / \left\langle \hat{\theta}_e \right\rangle^2 \ll 1$, is violated across roughly a third of the parameter space in moderately dry conditions ($\left\langle h \right\rangle = 100$ cm), and across more than one half of the parameter space under very dry conditions($\left\langle h \right\rangle = 900$ cm). When the mean tension is sufficiently high, e.g., $\left\langle h \right\rangle = 1000$ cm, and contact errors are present, the assumption is violated across the entire parameter space.

Where critical assumptions are valid stochastic-model results show significant error. The magnitude and pattern of error changes with mean tension. Mean velocities

144

may be overestimated (wet conditions) or underestimated (dry conditions) by roughly an order of magnitude. Errors in velocity variances change with the dimensionality of flow, and the magnitude of the error decreases with mean tension. Errors are generally much worse for 1D stochastic flow, because all heterogeneity is sampled. The velocity variance is overestimated by up to three orders of magnitude during 3D flow and eight orders of magnitude during 1D flow. The 1D velocity integral scale varies as the inverse of the velocity variance. Consequently, it is generally underestimated by as much as five orders of magnitude. The estimate of the 1D longitudinal macrodispersivity is surprisingly robust. It generally shows relatively small error across most of the parameter space.

When only observation errors occur a sweet spot develops in parameter space coincident with poorly sorted, coarse sand (low α and large K_s). In the sweet spot, all stochastic model results are accurate, because the spatial statistics of $\hat{f}(\mathbf{x})$ and $\hat{\alpha}(\mathbf{x})$ are accurate. When contact errors are present, no sweet spot develops, because the accurate regions for the spatial statistics of $\hat{f}(\mathbf{x})$ and $\hat{\alpha}(\mathbf{x})$ do not overlap.

Our results suggest that property-measurement errors can significantly impact stochastic-model results and, by implication, the decisions based on these results. If property-measurement errors are known and can be quantified, as in our case, it is possible to remove the effects of these errors. Unfortunately, it is impossible to explicitly know all errors *a priori*, and the number and potential effect of measurement errors is great. The consequences of unknown property errors are potentially severe. For the types of error considered here, one could unknowingly underpredict mean travel times by over

an order of magnitude under wet conditions and overestimate travel times by nearly an order of magnitude under drier conditions.

Our results also illustrate an important limitation of stochastic models. If input spatial statistics are not accurate, the magnitude of stochastic-model errors changes with flow conditions. A sweet spot only occurs in that part of parameter space where all input spatial statistics are accurately estimated. When measurements are affected by only observation errors, it is more likely that a sweet spot will develop in some part of a parameter space. When inversion-model errors affect measurements, it is less likely that the spatial statistics will be accurately estimated in an overlapping portion of parameter space, and there will be no sweet spot. Similar behavior is likely when multiple properties are estimated from different methods, with varying measurement support, or at dissimilar time scales.

Most practical applications of stochastic models involve conditioning on site-specific data and the use of boundary conditions and parameter fields that produce non-stationary flow conditions. When used in a decision-making process these models offer an advantage, because solutions are constrained by site-specific data and estimated second and higher moments are smaller, implying lower uncertainty and increased confidence in the results. When the hydraulic property data have been estimated in the presence of observation or inversion-model errors, however, the increased confidence may not be warranted, as bias in the results may erode the advantages of conditional approaches. This issue should be the subject of future research.

4.9   REFERENCES CITED

Ankeny, M. D., T. C. Kaspar, and R. Horton, 1988, Design for an automated tension infiltrometer, *Soil Science Society of America Journal*, v. 52, p. 893-896.

Deutsch, C. V., and A. G. Journel, GSLIB: *Geostatistical software library and user's guide*, 2nd ed., Oxford University Press, New York, NY, 369 pp.

DOE, 1993, *Hydrogeologic data for existing excavations at the Area 5 Radioactive Waste Management site, Nevada Test Site, Nye County, Nevada*, DOE/NV/11432-40, U. S. Department of Energy Nevada Operations Office, Las Vegas, NV.

Freeze, R. A., 1975, Stochastic-conceptual analysis of one-dimensional groundwater flow in non-uniform homogeneous media, *Water Resources Research*, v. 9, p. 725-741.

Gardner, W. R., 1958, Some steady state solutions of unsaturated moisture flow equations with application to evaporation for a water table, *Soil Science*, v. 85, p. 228-232.

Harter, T., and T. –C. Jim Yeh, 1996, Stochastic analysis of solute transport in heterogeneous, variably saturated soils, *Water Resources Research*, v. 32, p. 1585-1595.

Indelman, P., D. Or, and Y. Rubin, 1993, Stochastic analysis of unsaturated steady state flow through bounded heterogeneous formations, *Water Resources Research*, v. 29, p. 1141-1148.

Jarvis, N. J., and I. Messing, 1995, Near-saturated hydraulic conductivity in soils of contrasting texture measured by tension infiltrometers, *Soil Science Society of America Journal*, v. 59, p. 27-34.

Mantoglou, A. and L. W. Gelhar, 1987a, Capillary tension head variance, mean soil moisture content, and effective specific soil moisture capacity of transient unsaturated flow in stratified soils, *Water Resources Research*, v. 23, p. 47-56.

Mantoglou, A. and L. W. Gelhar, 1987b, Effective hydraulic conductivities of transient unsaturated flow in stratified soils, *Water Resources Research*, v. 23, p. 57-67.

Mohanty, B. P., M. D. Ankeny, R. Horton, and R. S. Kanwar, 1994, Spatial analysis of hydraulic conductivity measured using disc infiltrometers, *Water Resources Research*, v. 30, p. 2489-2498.

Reynolds, W. D., and D. W. Elrick, 1991, Determination of hydraulic conductivity using a tension infiltrometer, *Soil Science Society of America Journal*, v. 55, p. 633-639.

Robin, M. J. L., A. L. Gutjahr, E. A. Sudicky, and J. L. Wilson, 1993, Cross-correlated random field generation with the direct Fourier transform method, *Water Resources Research*, v. 29, p. 2385-2397.

Russo, D., 1988, Determining soil hydraulic properties by parameter estimation: On the selection of a model for the hydraulic properties, *Water Resources Research*, v. 24, p. 453-459.

Russo, D., 1993, Stochastic modeling of macrodispersion for solute transport in heterogeneous unsaturated porous formations, *Water Resources Research*, v. 29, p. 383-397.

Russo, D., 1995, Stochastic analysis of the velocity covariance and the displacement covariance tensors in partially saturated heterogeneous anisotropic porous formations, *Water Resources Research*, v. 31, p. 1647-1658.

Shouse, P. J., and B. P. Mohanty, 1998, Scaling of near-saturated hydraulic conductivity measured using disc infiltrometers, *Water Resources Research*, v. 23, p. 1195-1205.

Wooding, R. A., 1968, Steady infiltration from a shallow circular pond, *Water Resources Research*, v. 4, p. 1259-1273.

Yang, J., R. Zhang, and J. Wu, 1996, An analytical solution of macrodispersivity for adsorbing solute transport in unsaturated soils, *Water Resources Research*, v. 32, p. 355-362.

Yeh, T. –C. Jim, L. W. Gelhar, and A. L. Gutjahr, 1985a, Stochastic analysis of unsaturated flow in heterogeneous soils: 1. Statistically isotropic media, *Water Resources Research*, v. 21, p. 447-456.

Yeh, T. –C. Jim, L. W. Gelhar, and A. L. Gutjahr, 1985b, Stochastic analysis of unsaturated flow in heterogeneous soils: 2. Statistically isotropic media with variable α, *Water Resources Research*, v. 21, p. 457-464.

Yeh, T. –C. Jim, L. W. Gelhar, and A. L. Gutjahr, 1985c, Stochastic analysis of unsaturated flow in heterogeneous soils: 3. Observations and applications, *Water Resources Research*, v. 21, p. 465-471.

Zhang, D. Z., T. C. Wallstrom, and C. L. Winter, 1998, Stochastic analysis of steady-state unsaturated flow in heterogeneous media: Comparison of the Brooks-Corey and Gardner-Russo models, *Water Resources Research*, v. 34, p. 1437-1449.

5.0   CONCLUSIONS AND RECOMMENDATIONS

In this dissertation, we show for the first time that bias in property measurements adversely affects our ability to characterize spatial variability and model flow and transport in heterogeneous systems. Measured hydraulic properties become biased when random observation errors are propagated through non-linear inversion models that may also incorrectly describe experimental physics. In engineering and physics, measurement bias can be experimentally evaluated and removed through the use of calibration standards. The entire instrument, including the inversion model, must be calibrated to overcome the inversion non-linearity. This is often infeasible in hydrology because physical standards do not exist and inversion-model errors vary unpredictably between individual samples. In spatial variability studies, it is also impossible to fully calibrate estimates of the spatial statistics. Therefore, the effect of bias on spatial statistics cannot be directly quantified, and instead must be examined indirectly.

We develop a new Monte Carlo approach to indirectly determine spatial bias in estimates of hydraulic properties subject to simple observation and inversion-model errors and to quantify its potential effect on stochastic model results. In Chapter 2, we evaluate measurement-error-induced bias in the spatial statistics of tension infiltrometer estimates of the saturated hydraulic conductivity and the exponential relative permeability parameter. We include only small simple observation errors of infiltrometer flux and the applied tension at the disk source, and a boundary condition or inversion model error concerning disk contact with the soil surface. In Chapter 3 we consider laboratory estimates of the saturated hydraulic, porosity, and the van Genuchten parameters (α and

150

n). We simulate laboratory measurements in the presence of simple observation errors and inversion model errors, including equilibrium errors, heterogeneity at the base of the sample, and sample repacking. Because most applied spatial variability studies rely on a limited number of samples, we also examined the uncertainty in spatial statistics as a function of the number of samples. In Chapter 4 we determine the impact of measurement errors on 1D and 3D unconditional unsaturated stochastic models of unsaturated flow and transport. The major conclusions of this dissertation and some recommendations for future research are presented below.

5.1 CONCLUSIONS

In this dissertation, we found that small errors in observations and simple inversion-model errors can cause significant spatial bias in hydraulic property estimates when hydraulic properties are estimated with a non-linear inversion model. The bias originates because most hydraulic properties are not estimated directly. Instead, they are estimated using instruments that observe the response of a hydrologic system to perturbation and a non-linear mathematical-inversion model that infers property values from the observed responses. Bias results when observation errors are propagated through the inversion model or from errors in the inversion model itself. The extent of bias depends on the degree of non-linearity in the inversion model, the true values of the sampled hydraulic properties, and the nature of the observation and inversion-model errors.

Bias is manifested as a systematic distortion in space that affects quantitative measures of spatial variability including the mean, variance, variogram, and variogram model parameters and can lead to order-of-magnitude errors in these statistics (Chapters 2, 3, and 4). Artificial cross-correlation between estimated parameters results when multiple parameters are estimated from a single non-linear inversion model (Chapters 2 and 3). Measurement errors may lead to the inclusion of parameters in the inversion model that are simply artifacts of the errors (Chapter 3), yet show realistic spatial statistics. Measurement errors amplify uncertainty in experimental variograms due to limited sampling and can preclude identification of variogram-model parameters. The effects of observation and inversion model errors can be insidious, as hydraulic property estimates may appear reasonable and generate realistic looking spatial statistics which are, however, inaccurate and misleading.

The parameters that describe the slope of the moisture-characteristic or unsaturated hydraulic conductivity curves are particularly sensitive to measurement errors and show the greatest bias (Chapters 2, 3, and 4). It may be possible to accurately estimate spatial statistics of unsaturated scaling variables (saturated hydraulic conductivity, porosity, and parameters related to the air-entry pressure), especially if direct measurements with nearly-linear or linear inversion models are used (e.g., Chapter 3).

Robust estimation of unsaturated hydraulic properties for spatial variability studies is not possible with most current instruments and inversion models because multiple parameters are estimated using a single, nonlinear model. In addition, bias in spatial statistics of estimated hydraulic properties is extremely sensitive to different

inversion-model errors, and it is not possible to identify *a priori* all types of inversion-model error that can affect a particular property estimation method. Therefore, error analyses cannot be used to uniquely identify all material types or conditions under which a particular instrument or inversion model will perform best or to remove bias caused by measurement errors.

Our results suggest that property-measurement errors can significantly impact stochastic-model results and, by implication, the decisions based on these results. We observe order-of-magnitude scale errors in the results of analytical stochastic models for unsaturated flow and transport (Chapter 4). These errors originate in two ways: 1) critical model assumptions may be violated, limiting the parameter space usable in the model and 2) model results become biased or systematic distorted. Model assumptions are violated most when flow occurs under dry conditions. We also found that errors were greatest (several orders of magnitude) for estimates of the velocity variance and integral scale, which depend on variogram-model parameters, modest for estimates of the ensemble mean velocity (an order of magnitude), and least for estimates of the macrodispersivity (under a factor of 2), due to compensating errors.

If input spatial statistics are not accurate the magnitude of stochastic-model errors change with flow conditions. A sweet spot, where estimates of ensemble velocity parameters remain accurate regardless of tension, only occurs in that part of parameter space where all input spatial statistics are accurately estimated. When measurements are affected by only observation errors, it is likely that a sweet spot will develop in some part of a parameter space. When inversion-model errors affect measurements, it is less likely that the spatial statistics will be accurately estimated in an overlapping portion of

parameter space, and there will be no sweet spot. Similar behavior is likely when multiple properties are estimated from different methods, with varying measurement support, or at dissimilar time scales.

Bias in property measurements is a critical problem in groundwater hydrology with wide reaching implications. It potentially impairs our ability to directly characterize property heterogeneity and accurately model flow and transport at contaminated sites. It may adversely affect the design, final cost, and effectiveness of remedial actions at contaminated sites. Given the scope of the environmental problem in the United States, additional research related to property measurement bias and related spatial bias is imperative.

5.2   RECOMMENDATIONS

The primary purpose for characterization activities is to provide data for conceptual and predictive subsurface models, including probabilistic models of contaminant transport for decision making. Although many techniques exist for incorporating site-specific observations of hydraulic parameter heterogeneity into a probabilistic risk framework for decision analysis, they cannot be reliably applied without first quantifying the uncertainty in hydraulic parameter data. If the character and extent of spatial bias is unknown, parameter estimates may be overvalued, resulting in costly site-characterization and poor remedial decisions. Until now, the effects of spatial bias due to measurement errors were ignored. While this dissertation represents an important first step, we must take a step back and evaluate the impact of spatial bias on nearly all of

154

our property-estimation methods and the models that require these hydraulic properties. Some the work that should be done is described below. While this listing is by no means comprehensive, it does provide initial direction for future research activities.

Evaluate Other Property-Estimation Methods. Although we have considered several of the standard methods for estimating unsaturated hydraulic properties, a number of current techniques remain unevaluated, including centrifugal methods for estimating moisture characteristic curves, numerical inversion of tension infiltrometer data, and pedotransfer functions. The impact of measurement errors on the spatial statistics of properties estimated with current methods should be determined.

Consider Spatial Bias in the Design of New and Emerging Technologies. New techniques for estimating properties, including geophysically based methods, should be developed with consideration of measurement-error-induced spatial bias. A systematic design approach could be employed, where design decisions, component selection, and implementation methods are chosen to minimize spatial bias, ensuring maximum data value.

Consider the Impact of Measurement Error on Data Worth. Although a large body of research has focused on evaluations of data worth, with the goal of optimizing data sampling locations, the impact of realistic measurement errors have been neglected. Most treatments of data worth assume that hydraulic

parameter measurement errors are unbiased and that parameter uncertainty only arises from incomplete sampling and non-ideal sample locations. However, these assumptions are generally invalid because measurement errors can be spatially biased, and this bias amplifies sampling uncertainty. The impact of measurement-error-induced spatial bias should be considered when evaluating site-specific data worth.

Evaluate Non-Parameteric Geostatistics. Indicator geostatistics are a very powerful non-parameteric tool for characterizing spatial variability. Indicator functions transform property value into a binary random variable, either 0 or 1, depending upon whether or not the property exceeds a threshold value. For non-categorical random space functions, threshold values are typically selected to represent quantiles (e.g., the median). Variograms of indicator functions are extremely robust, because their estimation does not depend on property values. Because indicator-variogram models contain only two unknowns (correlation length and nugget variance), they can be more reliably fit to indicator variograms. Indicator variograms may reveal the pattern of spatial variation for unsaturated hydraulic properties that cannot be evaluated using classical geostatistical techniques. The impact of measurement-error-induced spatial bias on indicator statistics should be evaluated.

Evaluate the Impact of Spatial Bias on Conditional Stochastic Models. Most practical applications of stochastic models involve conditioning on site-specific

data and the use of boundary conditions and parameter fields that produce non-stationary flow conditions. When used in a decision-making process these models offer an advantage, because solutions are constrained by site-specific data and estimated second and higher moments are smaller, implying lower uncertainty and increased confidence in the results. When the hydraulic property data have been estimated in the presence of observation or inversion-model errors, however, the increased confidence may not be warranted, as bias in the results erodes the advantages of conditional approaches. The impact of measurement-error-induced spatial bias on conditional stochastic models needs to be evaluated.

APPENDIX A - REPACKING ERRORS FOR VAN GENUCHTEN PARAMETERS

Haverkamp and Parlange (1986) developed an approach for pressure-saturation curves from cumulative grain size distributions and bulk density values. We modify their approach to allow us to adjust the values of α and n due to changes in bulk density when a sample is repacked. Haverkamp and Parlange (1986) assume that the particle diameter d (cm) can be related to the equivalent pore radius r (cm) by

$$d = \gamma r \qquad (A\text{-}1)$$

where γ is a packing parameter that is assumed constant. Using the Young-Laplace relationship, the matric potential (in cm) for water at 20°C is related to the particle diameter by

$$\psi = -\frac{0.149\gamma}{d} \qquad (A\text{-}2)$$

The parameter γ is only constant for stable packing arrangements of uniform-size particles. In real materials, particle sizes are not uniform, and γ varies as a function of pore radius (r). In addition, the Young-Laplace relationship (A-1) only applies to equilibrium conditions, when the pressure-saturation relationship is independent of pore-structure.

Haverkamp and Parlange (1986) fit a van Genuchten (1980) equation to the cumulative grain-size distribution [$F(d)$]

$$F(d) = \frac{1}{\left[1+\left(\dfrac{d_g}{d}\right)^{n_d}\right]^{1-1/n_d}} \qquad (A\text{-}3)$$

where d_g is a critical grain size and n_d is a parameter that is related to the standard deviation of the pore-size distribution. They assume that

$$n = a_1 \rho_b{}^{a_2} (n_d - 1) + 1 \qquad \text{(A-4)}$$

where a_1 is a constant equal to 0.0723 and a_2 is a constant equal to 3.8408. For a known value of n, drawn from our random field, we determine n_d using

$$n_d = \frac{n-1}{a_1 \rho_b{}^{a_2}} + 1 \qquad \text{(A-5)}$$

Using n_d and ρ_m, we can derive (3-17)

$$n_m = \left(\frac{\rho_m}{\rho_b}\right)^{a_2} (n-1) + 1 \qquad \text{(A-6)}$$

We relate the parameter α to d_g by

$$\alpha = \frac{d_g}{0.149 \gamma} \qquad \text{(A-7)}$$

The packing coefficient (γ) is determined from (Haverkamp and Parlange, 1986)

$$\gamma = b_1 + b_2(n-1) + b_3(n-1)^2 \qquad \text{(A-8)}$$

where $b_1 = 17.1736$, $b_2 = -4.7043$, and $b_3 = 0.1589$. We arbitrarily modify the value of b_3 to be equal to 0.4, because the value used by Haverkamp and Parlange (1986) yields negative values of γ at large n values ($n > 5.27$). The parameter d_g can be derived from

$$d_g = 0.149 \alpha \gamma \qquad \text{(A-9)}$$

A modified packing coefficient is determined from

$$\gamma_m = b_1 + b_2(n_m - 1) + b_3(n_m - 1)^2 \qquad \text{(A-10)}$$

Using d_g and γ_m, we can calculate a α parameter that is modified due to repacking

$$\alpha_m = \frac{d_g}{0.149\gamma_m} \qquad\qquad \text{(A-11)}$$

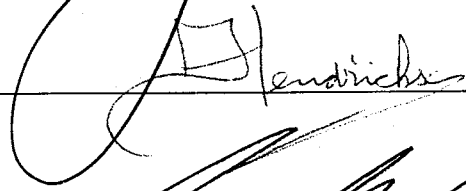Upon substitution, (A-11) can be rearranged to yield (3-18).

REFERENCES CITED

Haverkamp, R., and J. −Y. Parlange, 1986, Predicting the water-retention curve from

particle-size distribution: 1. Sandy soils without organic matter, *Soil Science*, v.

142, p. 325-339.

van Genuchten, M. Th., 1980, A closed −form equation for predicting the hydraulic

conductivity of unsaturated soils, *Soil Science Society of America Journal*, v. 44,

p. 892-898.

APPROVAL PAGE

This dissertation is accepted on behalf of the faculty of the Institute by the following
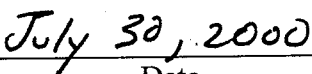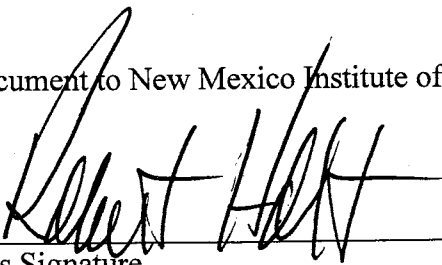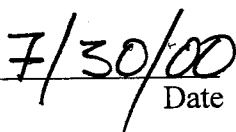
committee:

_____
Advisor

_____

_____

_____

_____

July 3∂, 2000
_____
Date

I release this document to New Mexico Institute of Mining and Technology

_____   7/30/00
Student's Signature   Date